APPENDIX

4. Spectral Reflectance

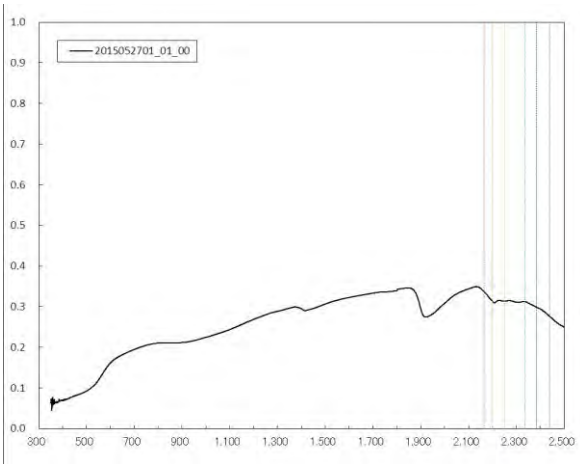

2015052701_01_00

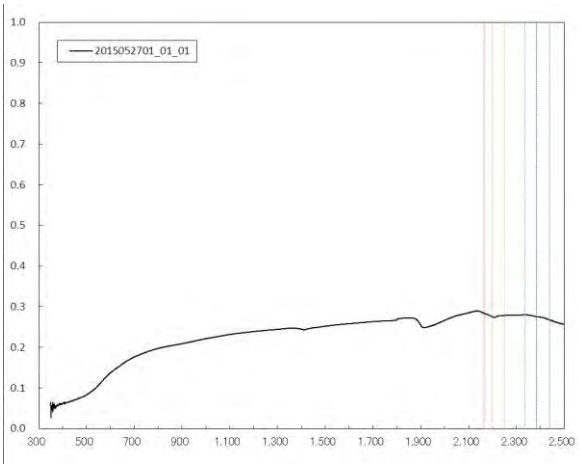

2015052701_01_01

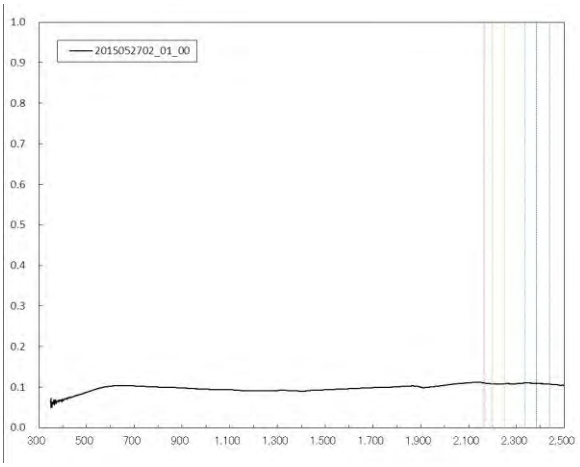

2015052702_01_00

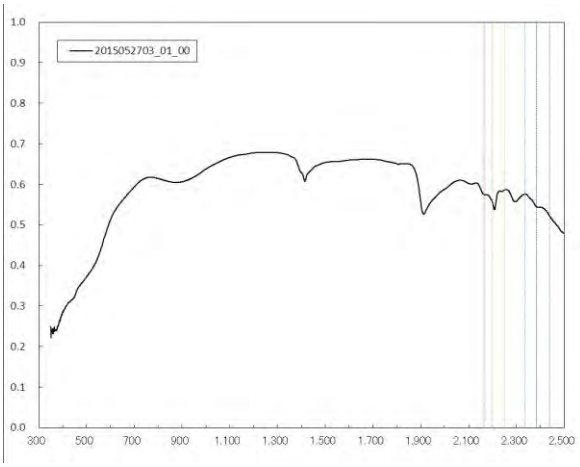

2015052703_01_00

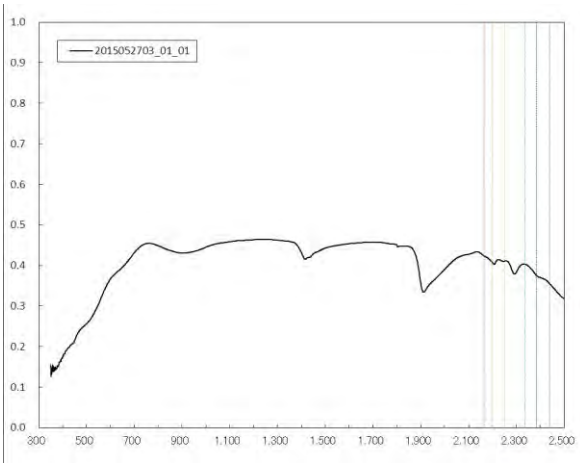

2015052703_01_01

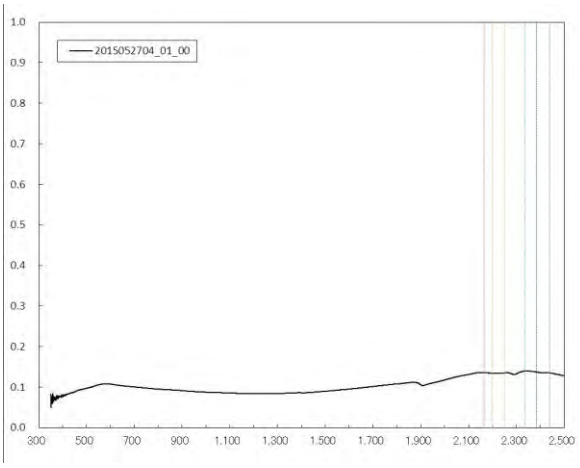

2015052704_01_00

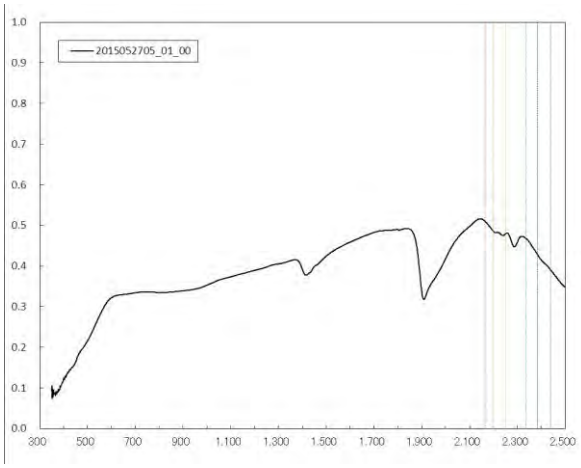

2015052705_01_00

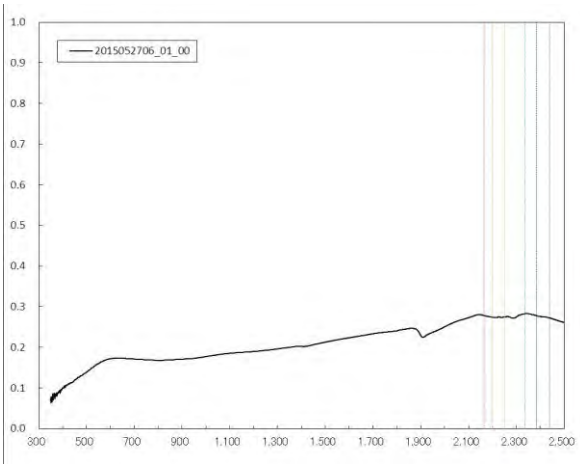

2015052706_01_00

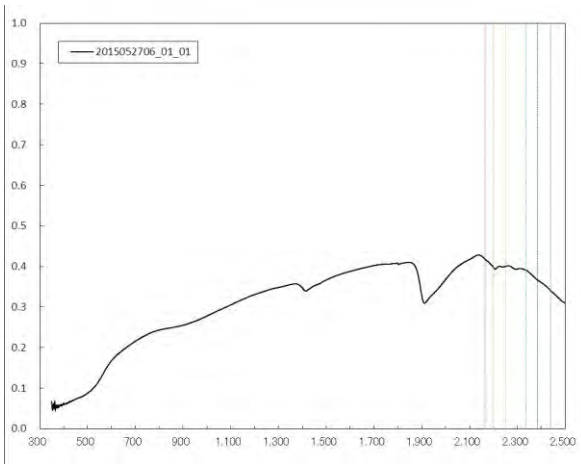

2015052706_01_01

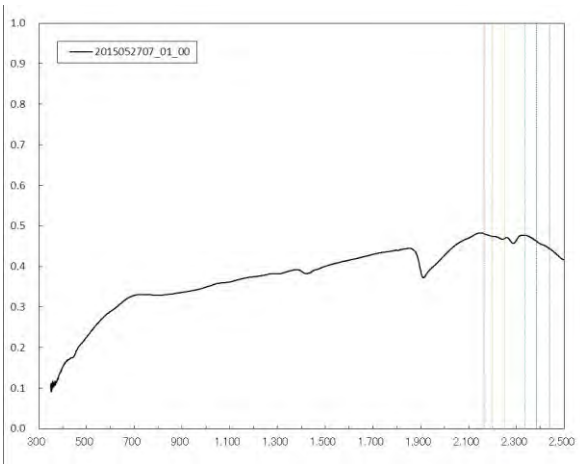

2015052707_01_00

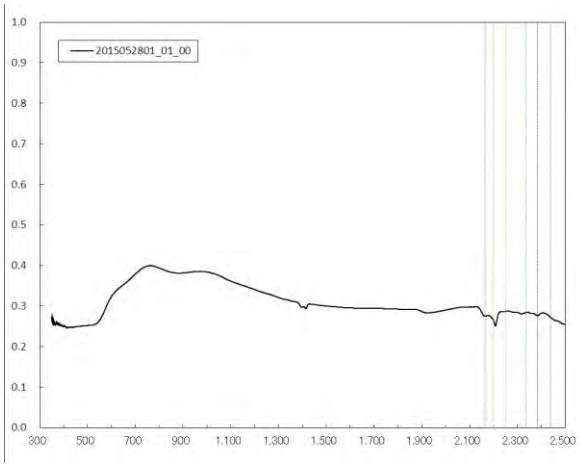

2015052801_01_00

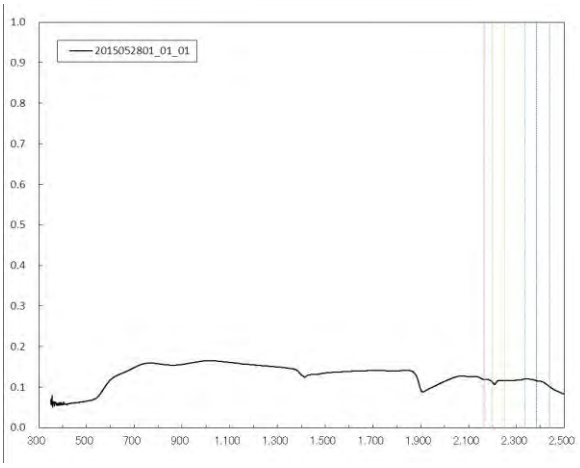

2015052801_01_01

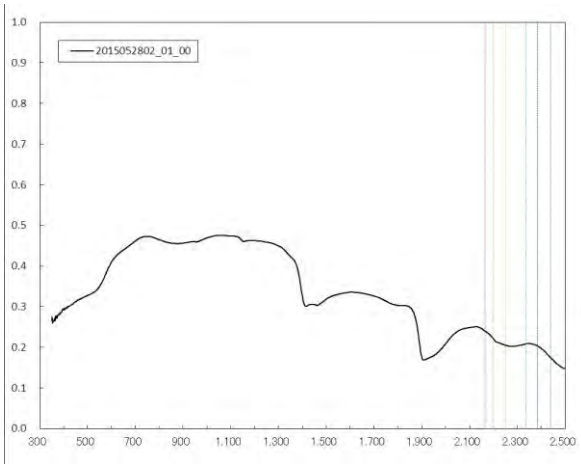

2015052802_01_00

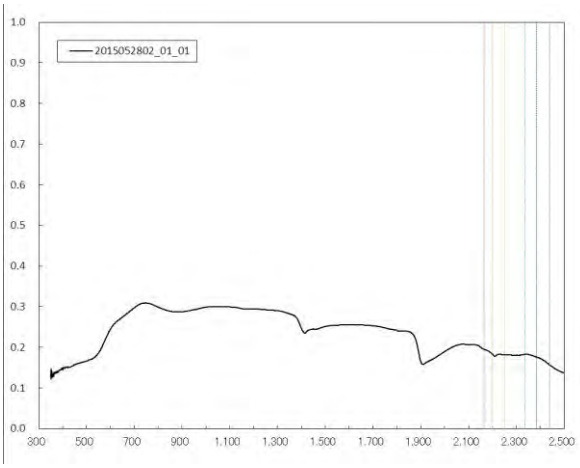

2015052802_01_01

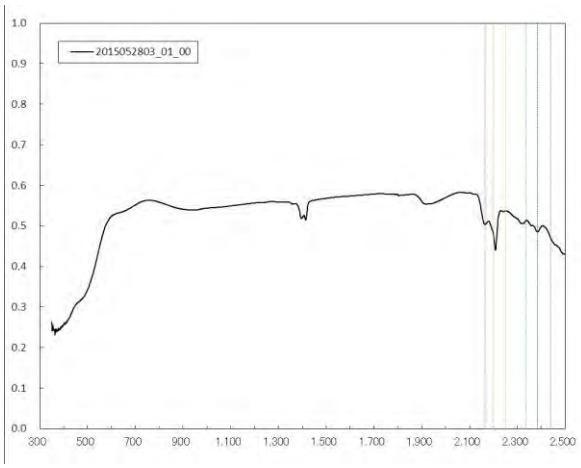

2015052803_01_00

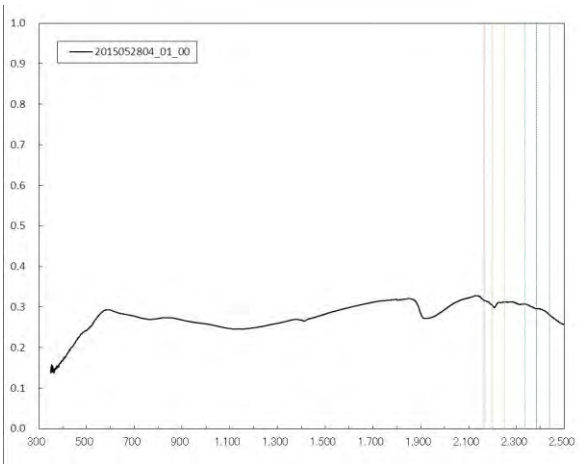

2015052804_01_00

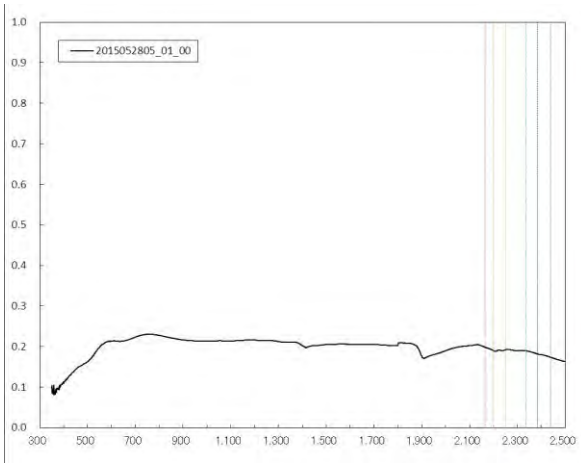

2015052805_01_00

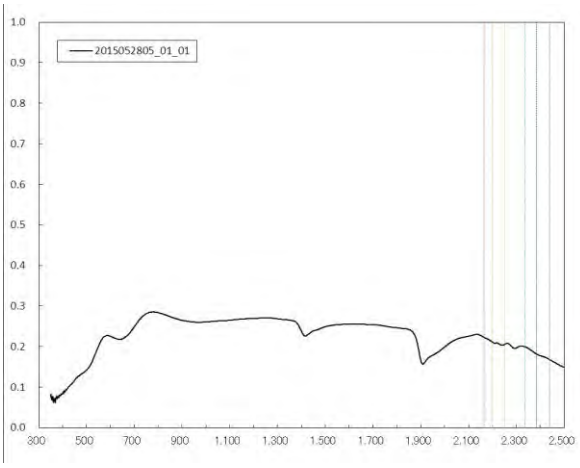

2015052805_01_01

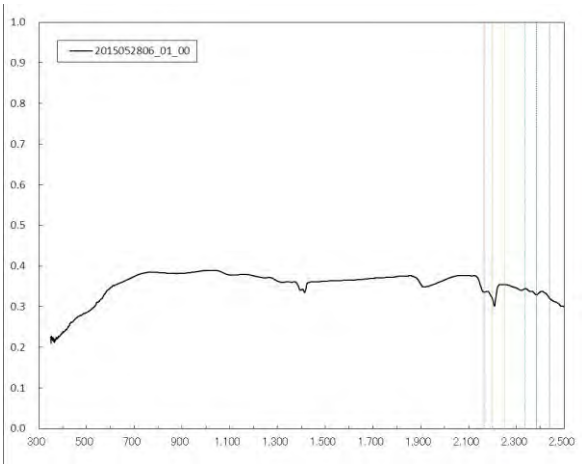

2015052806_01_00

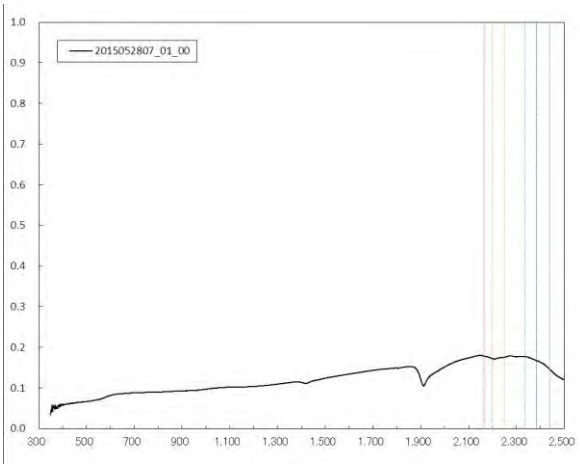

2015052807_01_00

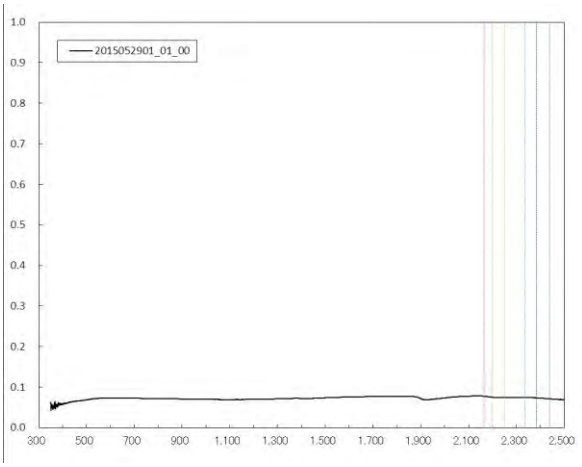

2015052901_01_00

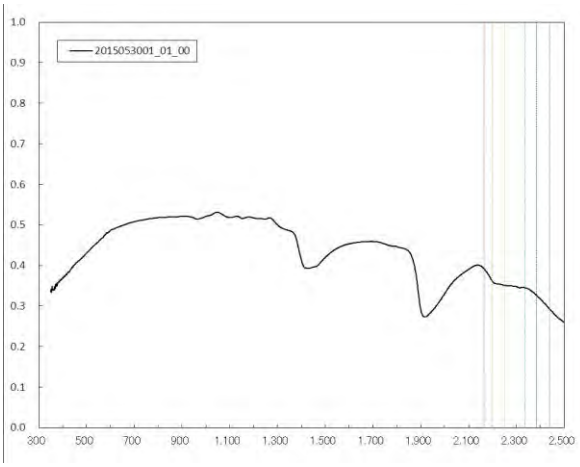

2015053001_01_00

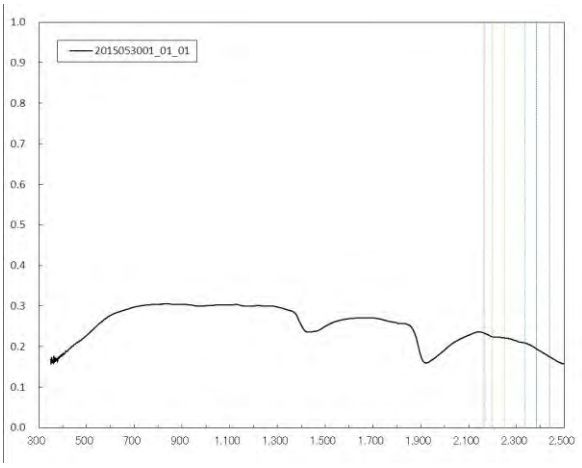

2015053001_01_01

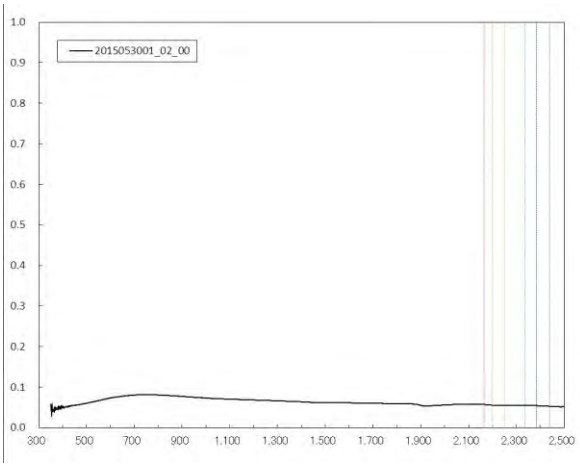

2015053001_02_00

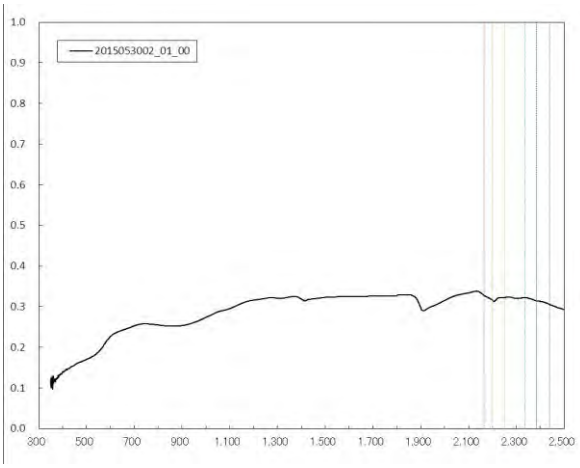

2015053002_01_00

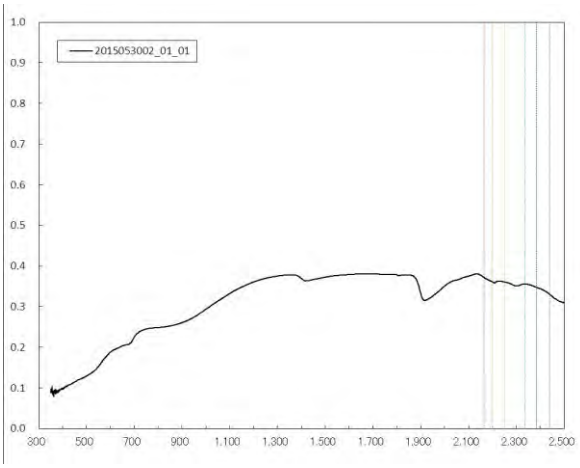

2015053002_01_01

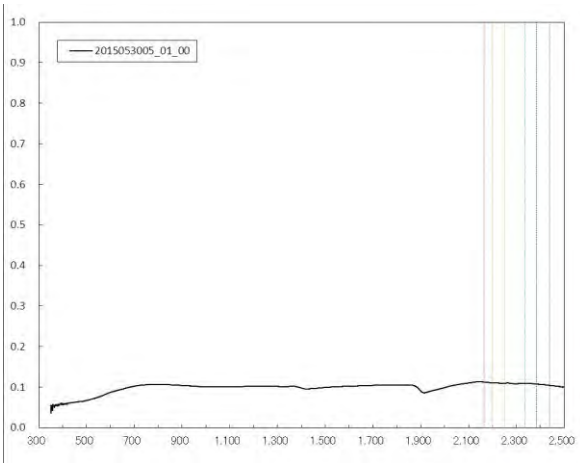

2015053005_01_00

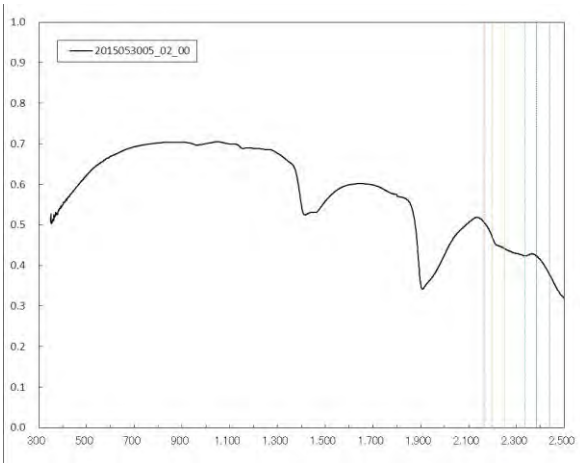

2015053005_02_00

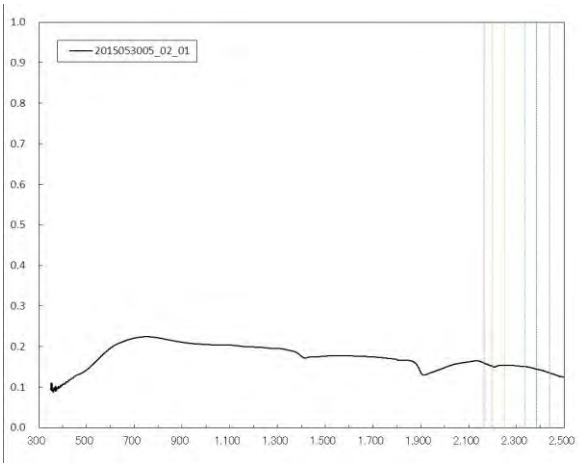

2015053005_02_01

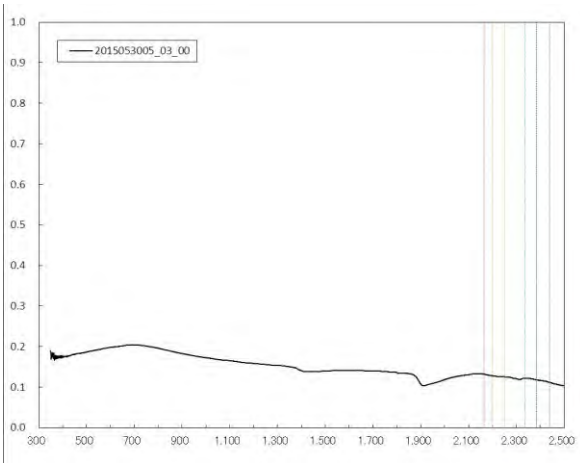

2015053005_03_00

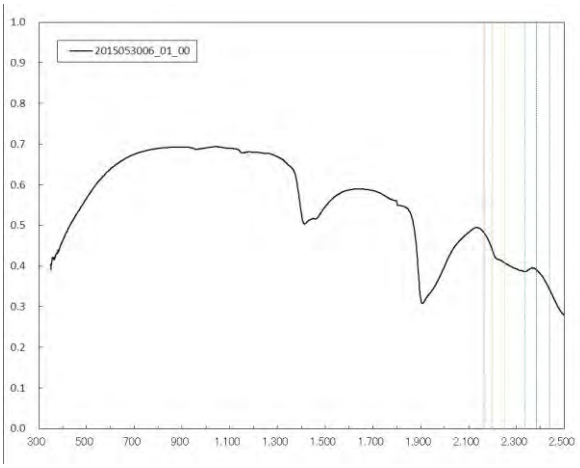

2015053006_01_00

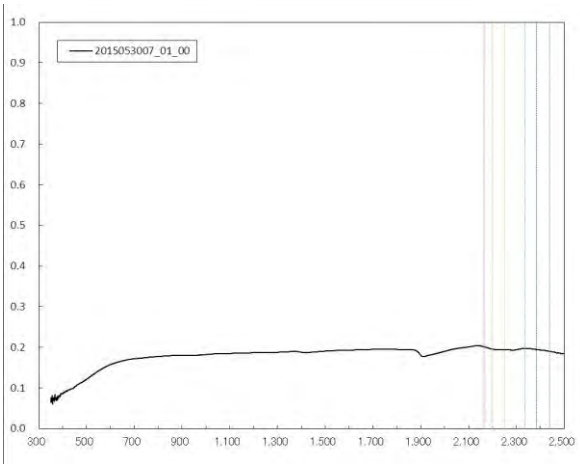

2015053007_01_00

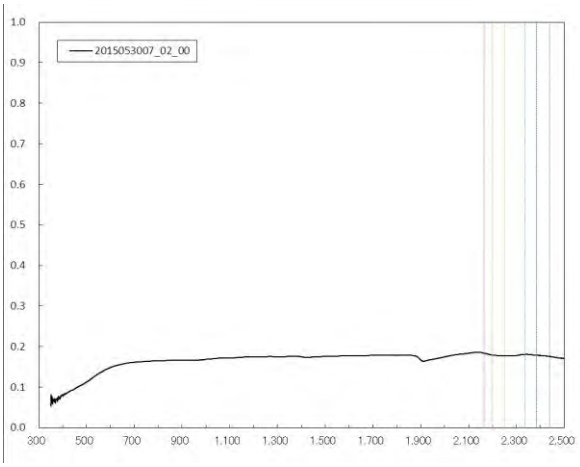

2015053007_02_00

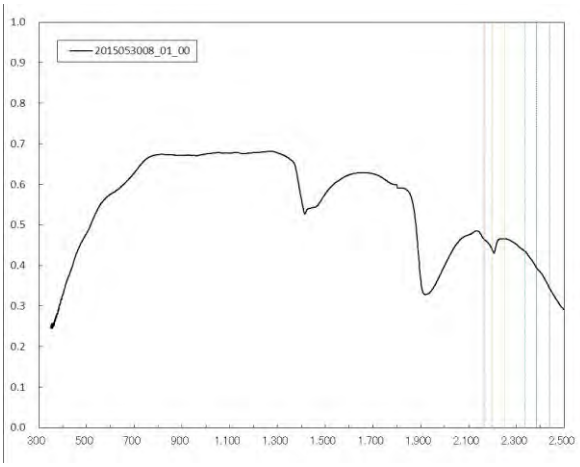

2015053008_01_00

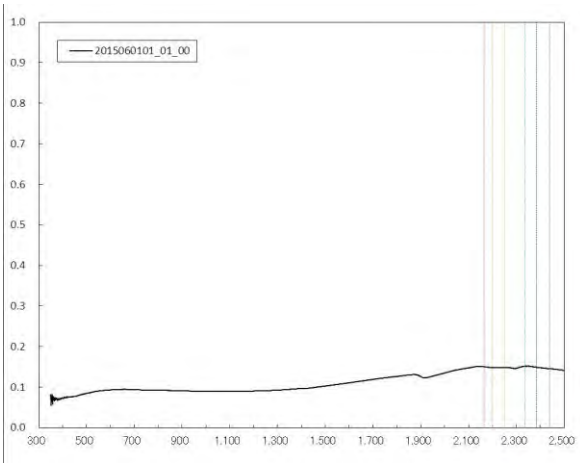

2015060101_01_00

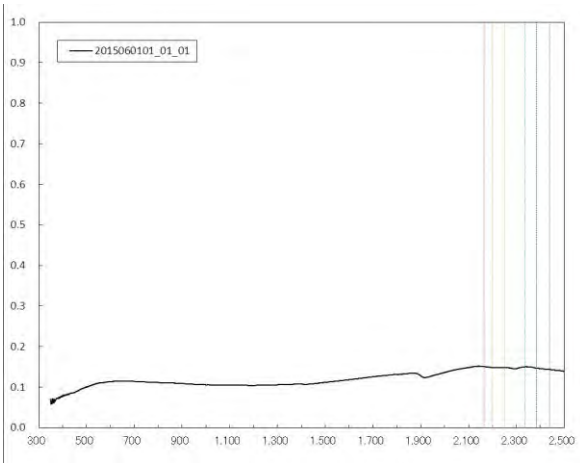

2015060101_01_01

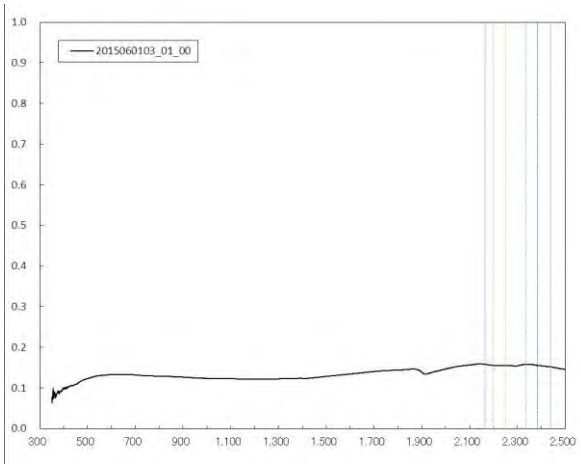

2015060103_01_00

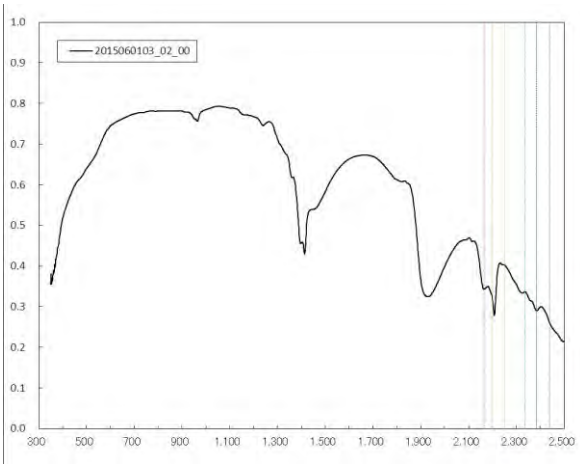

2015060103_02_00

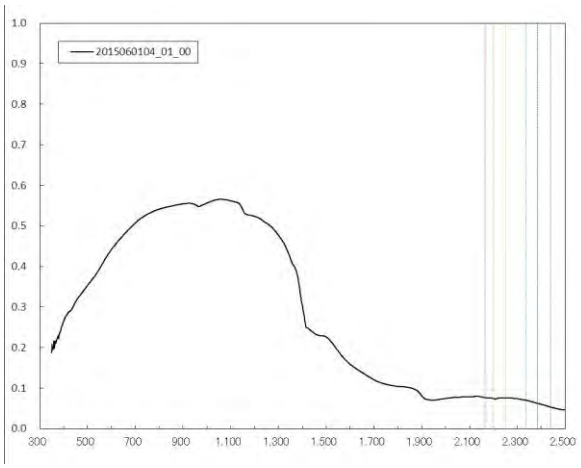

2015060104_01_00

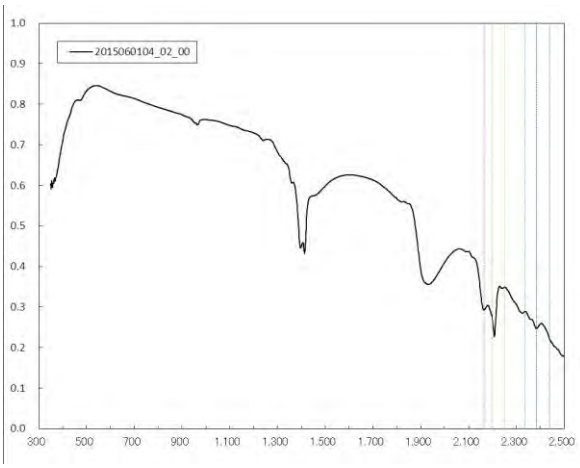

2015060104_02_00

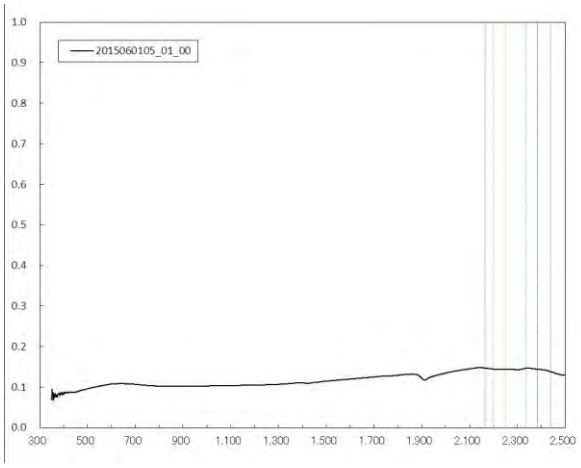

2015060105_01_00

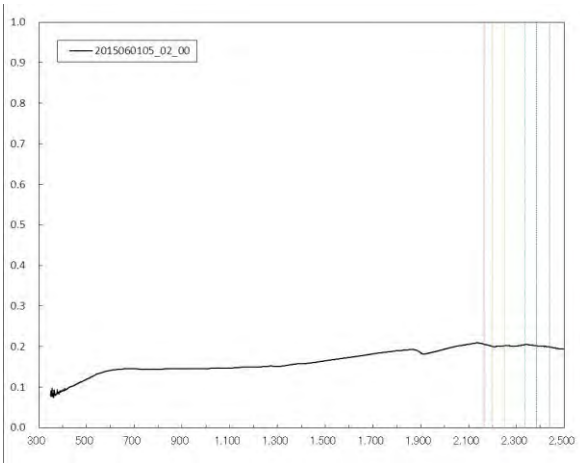

2015060105_02_00

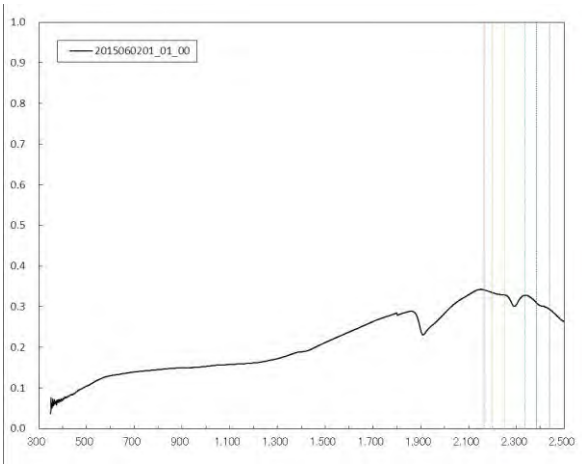

2015060201_01_00

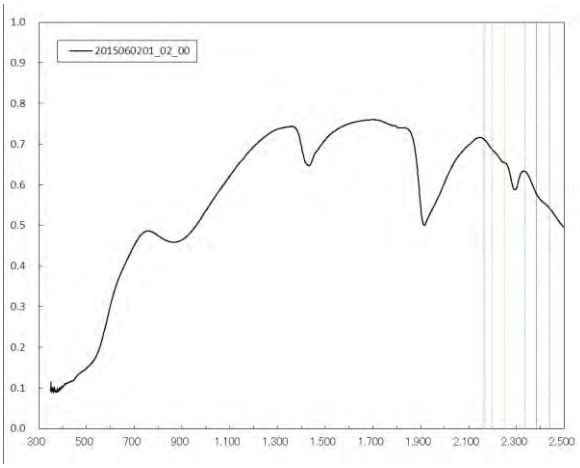

2015060201_02_00

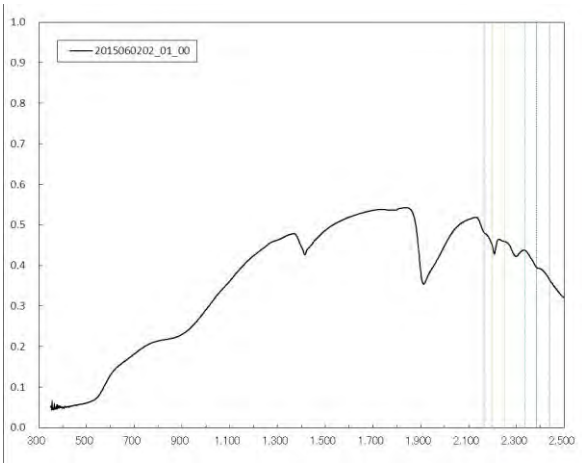

2015060202_01_00

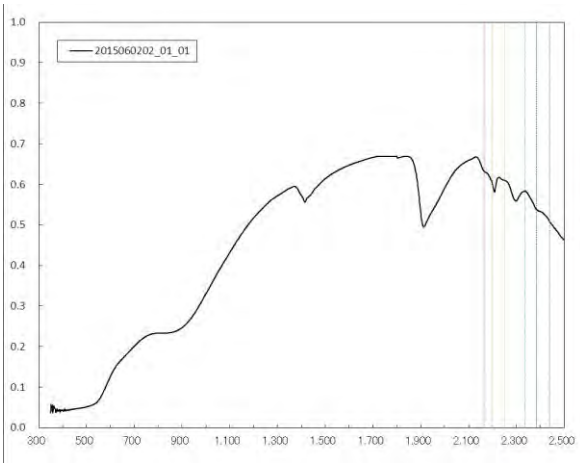

2015060202_01_01

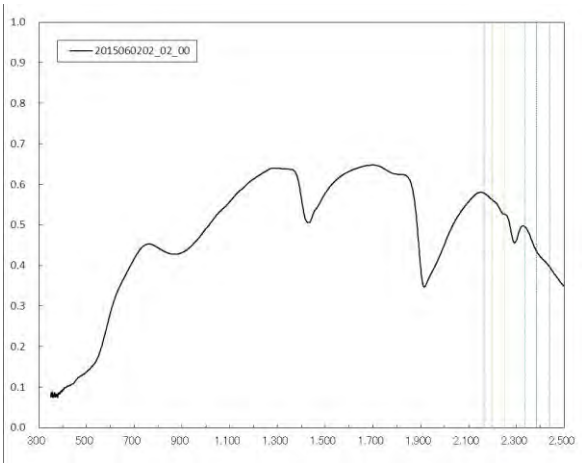

2015060202_02_00

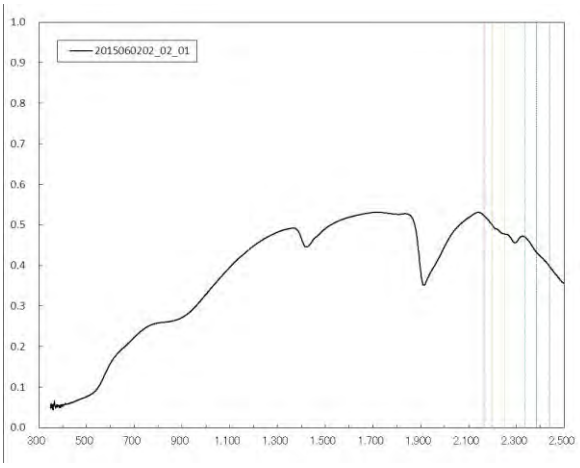

2015060202_02_01

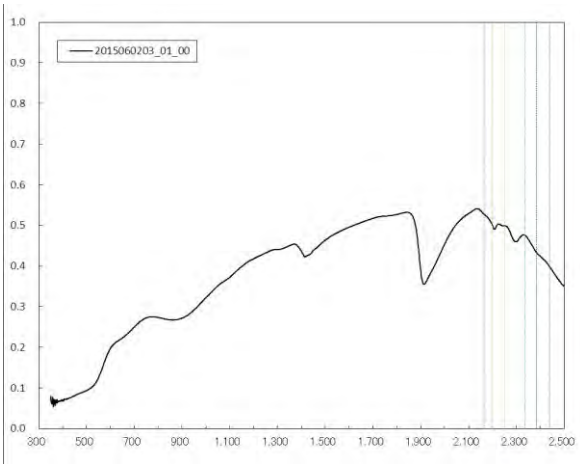

2015060203_01_00

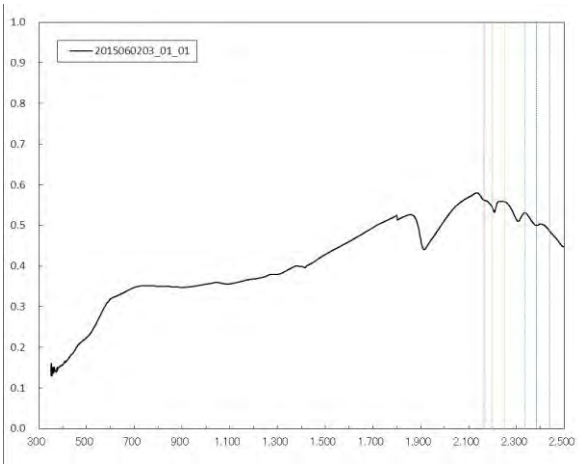

2015060203_01_01

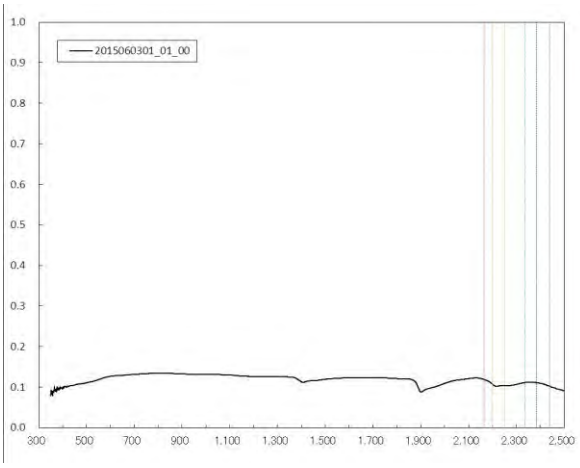

2015060301_01_00

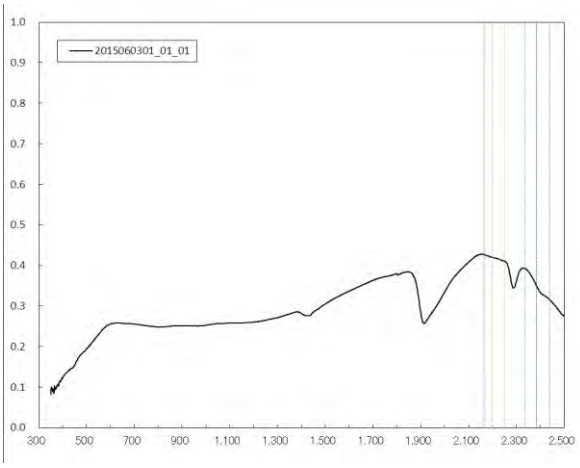

2015060301_01_01

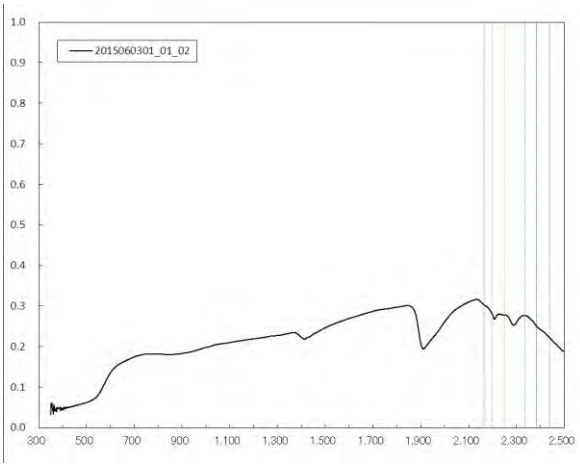

2015060301_01_02

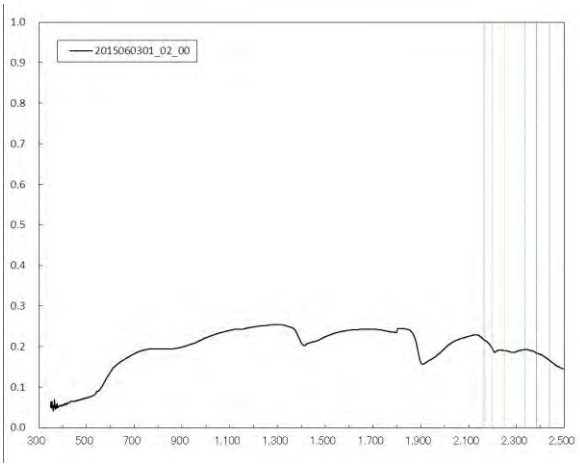

2015060301_02_00

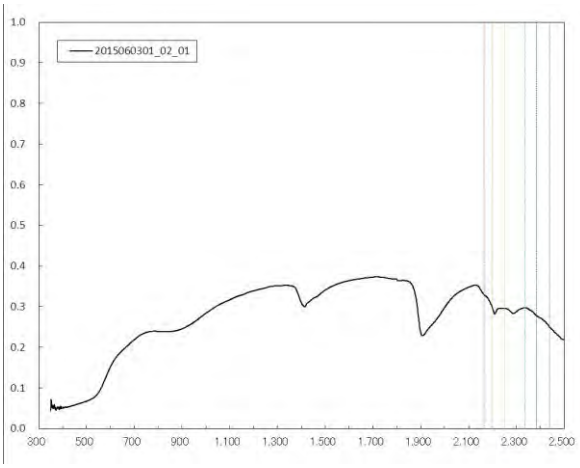

2015060301_02_01

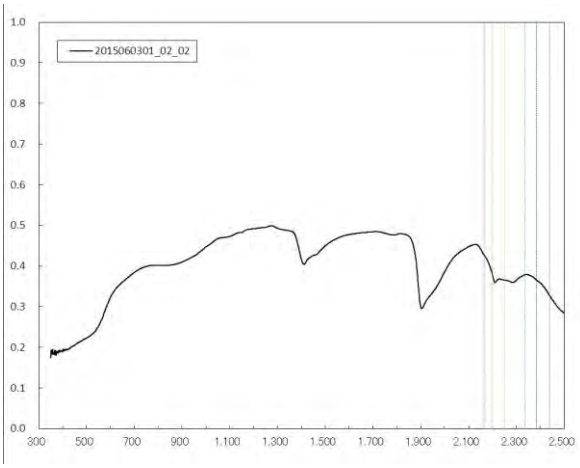

2015060301_02_02

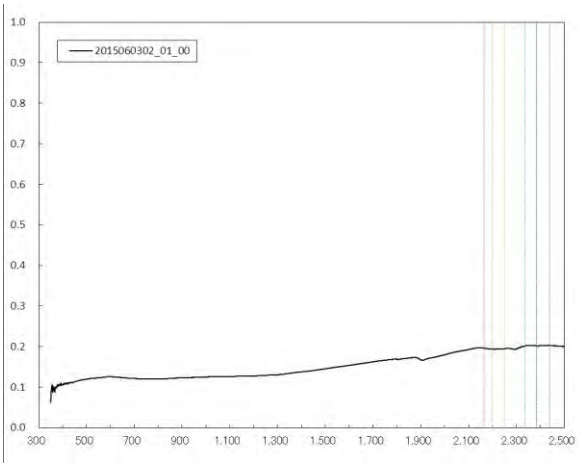

2015060302_01_00

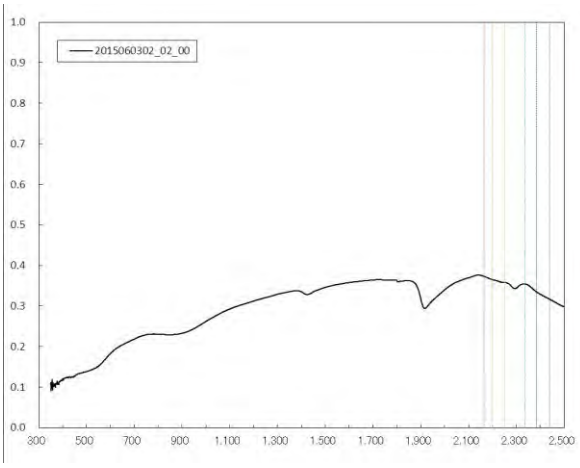

2015060302_02_00

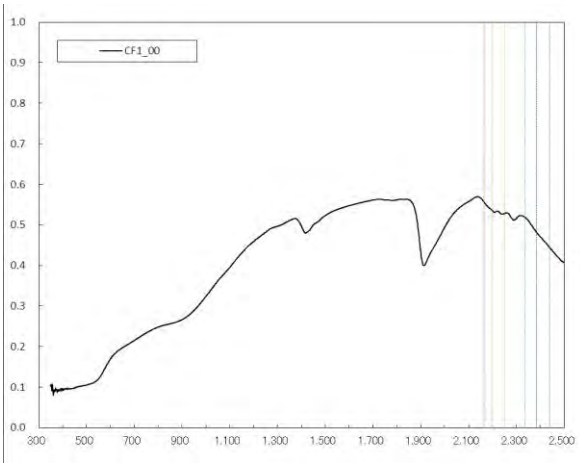

CF1_00

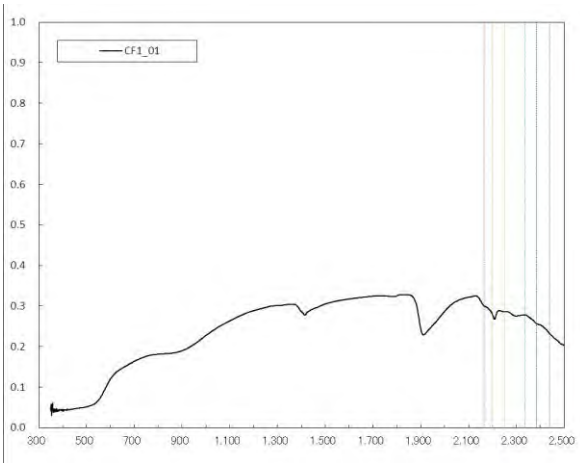

CF1_01

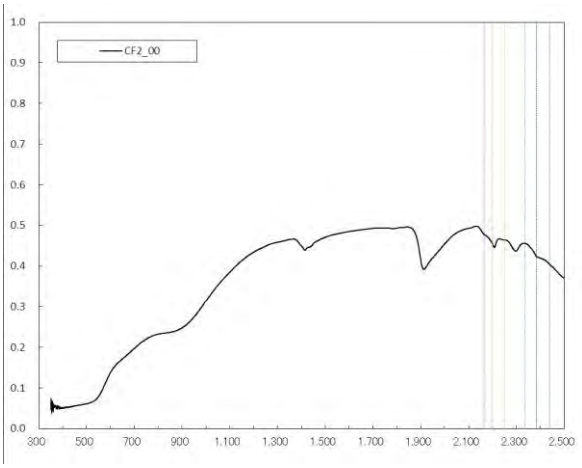

CF2_00

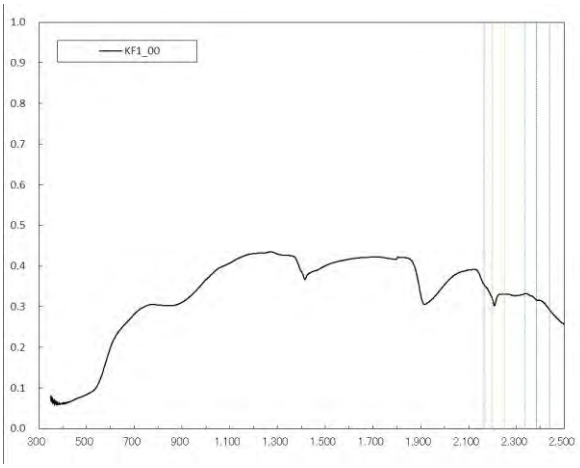

KF1_00

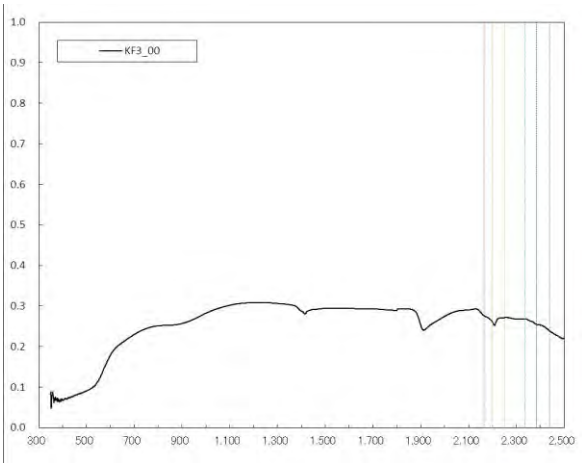

KF3_00

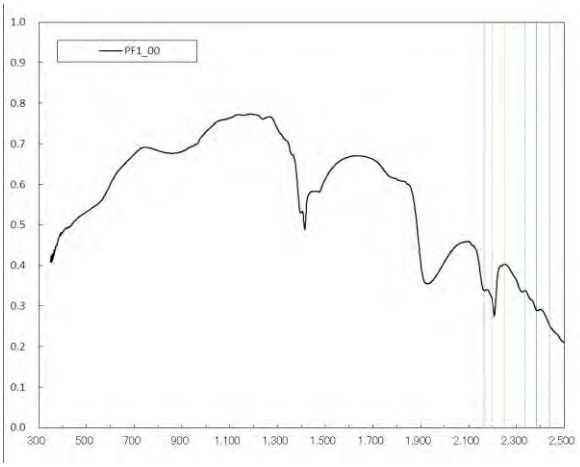

PF1_00

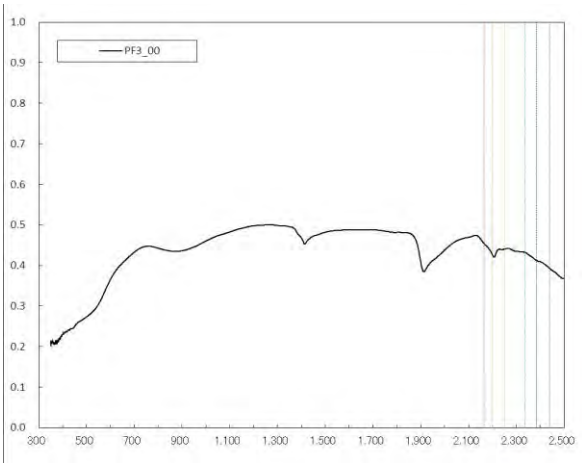

PF3_00

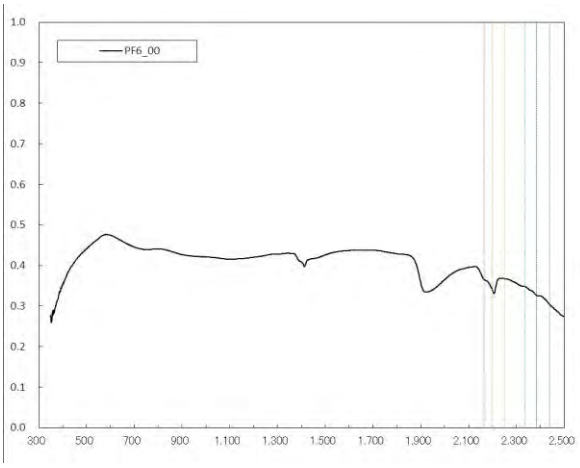

PF6_00

APPENDIX

5. Geochemical Diagrams for Each Geothermal Fields

Arus

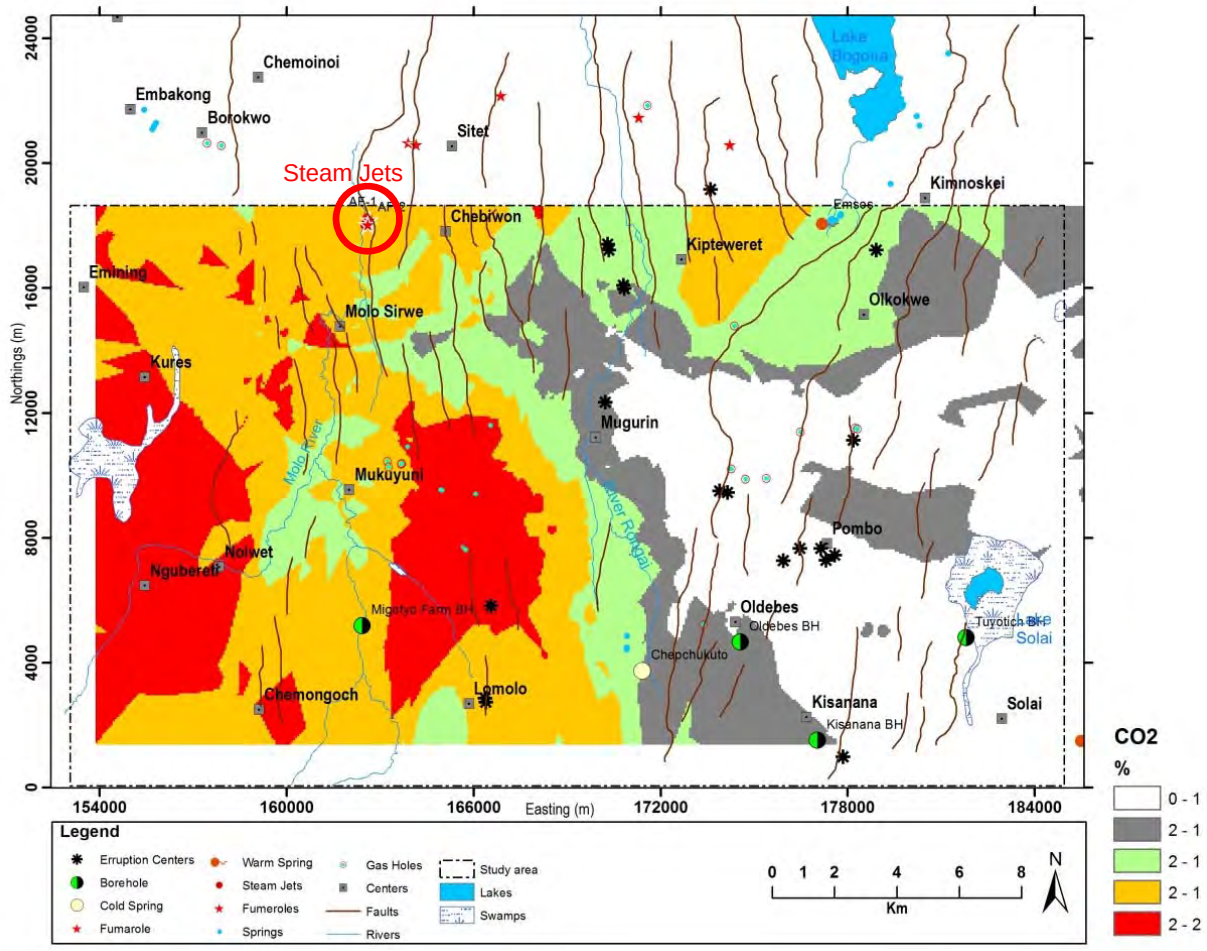

Location map of springs, boreholes and fumaroles (modified from GDC (2013))

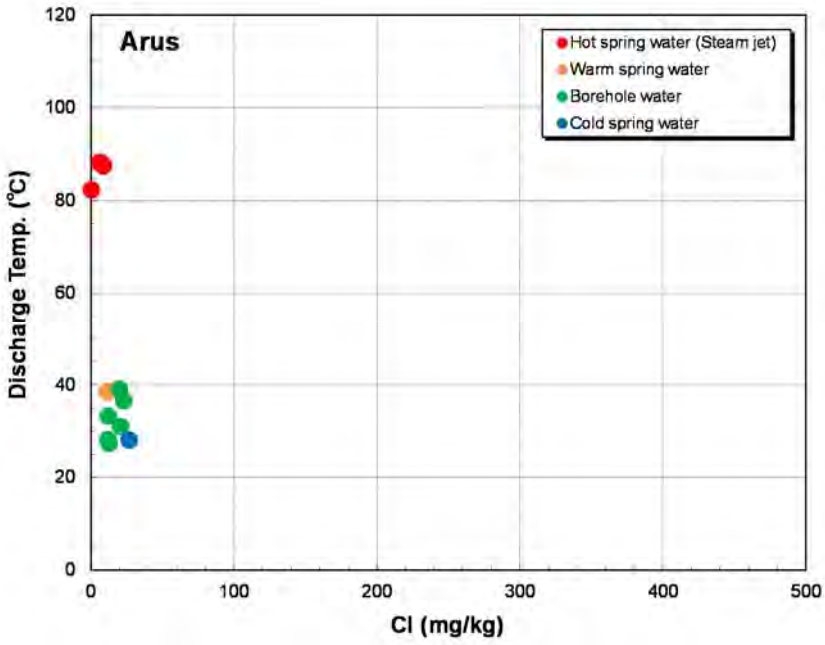

Plot of measured discharge temperature vs. Cl concentration for spring and borehole water

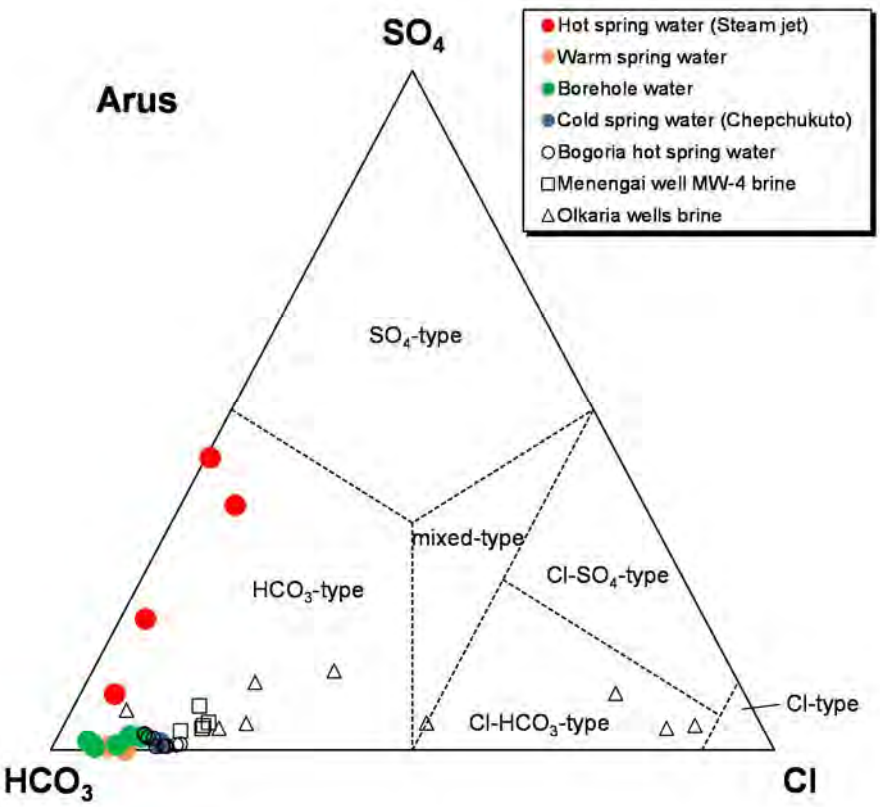

Ternary plot of major anion composition for spring and borehole water

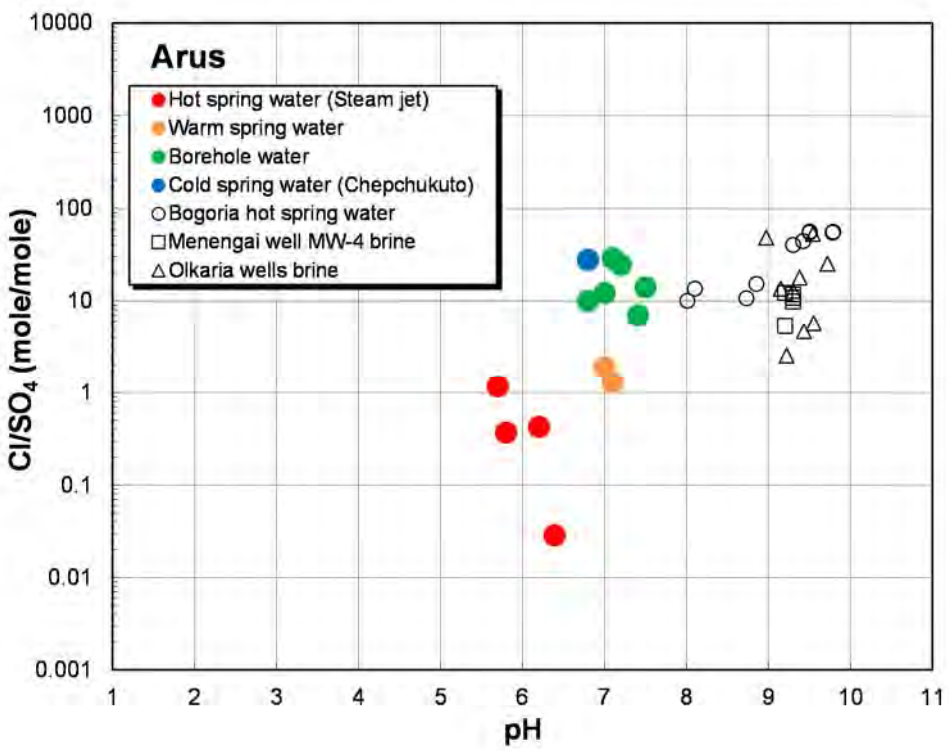

Plot of Cl/SO_4 ratio vs. pH for spring and borehole water

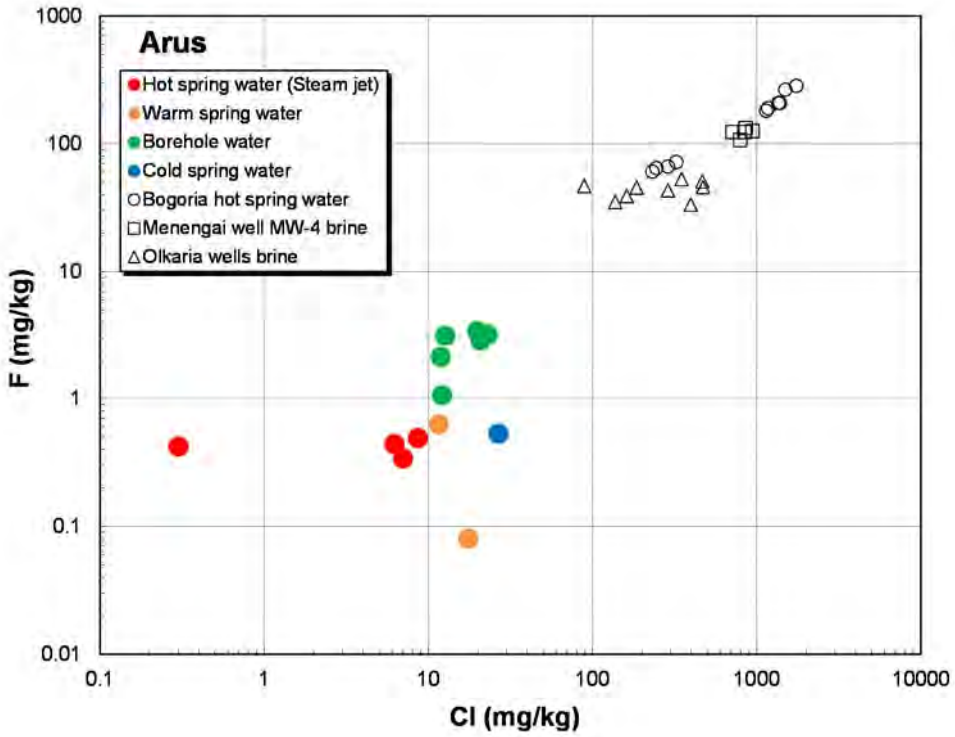

Plot of F vs. Cl concentration for spring and borehole water

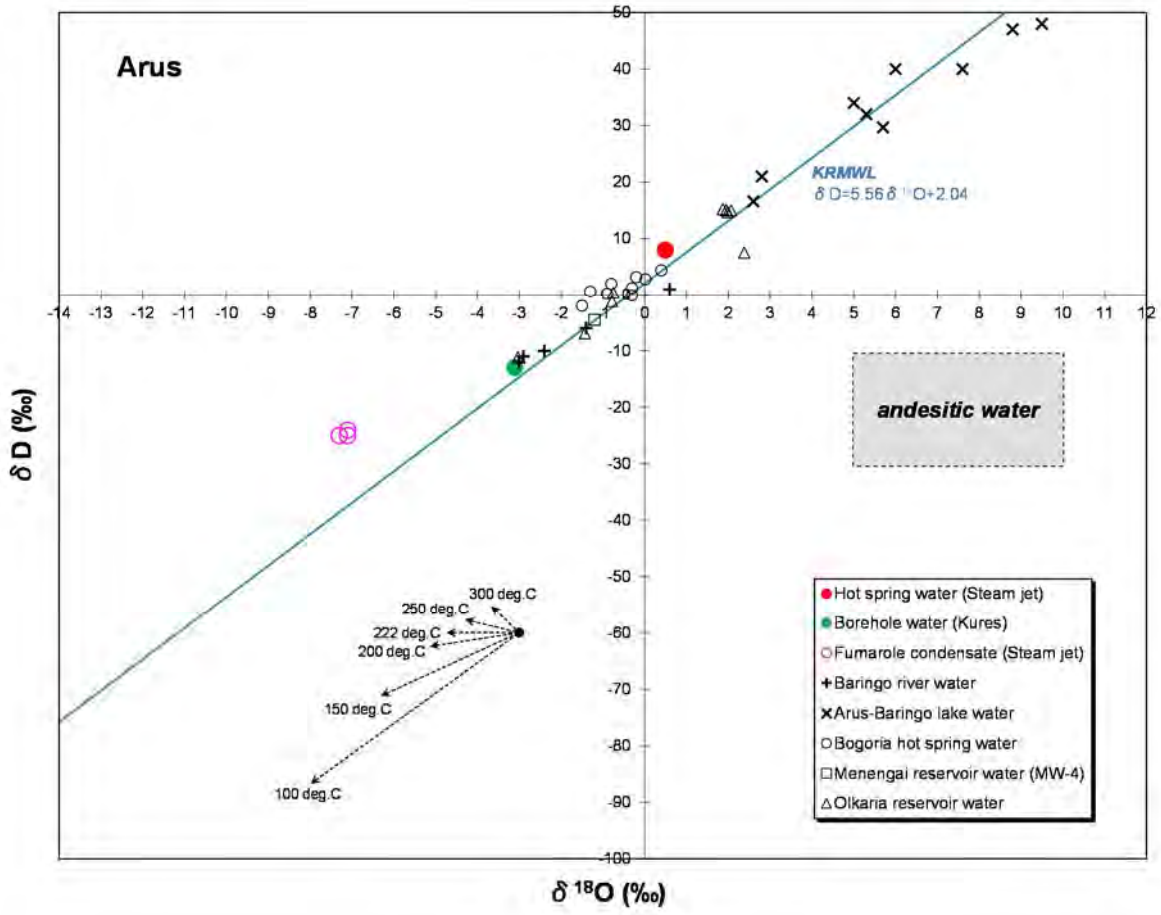

Hydrogen and oxygen isotopic composition

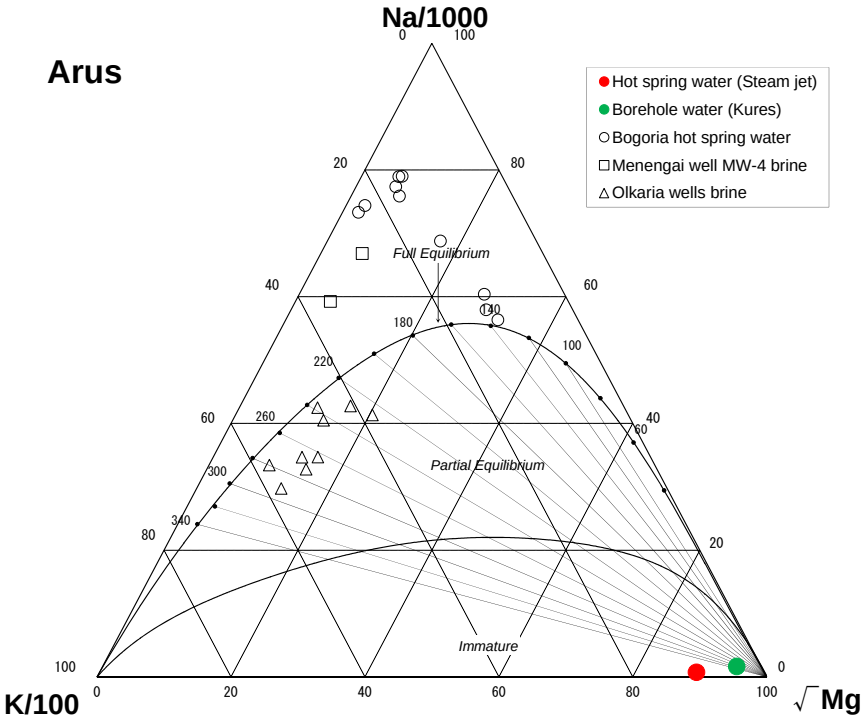

Ternary plot of Na-K-Mg composition for spring and borehole water

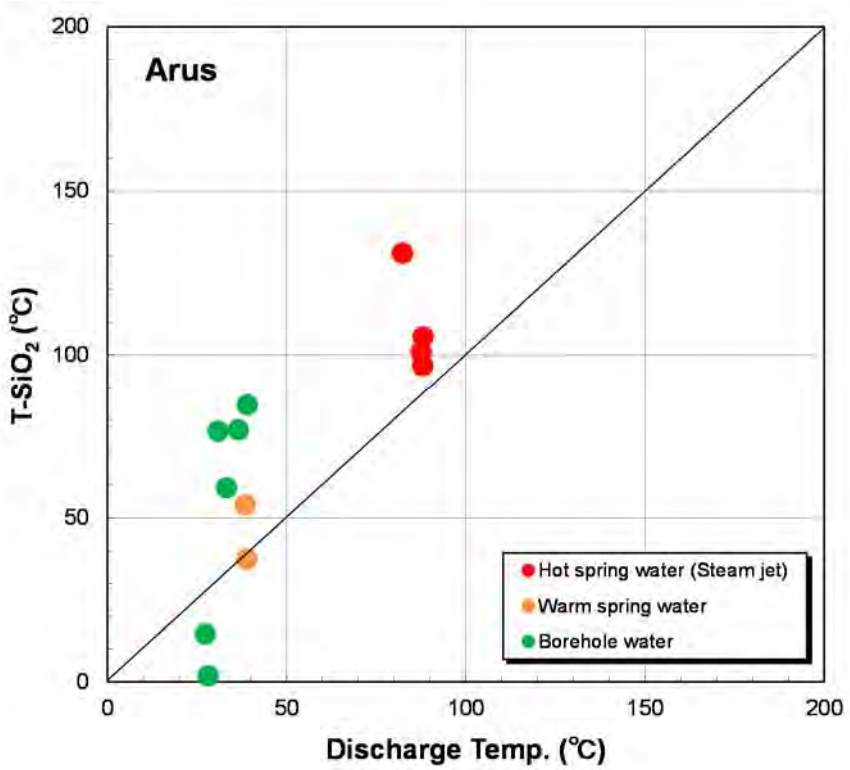

Comparison of measured discharge temperature and calculated silica temperature for spring and borehole water

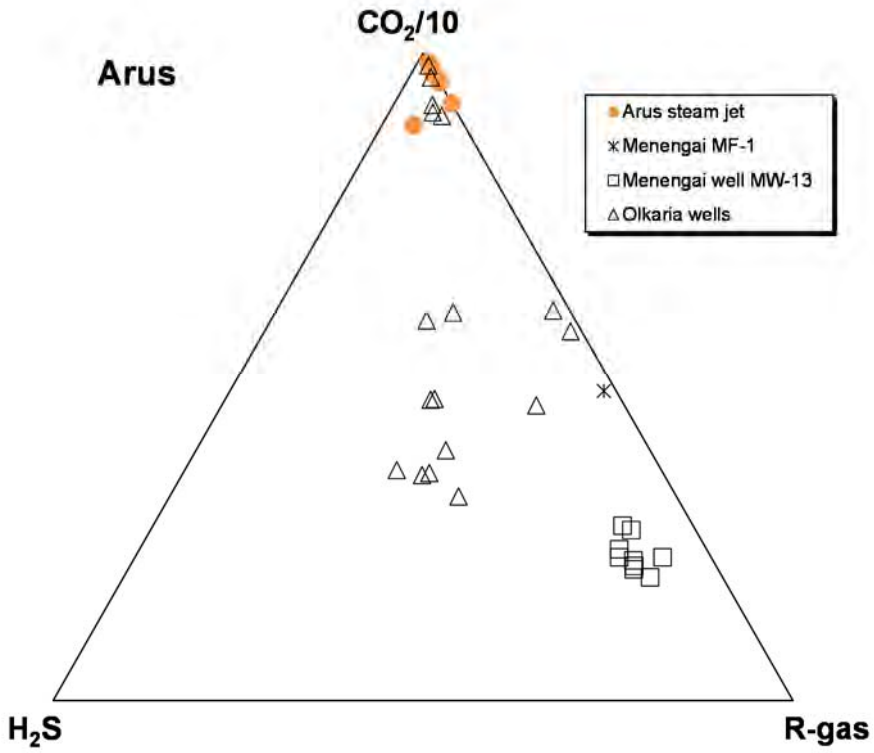

Ternary plot of major gas chemistry for geothermal gases

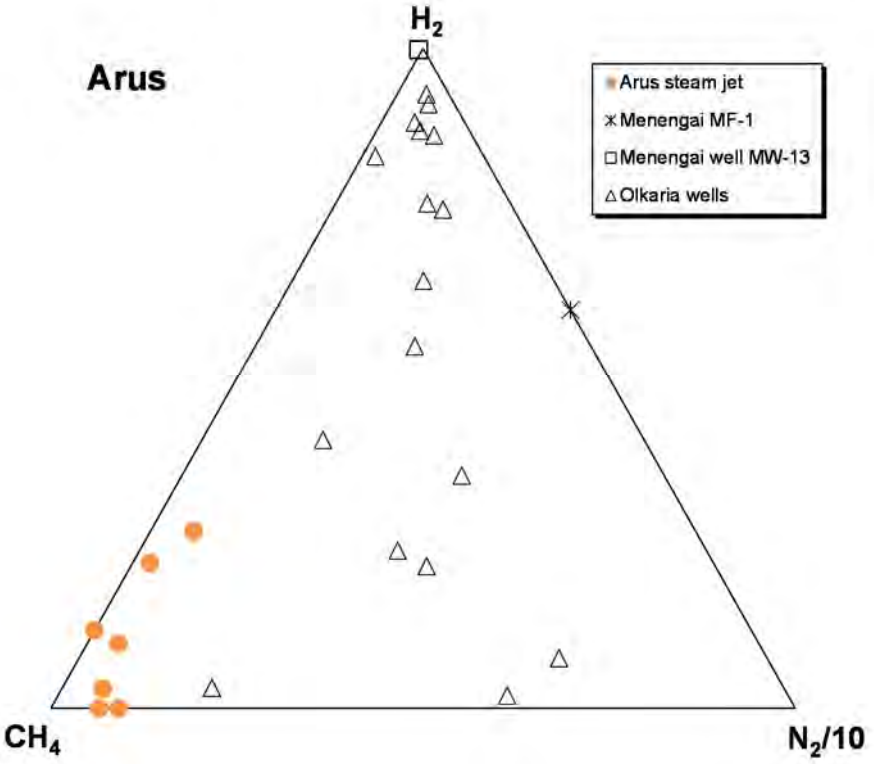

Ternary plot of minor gas chemistry for geothermal gases

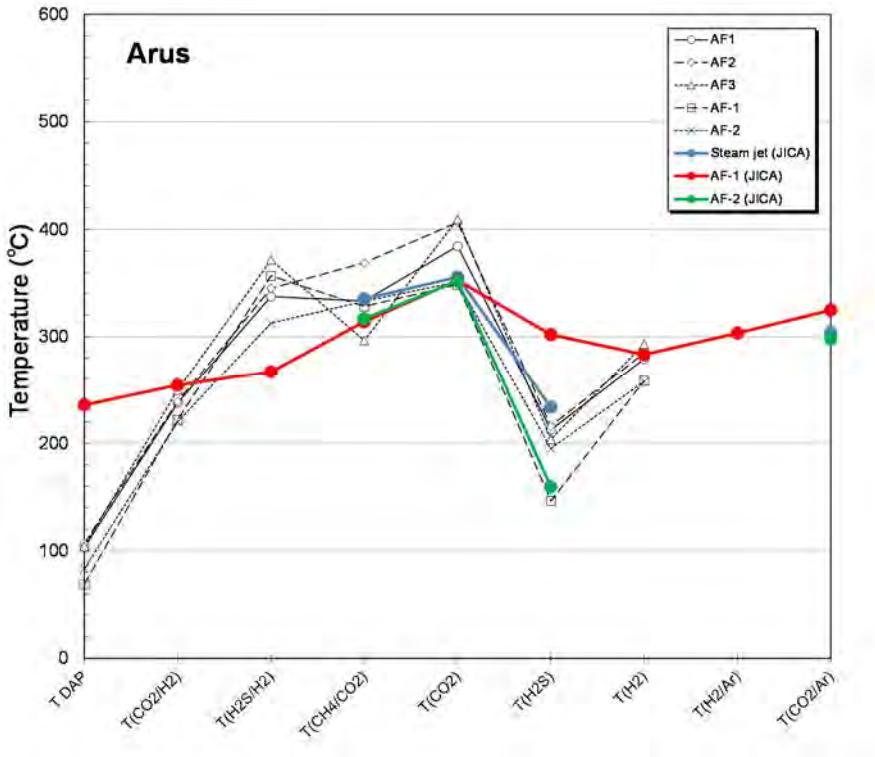

Comparison of gas chemical temperatures for fumarolic gases

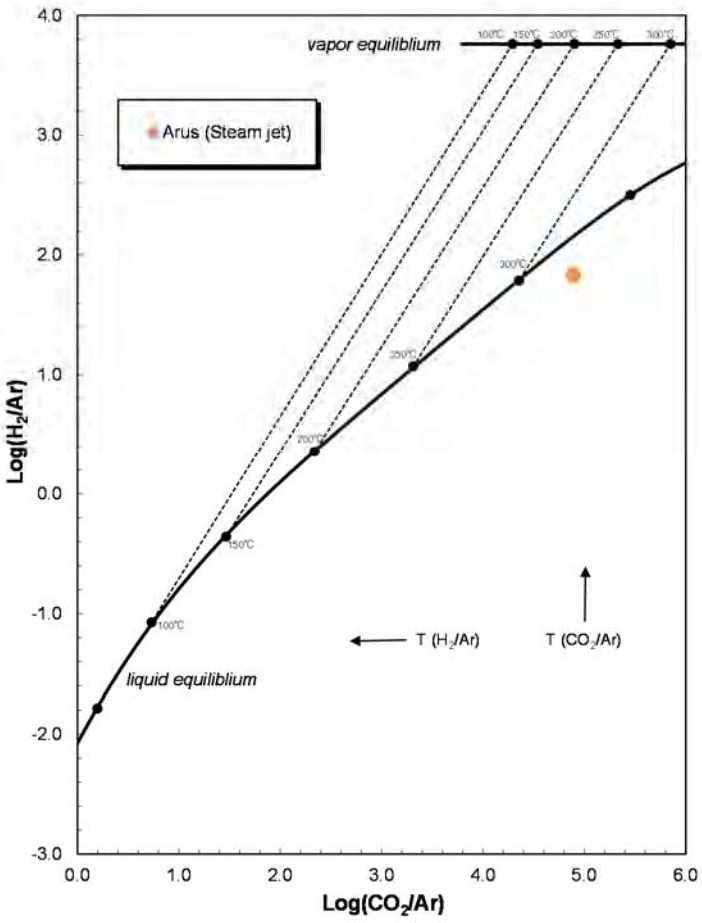

Plot of H_2/Ar vs. CO_2/Ar for fumarolic gas

Baringo

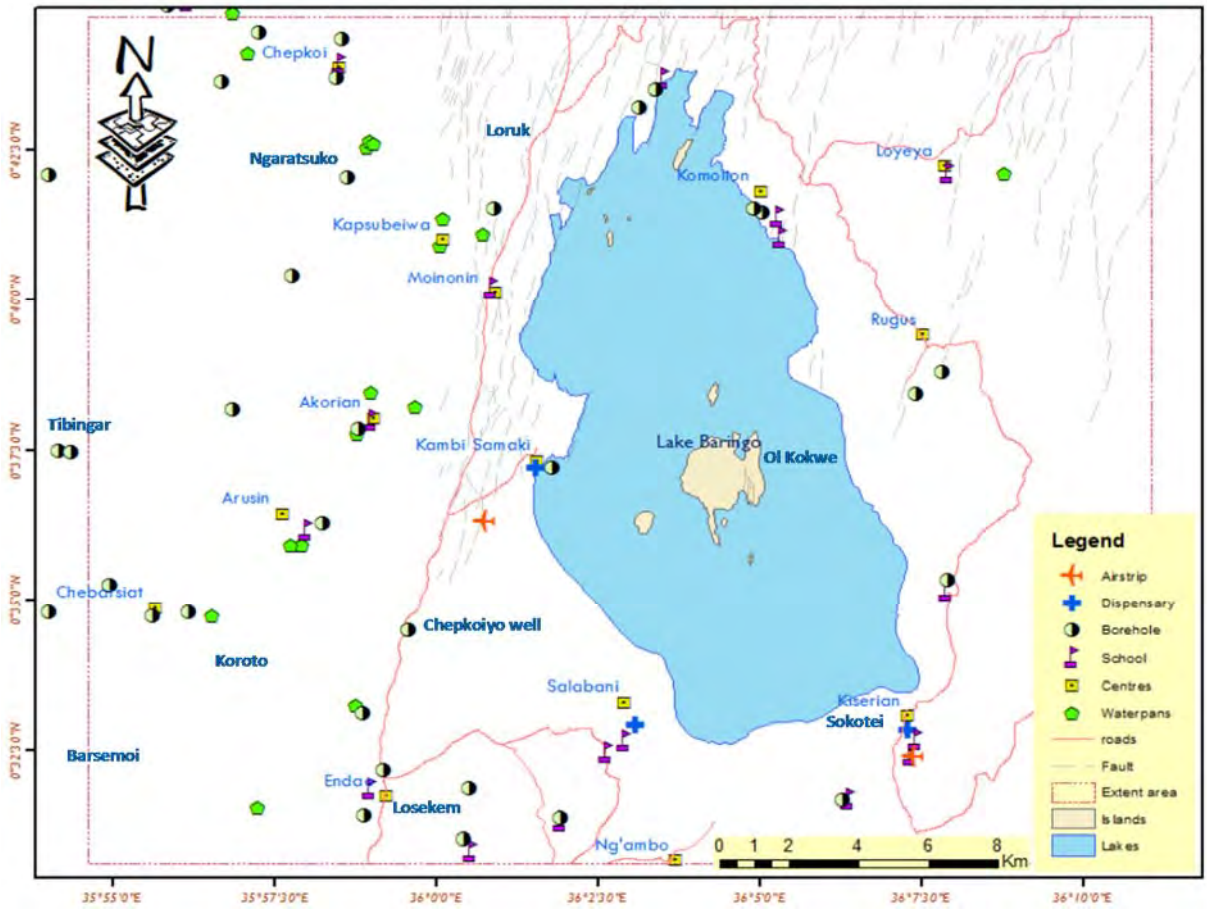

Location map of boreholes (modified from GDC (2011))

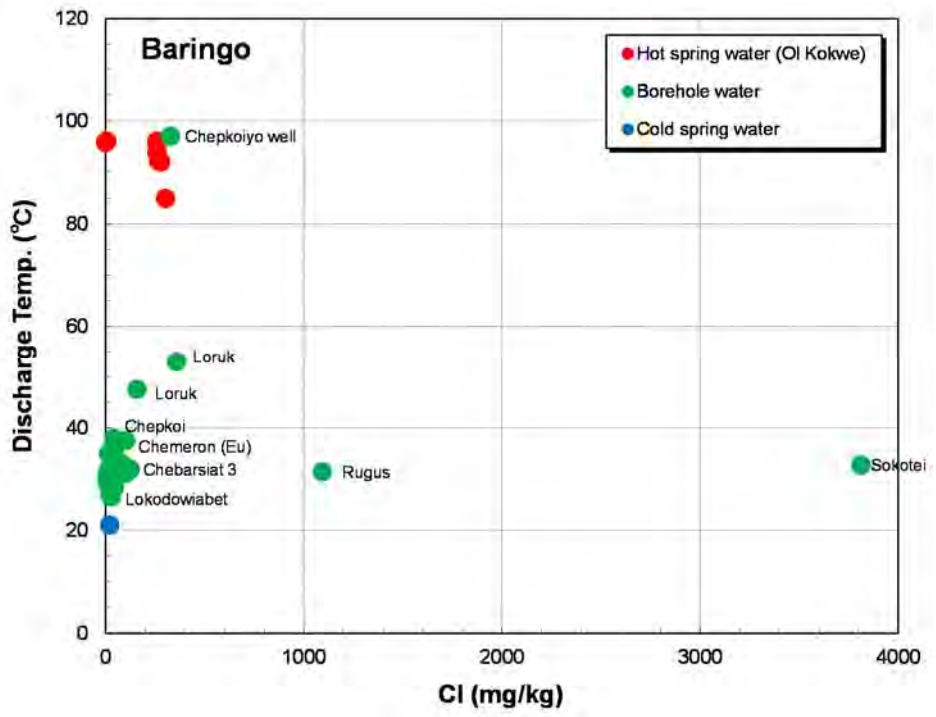

Plot of measured discharge temperature vs. Cl concentration for spring and borehole water

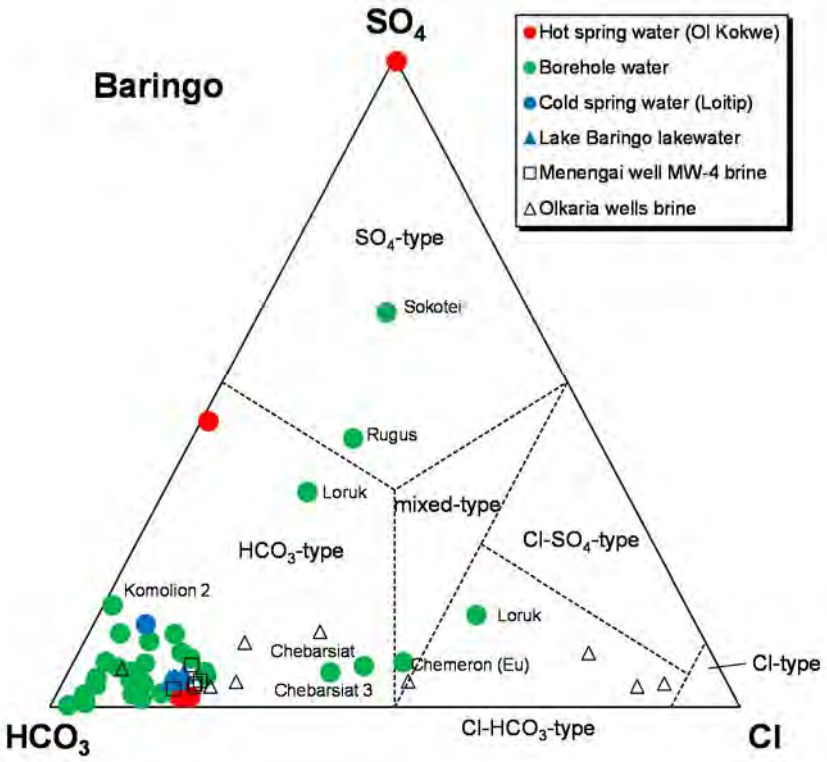

Ternary plot of major anion composition for spring and borehole water

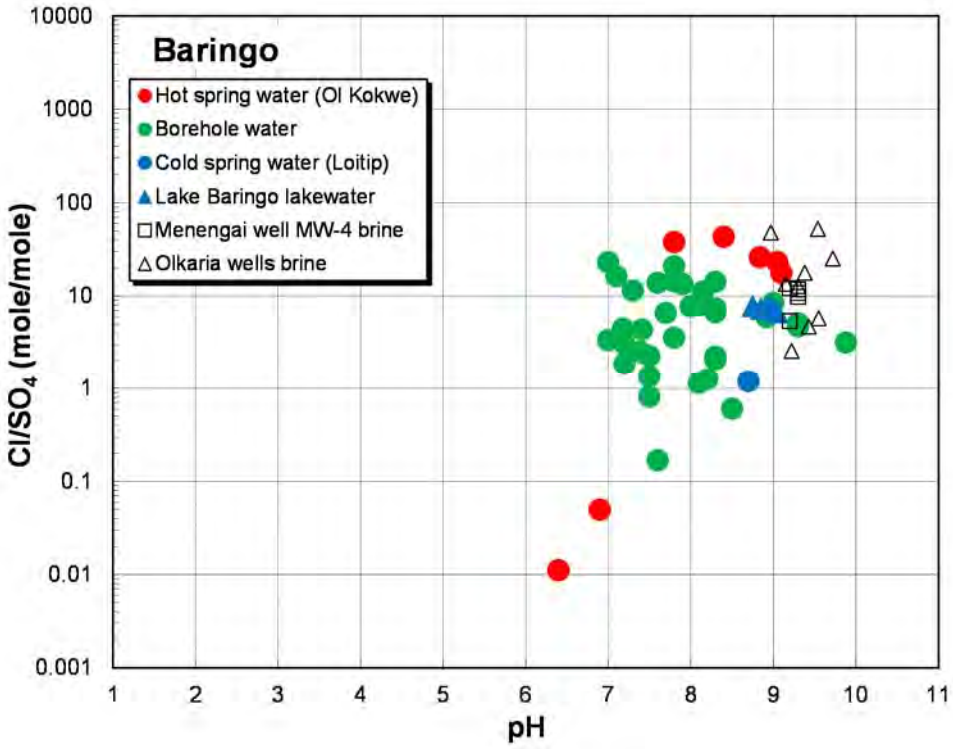

Plot of Cl/SO_4 ratio vs. pH for spring and borehole water

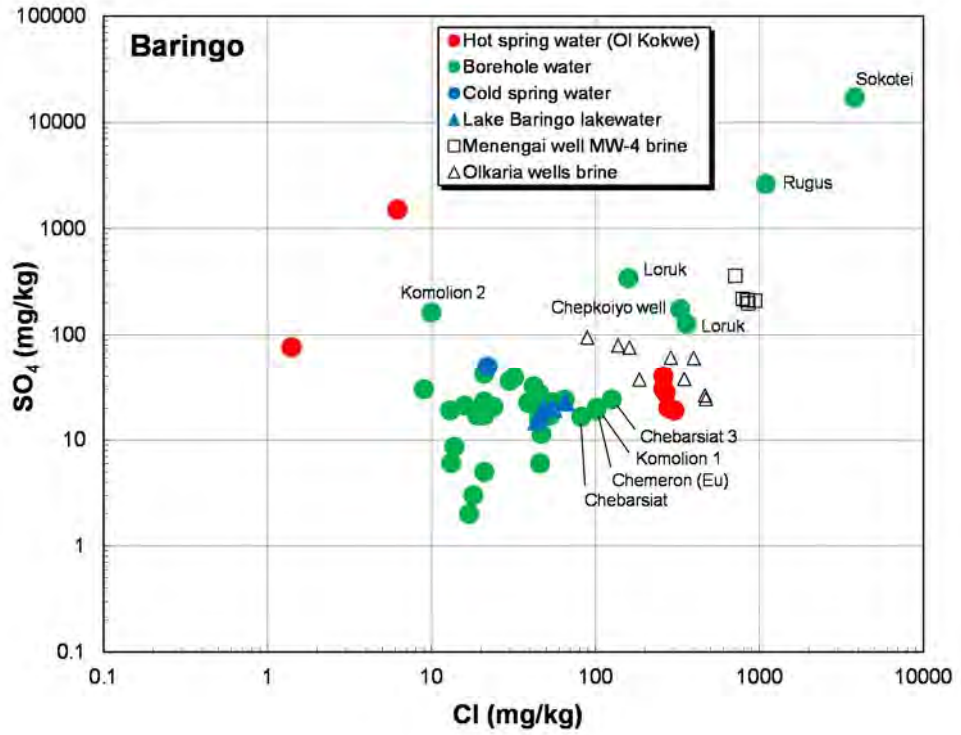

Plot of SO_4 vs. Cl concentration for spring and borehole water

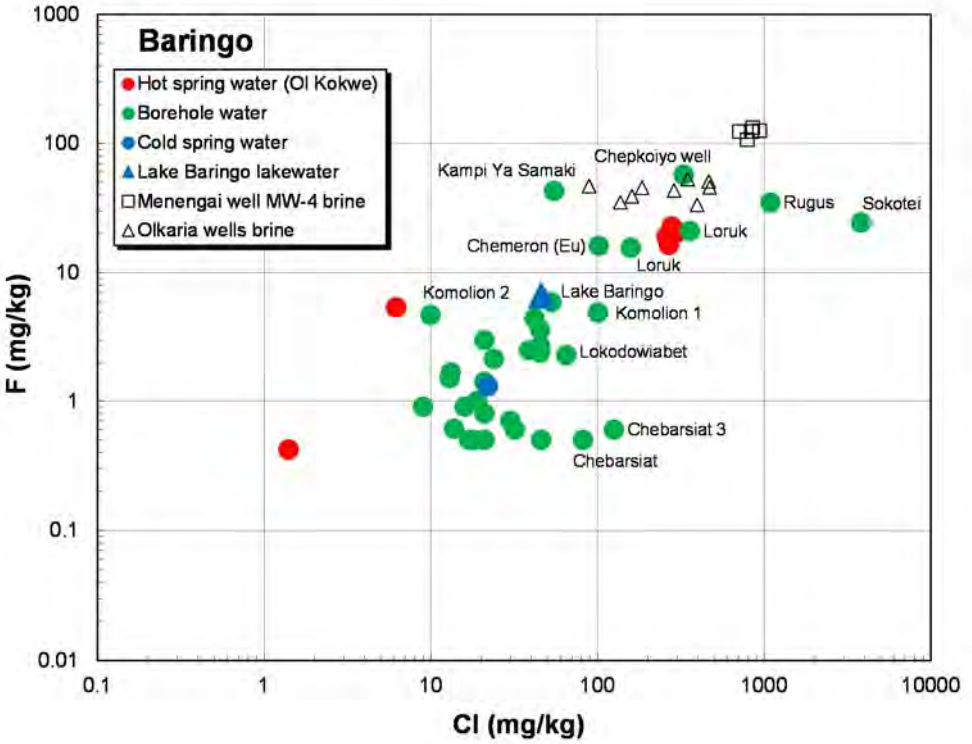

Plot of F vs. Cl concentration for spring and borehole water

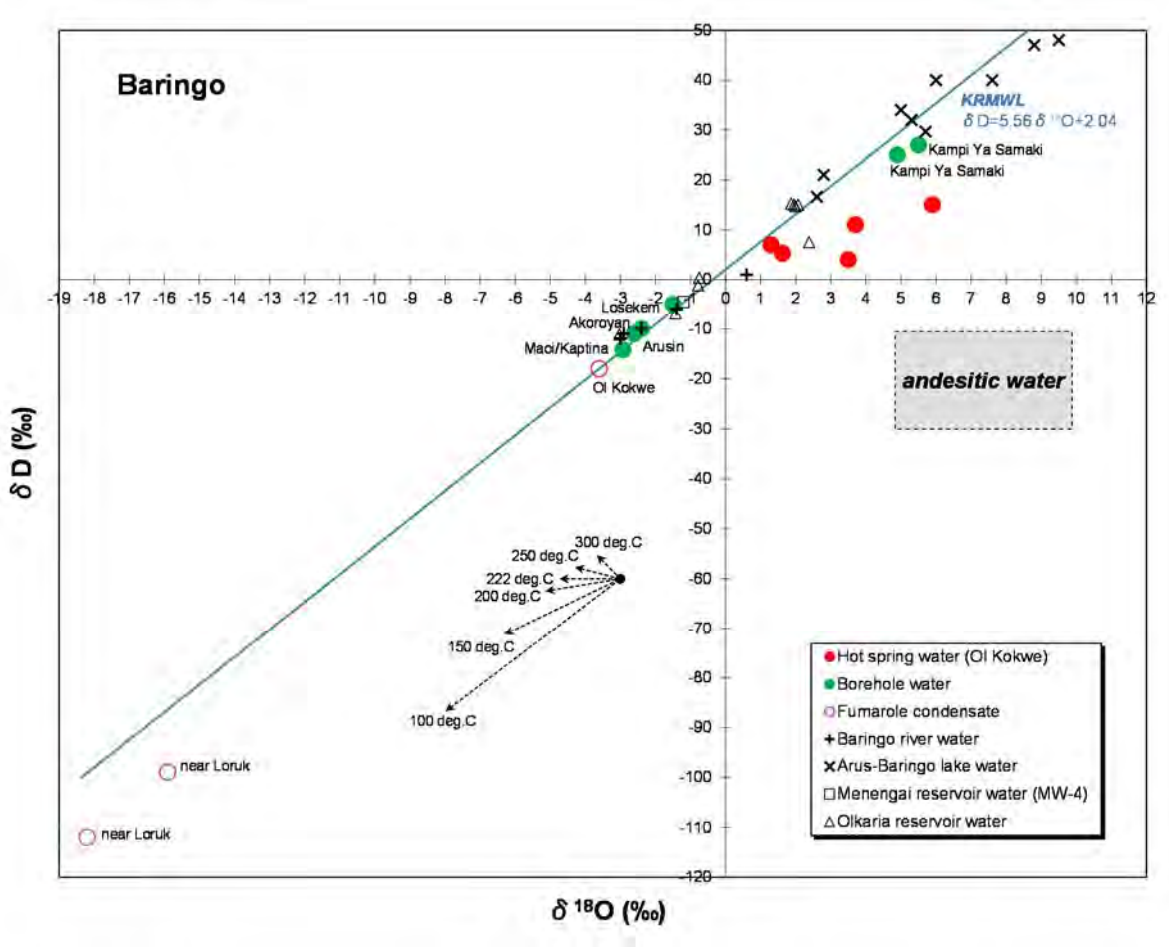

Hydrogen and oxygen isotopic composition

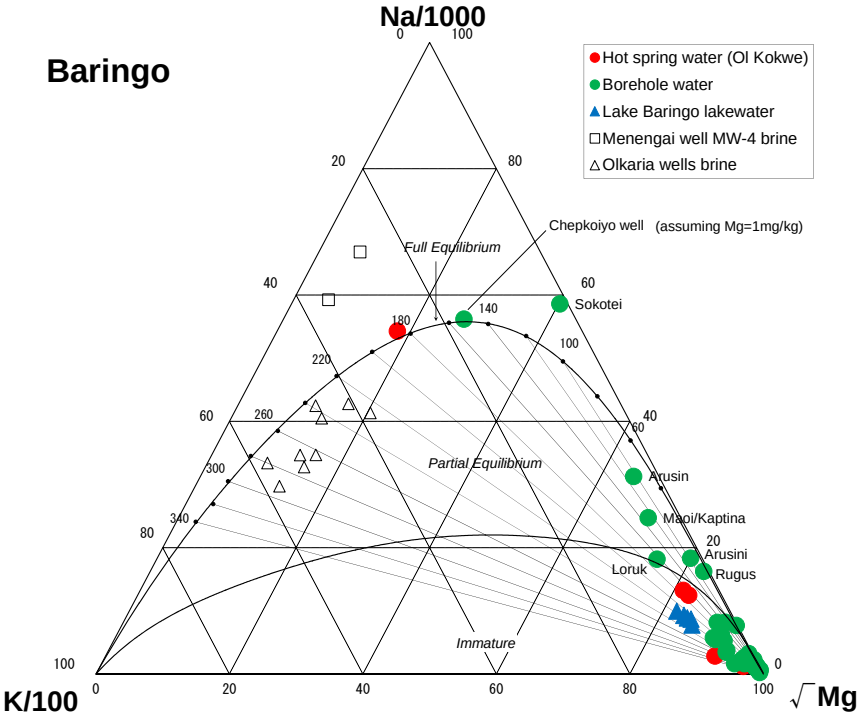

Ternary plot of Na-K-Mg composition for spring and borehole water

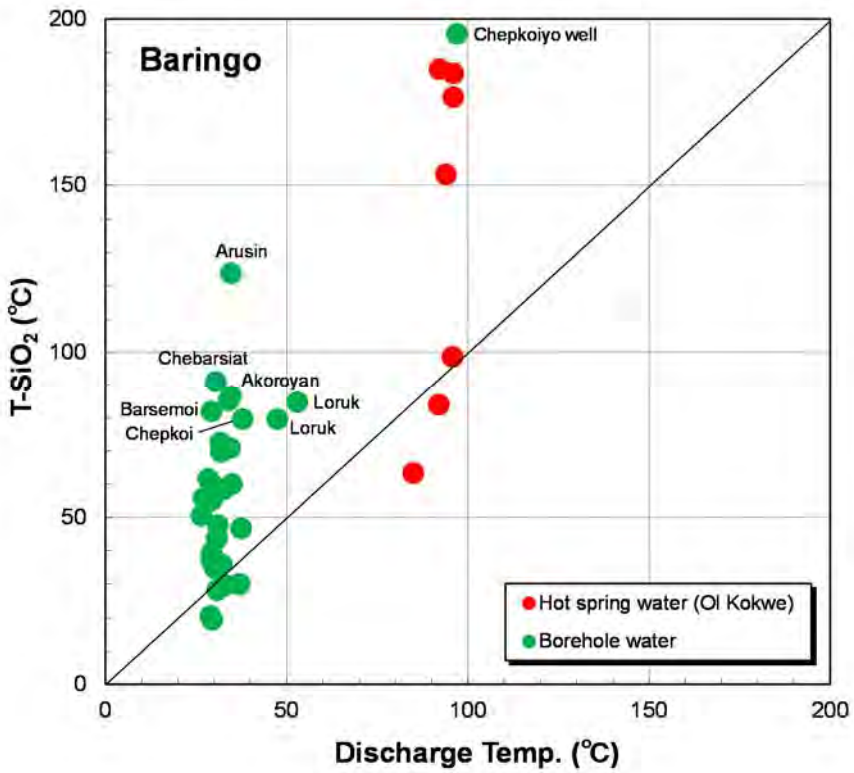

Comparison of measured discharge temperature and calculated silica temperature for spring and borehole water

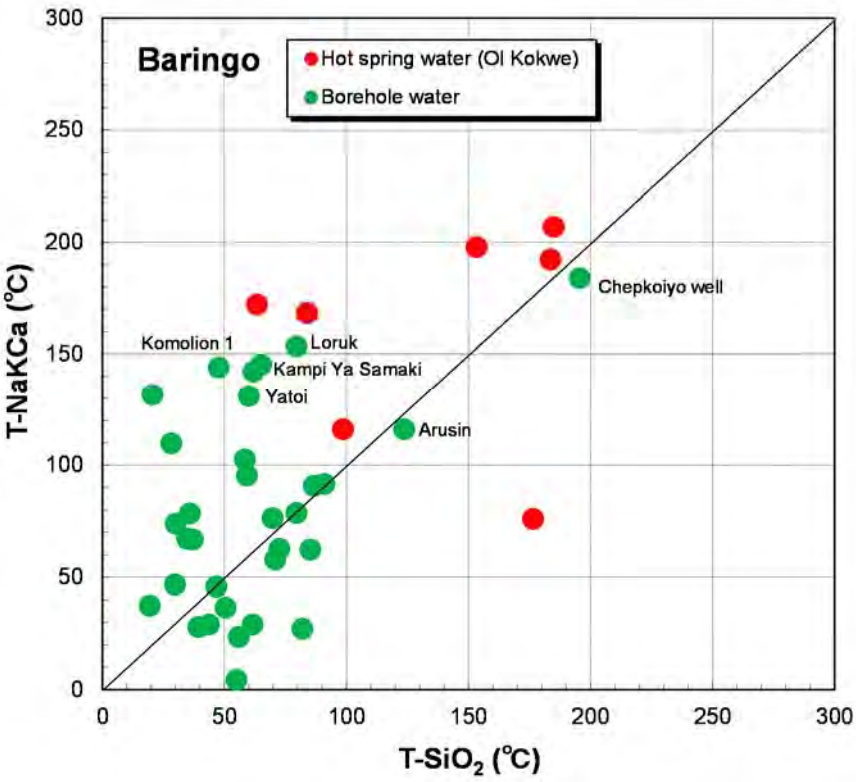

Comparison of silica temperature and NaKCa temperature for spring and borehole water

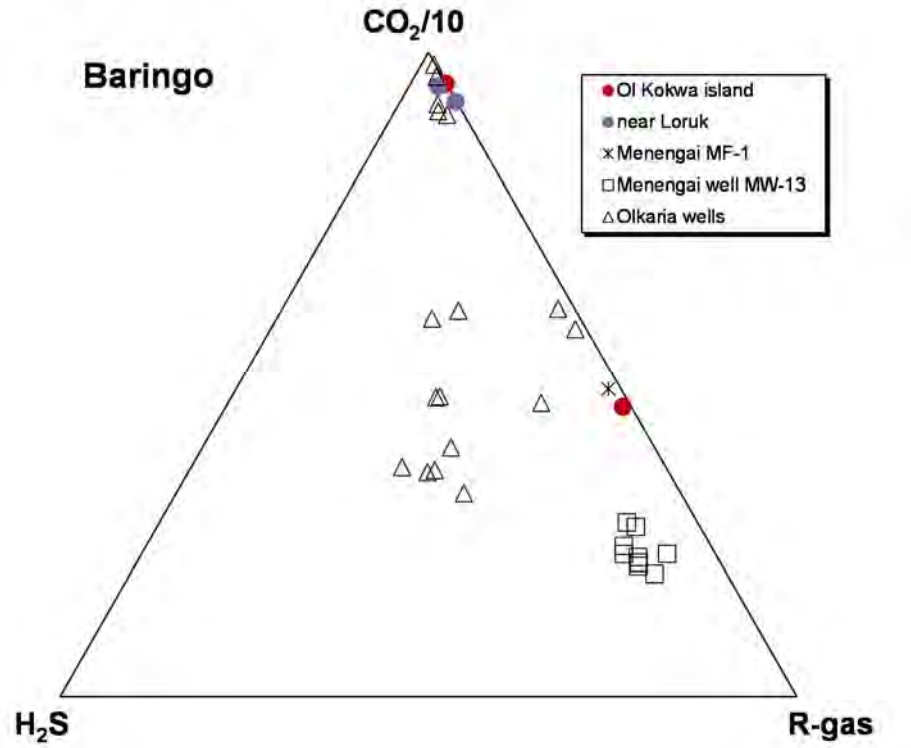

Ternary plot of major gas chemistry for geothermal gases

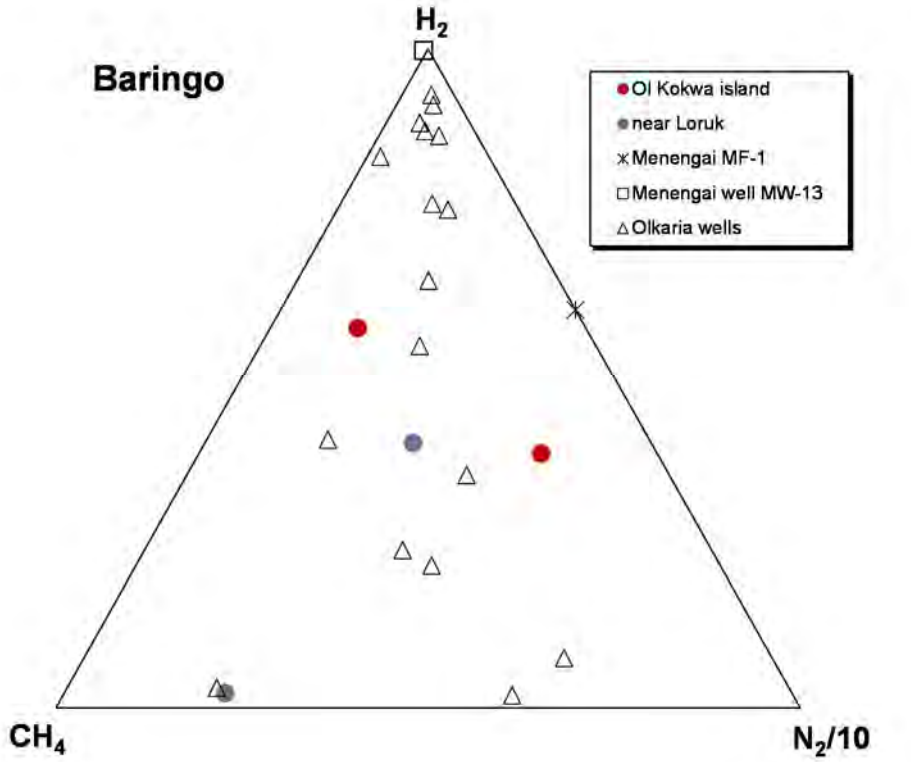

Ternary plot of minor gas chemistry for geothermal gases

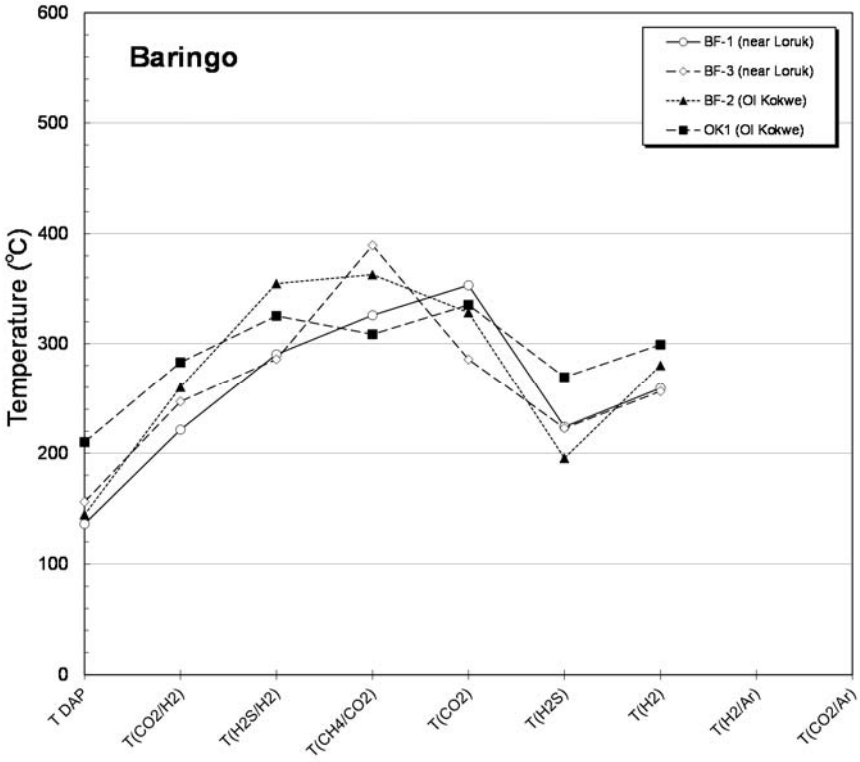

Comparison of gas chemical temperatures for fumarolic gases

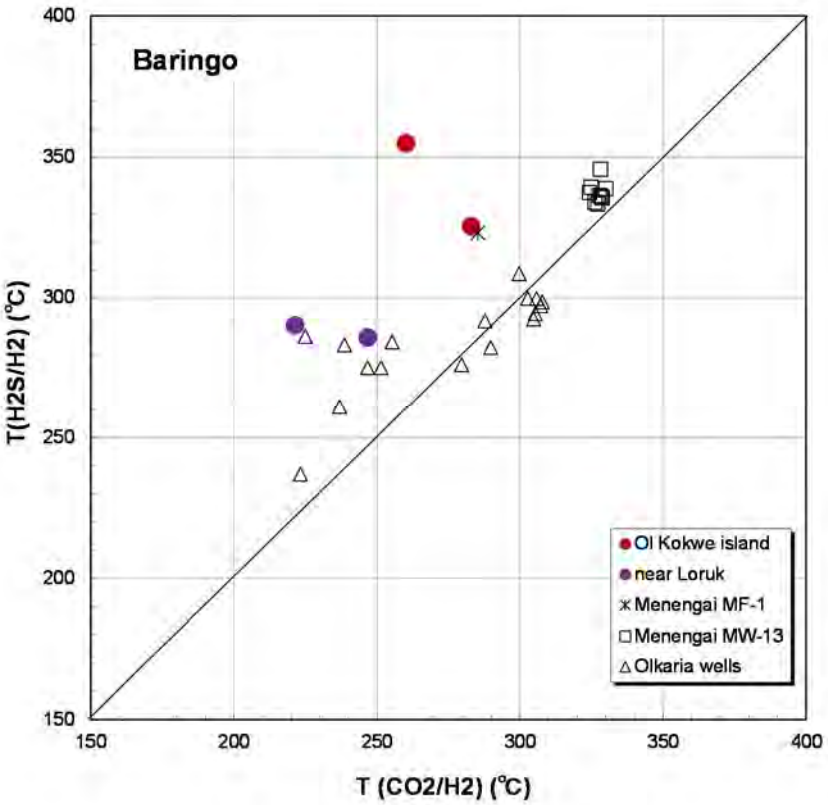

Comparison of H_2S/H_2 temperature and CO_2/H_2 temperature for geothermal gases

Korosi - Chepchuk

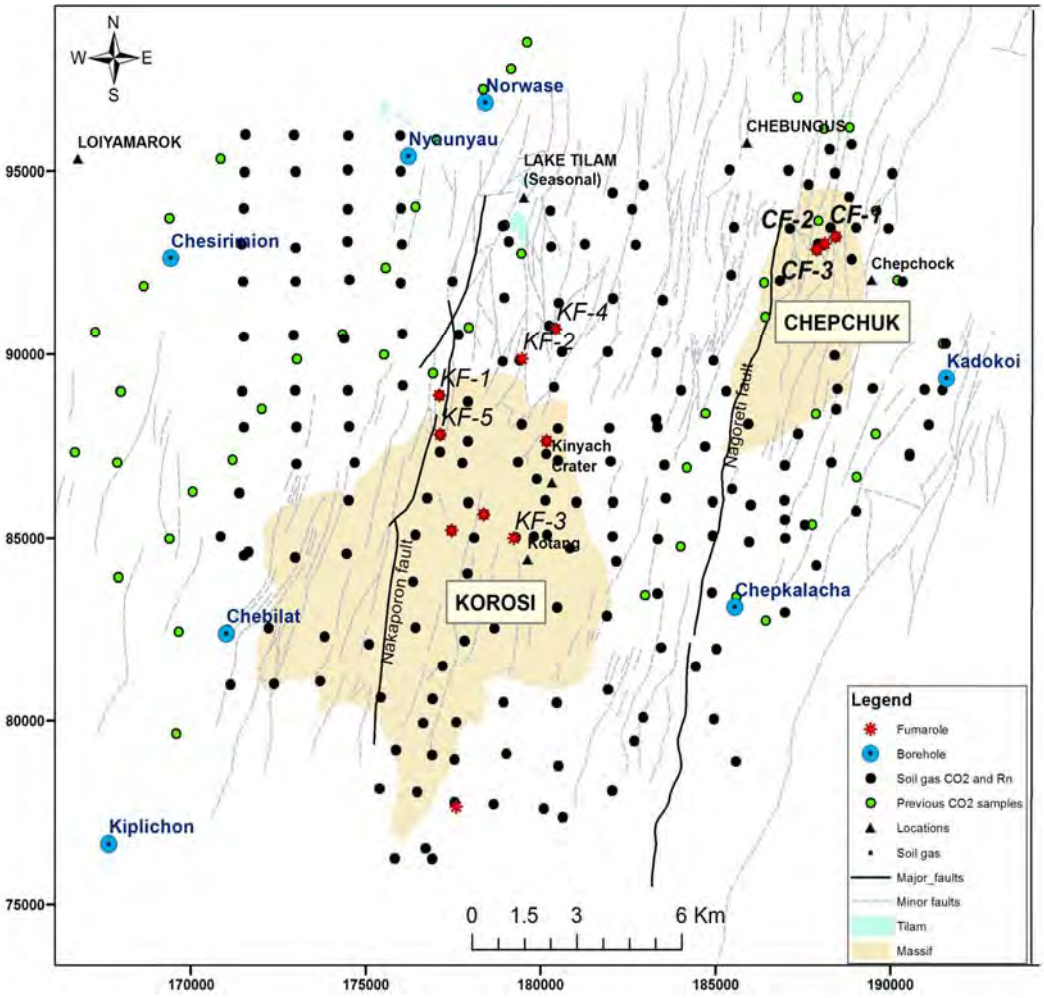

Location map of boreholes and fumaroles (GDC internal report)

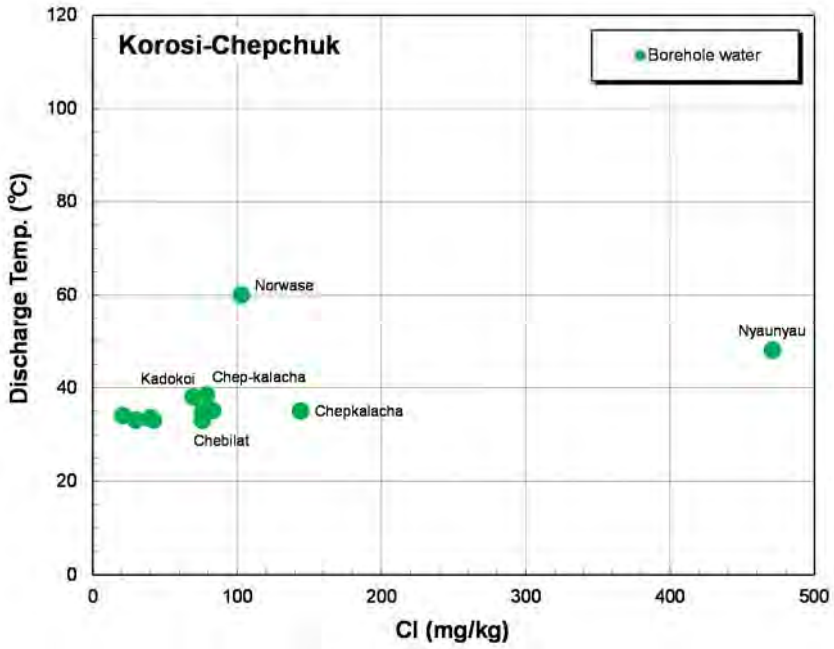

Plot of measured discharge temperature vs. Cl concentration for borehole water

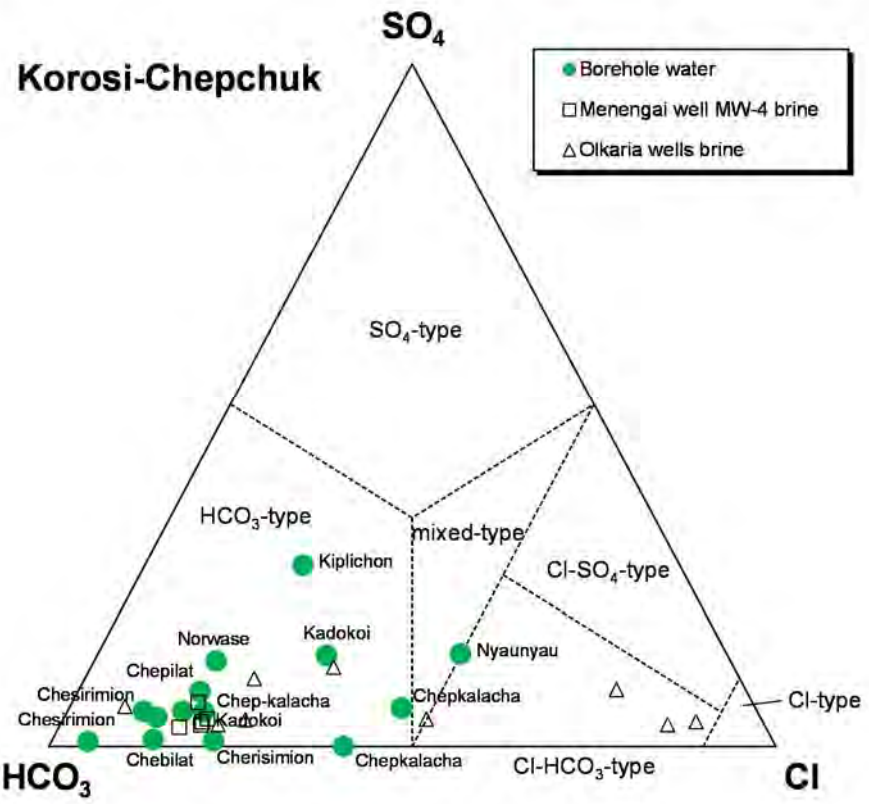

Ternary plot of major anion composition for borehole water

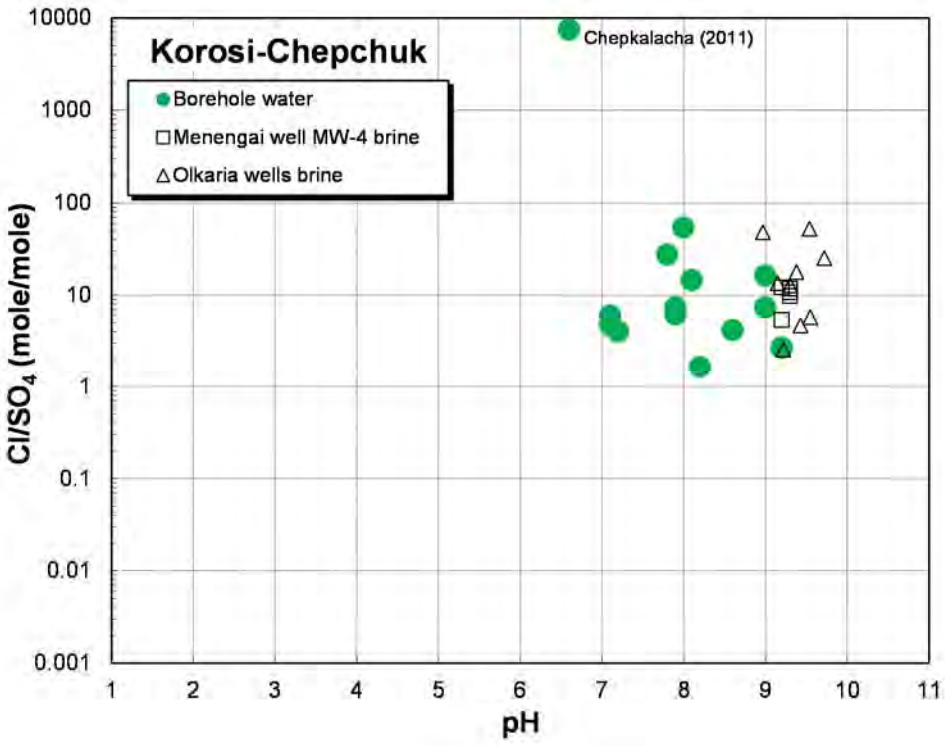

Plot of Cl/SO_4 ratio vs. pH for borehole water

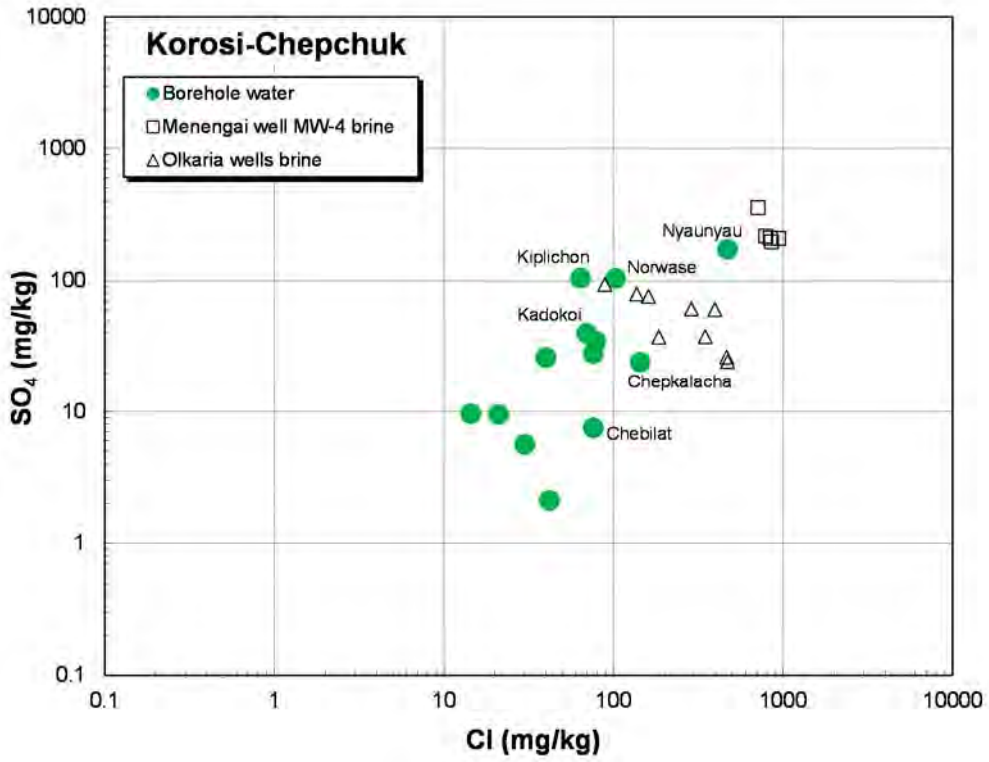

Plot of SO_4 vs. Cl concentration for borehole water

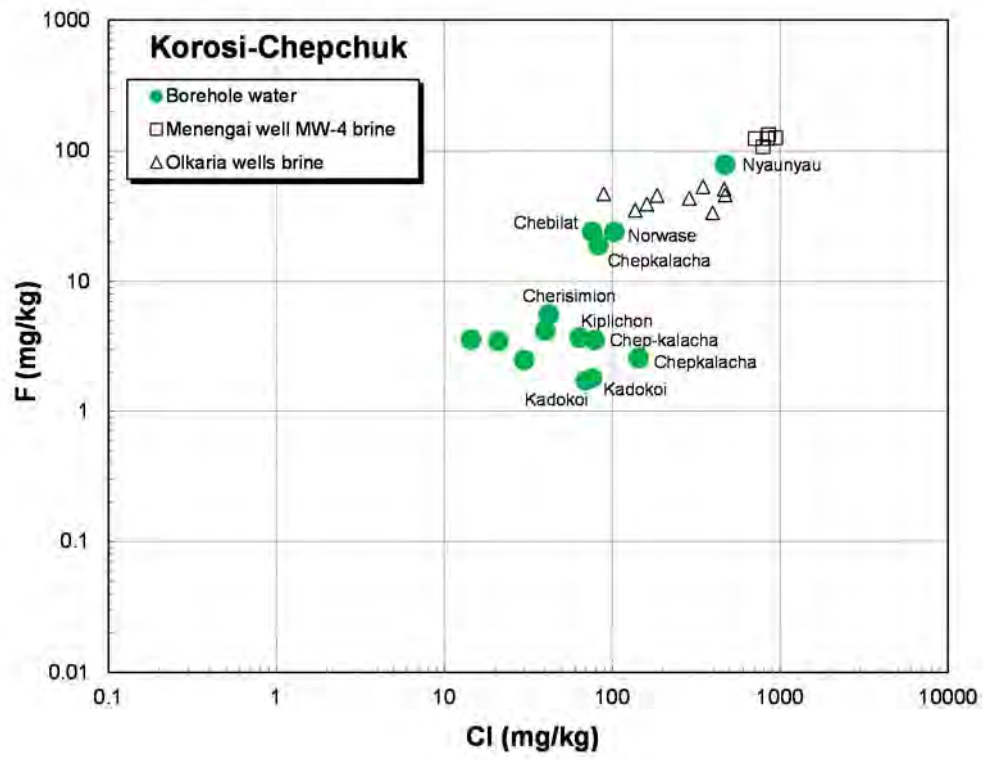

Plot of F vs. Cl concentration for spring and borehole water

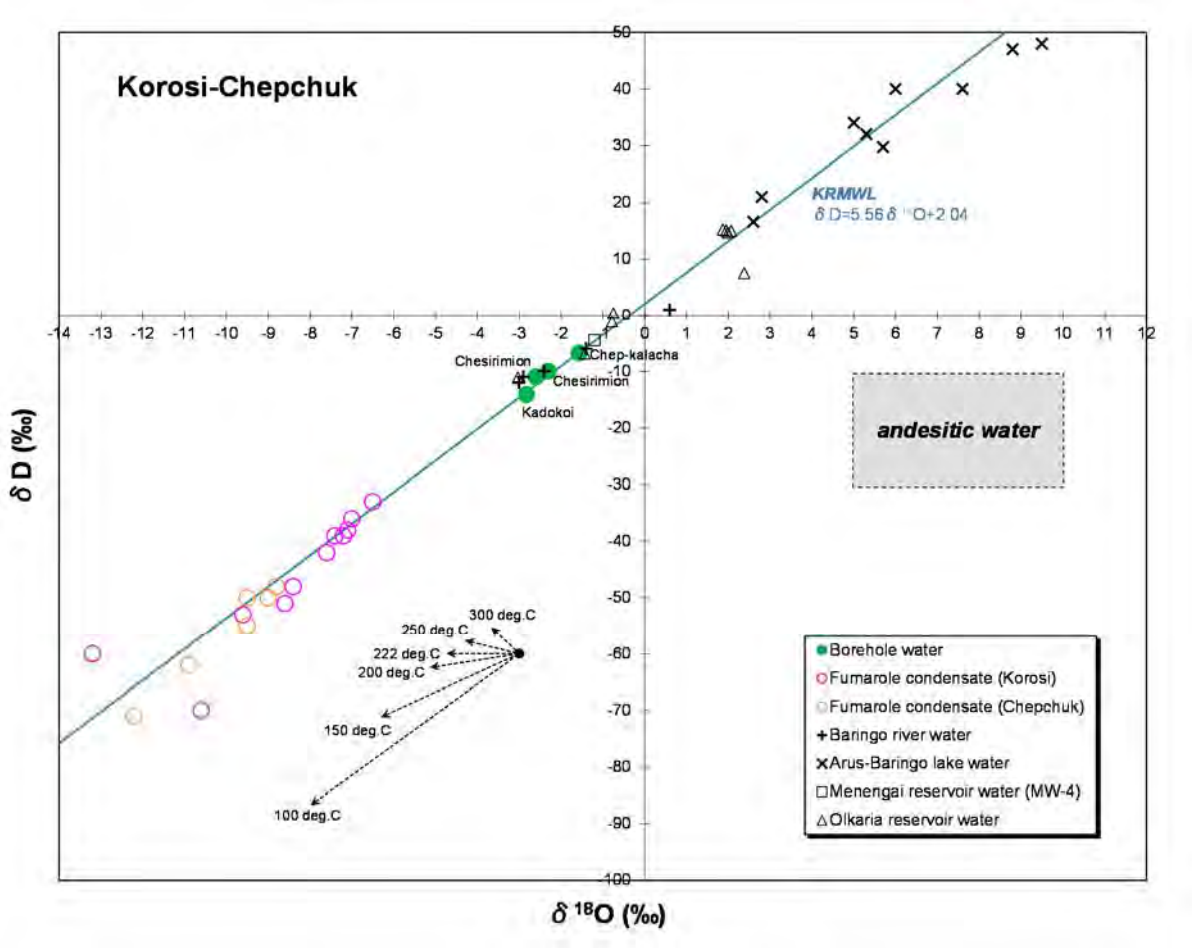

Hydrogen and oxygen isotopic composition

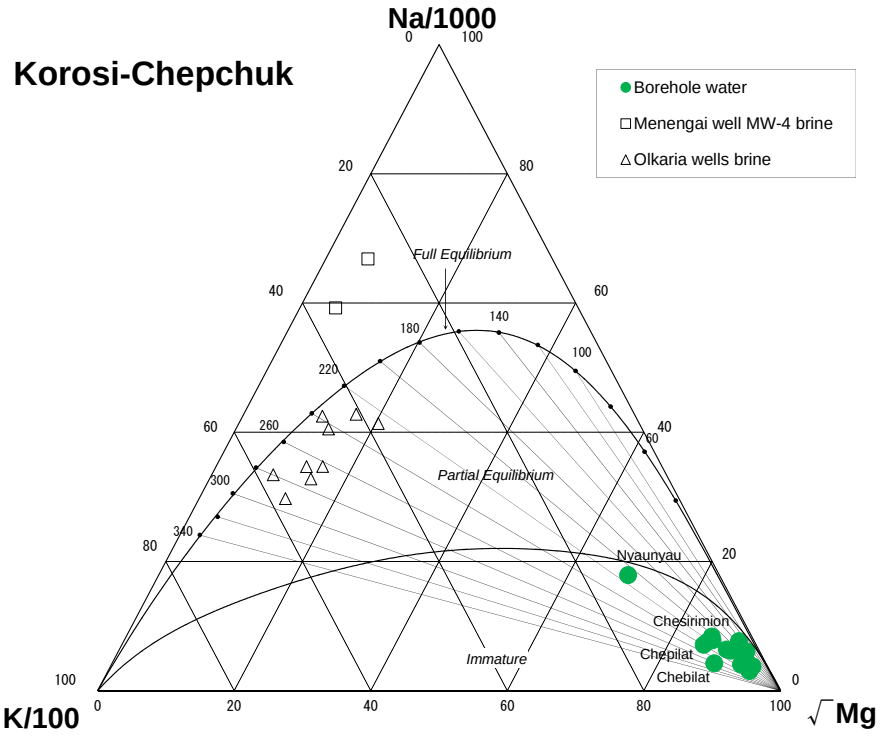

Ternary plot of Na-K-Mg composition for borehole water

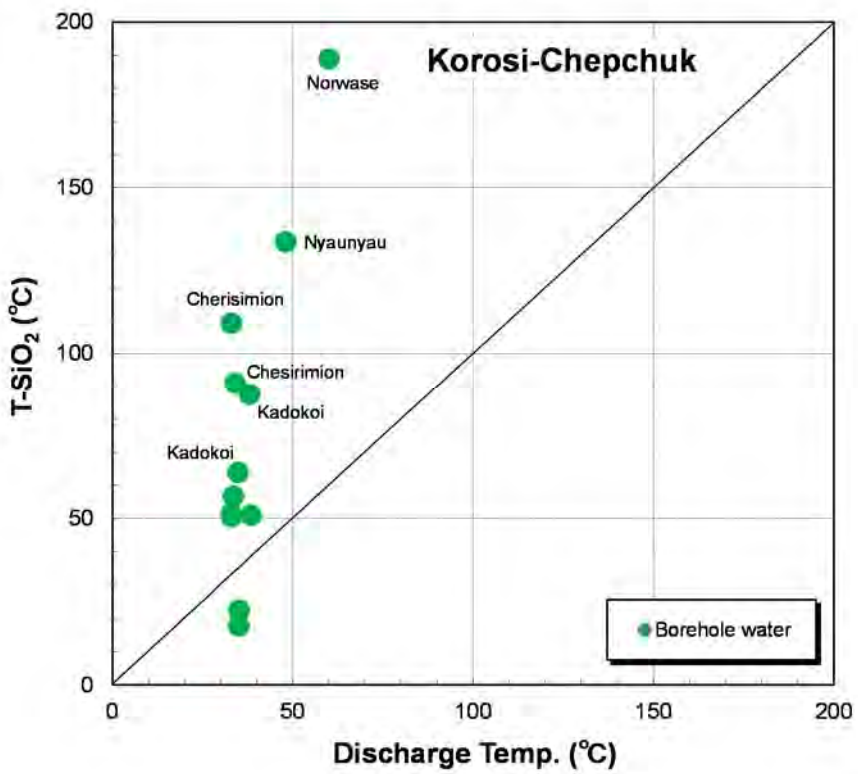

Comparison of measured discharge temperature and calculated silica temperature for borehole water

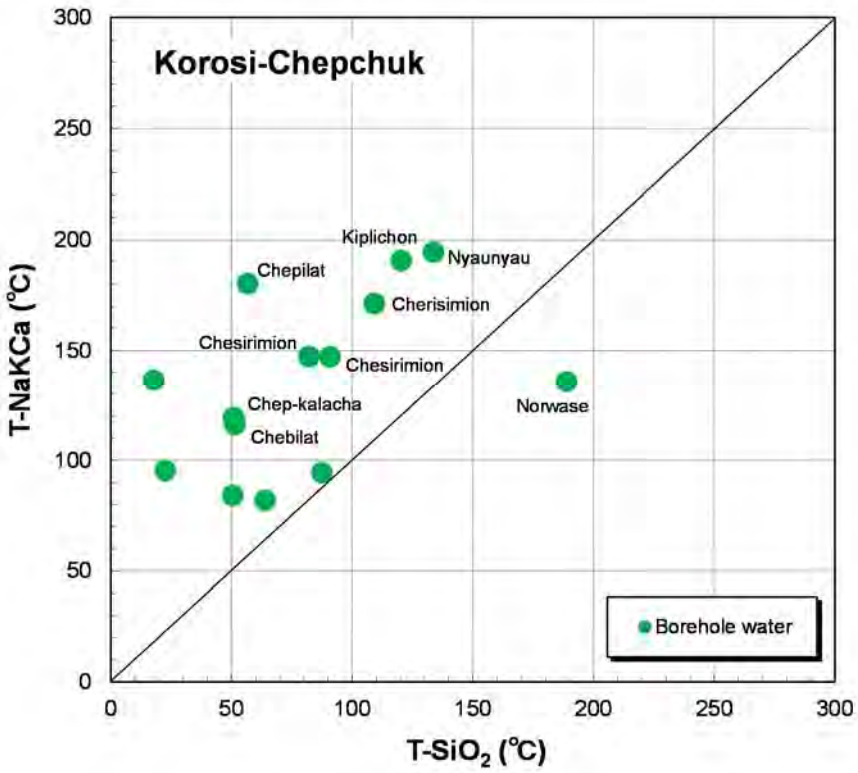

Comparison of silica temperature and NaKCa temperature for borehole water

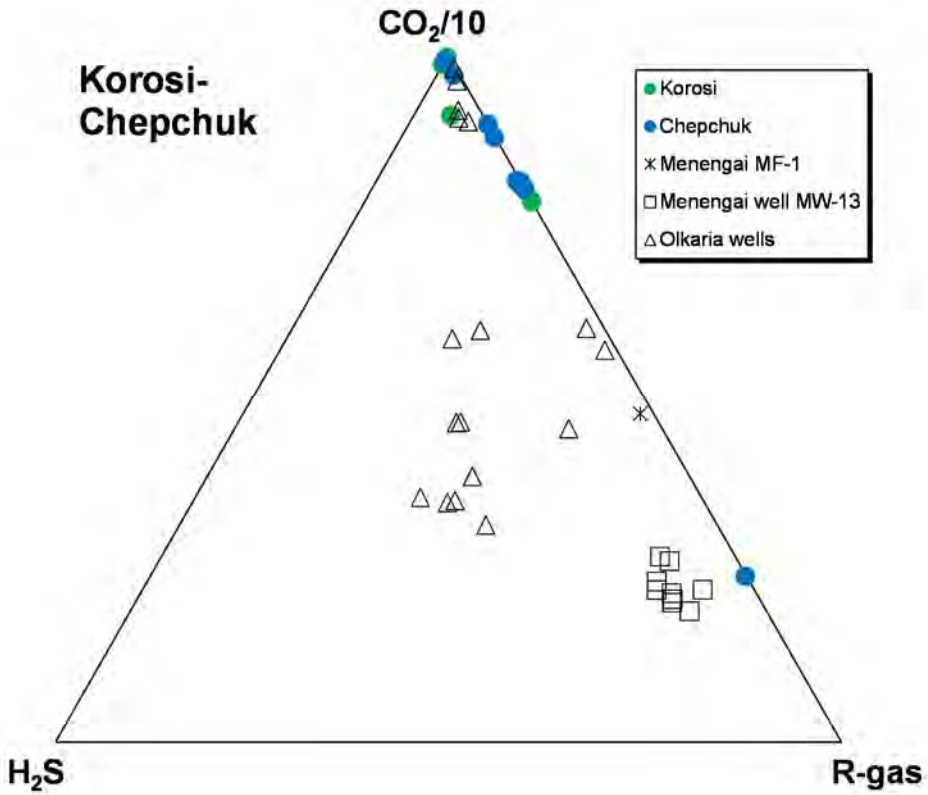

Ternary plot of major gas chemistry for geothermal gases

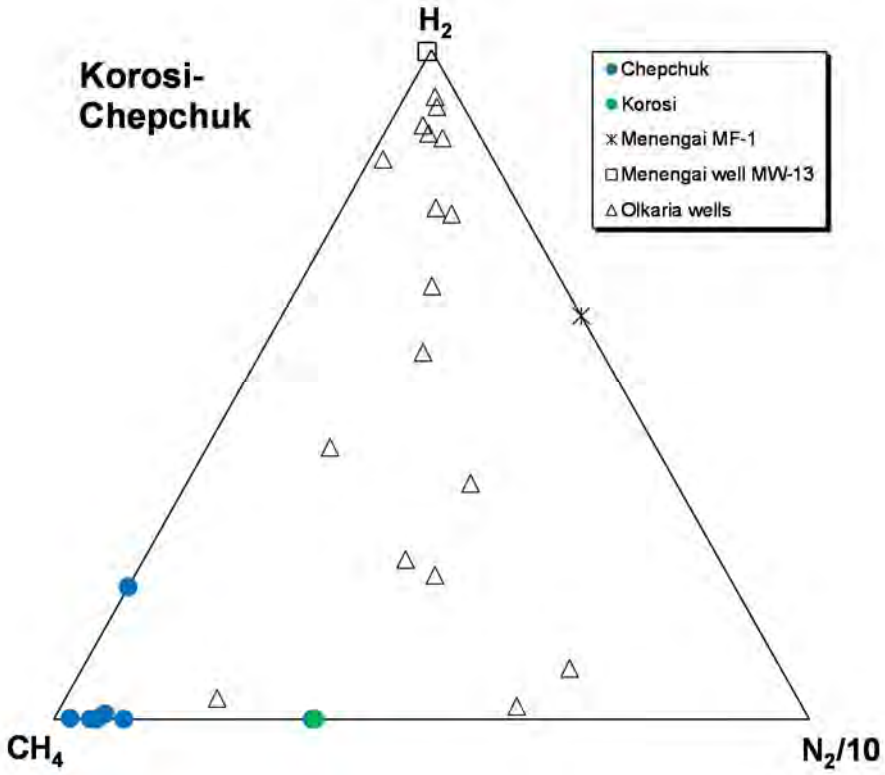

Ternary plot of minor gas chemistry for geothermal gases

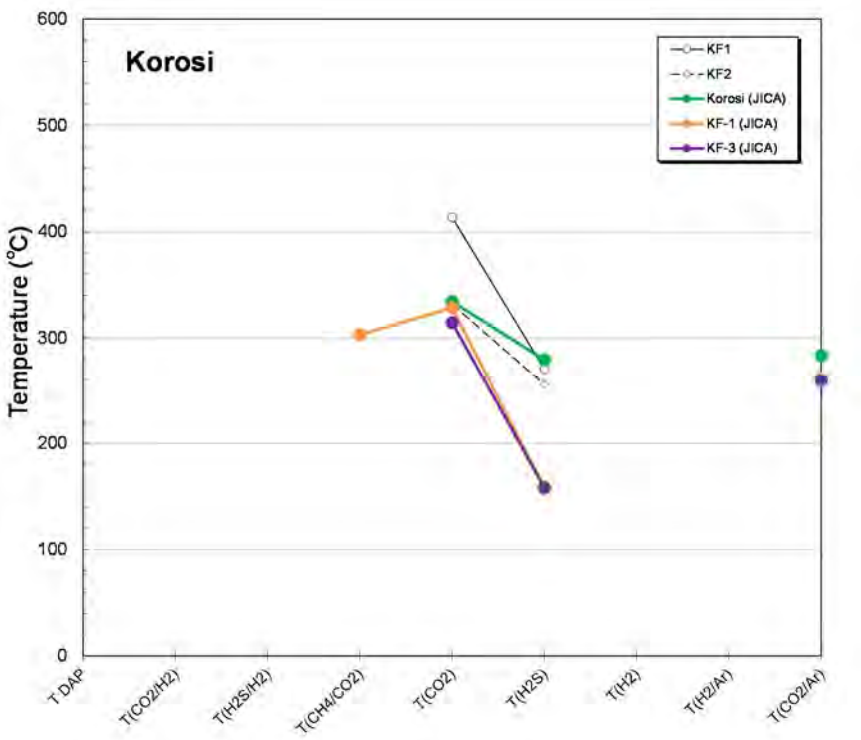

Comparison of gas chemical temperatures for fumarolic gases (Korosi)

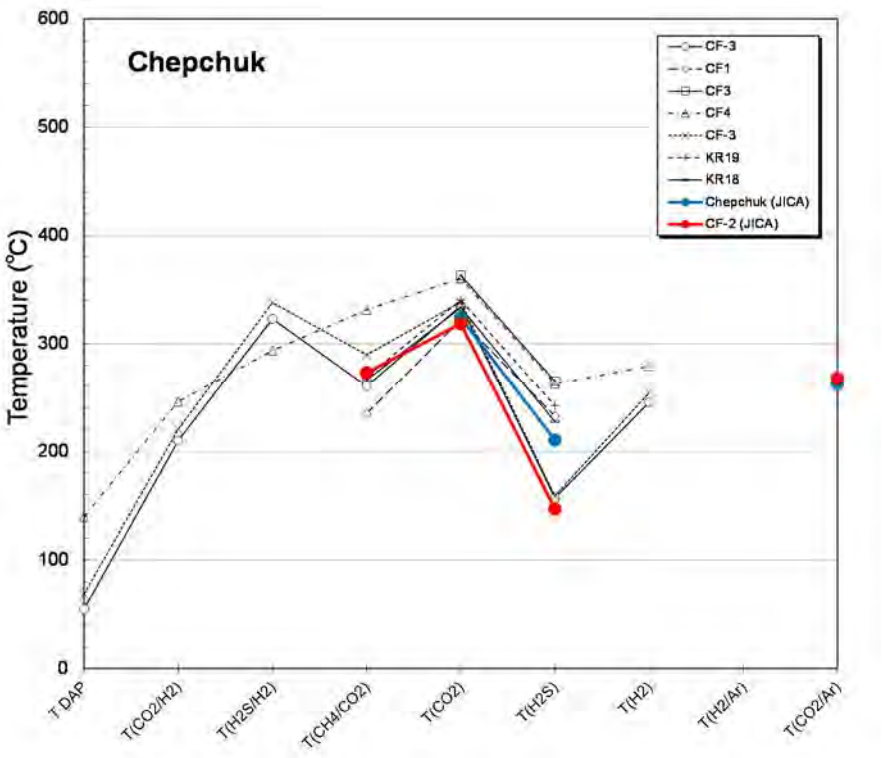

Comparison of gas chemical temperatures for fumarolic gases (Chepchuk)

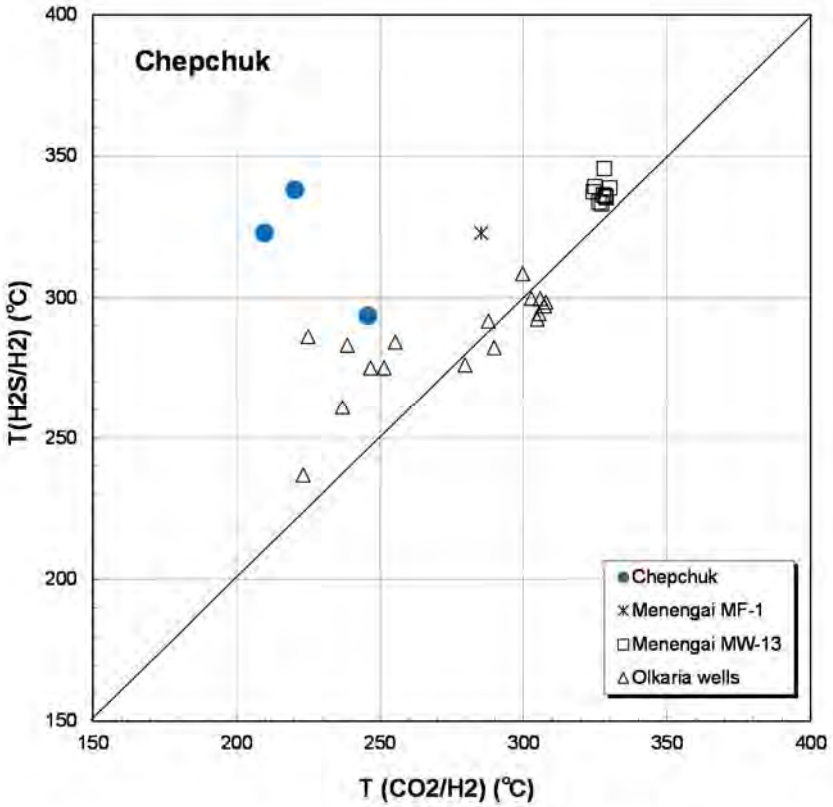

Comparison of H_2S/H_2 temperature and CO_2/H_2 temperature for geothermal gases (Chepchuk)

Paka

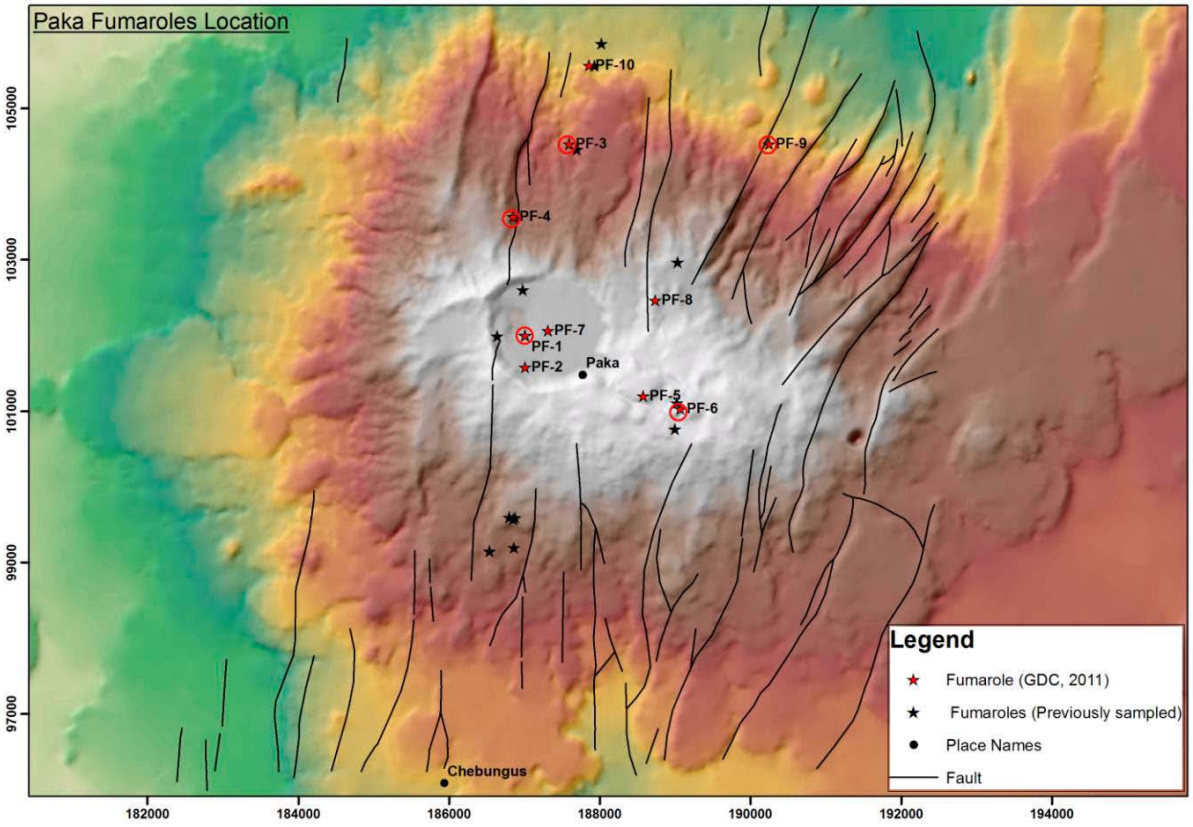

Location map of fumaroles (Kipng'ok and Nyamongo, 2013)

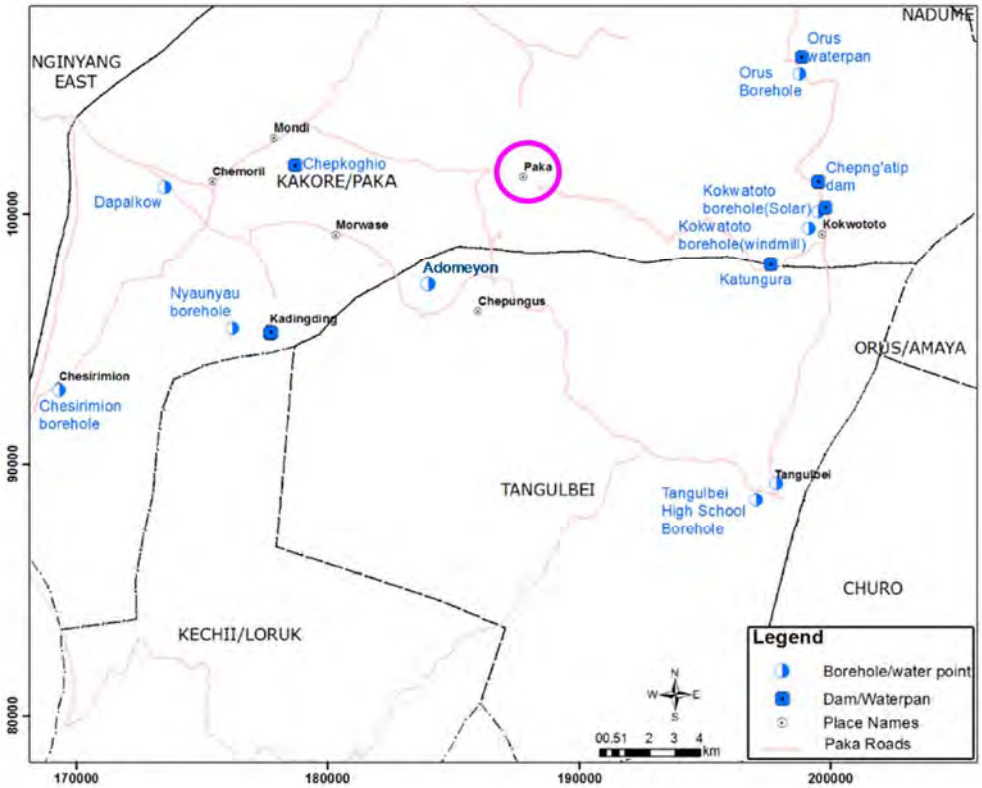

Location map of boreholes in surroundings (modified from GDC (2011))

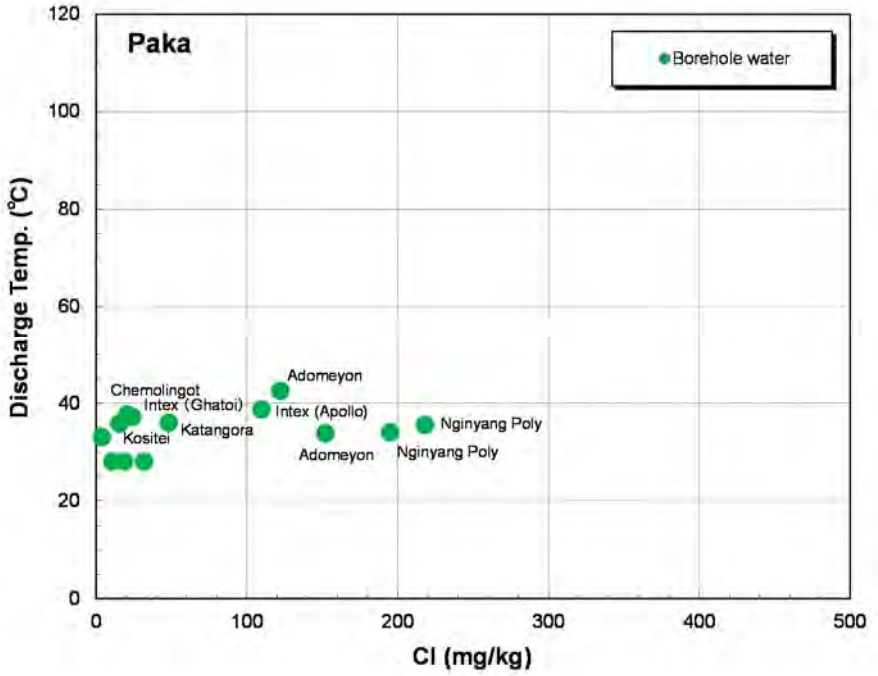

Plot of measured discharge temperature vs. Cl concentration for borehole water

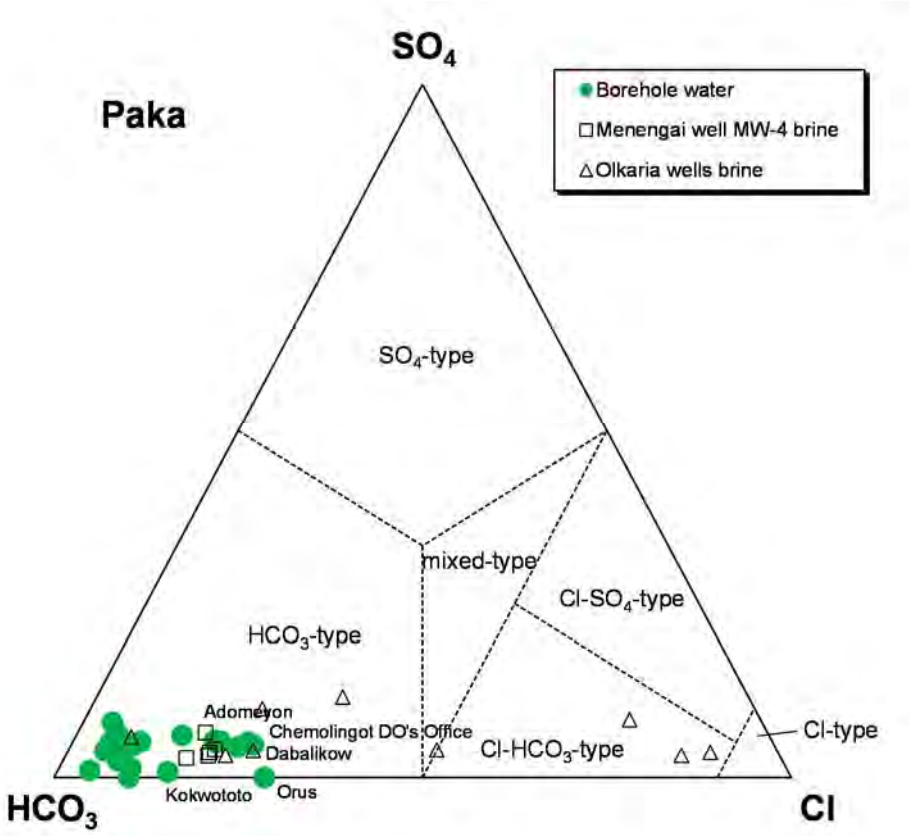

Ternary plot of major anion composition for borehole water

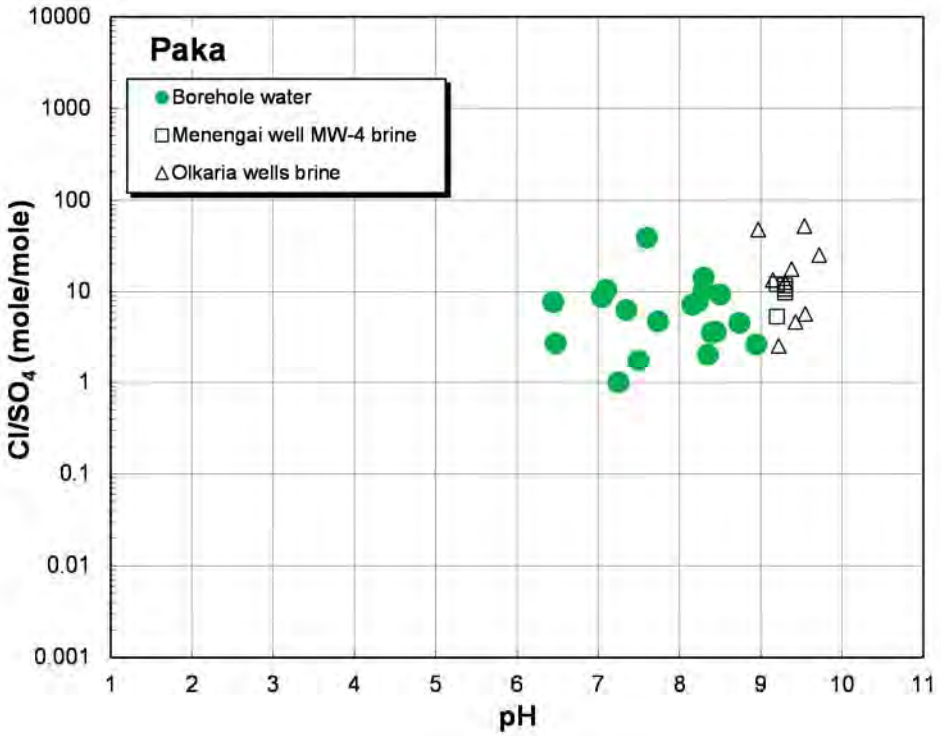

Plot of Cl/SO_4 ratio vs. pH for borehole water

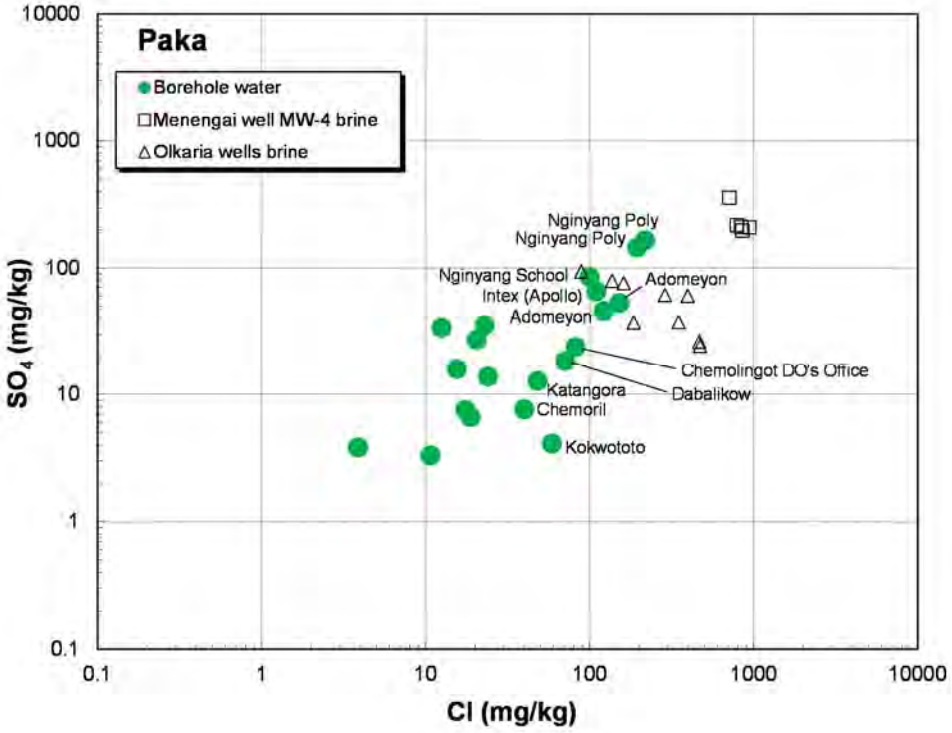

Plot of SO_4 vs. Cl concentration for borehole water

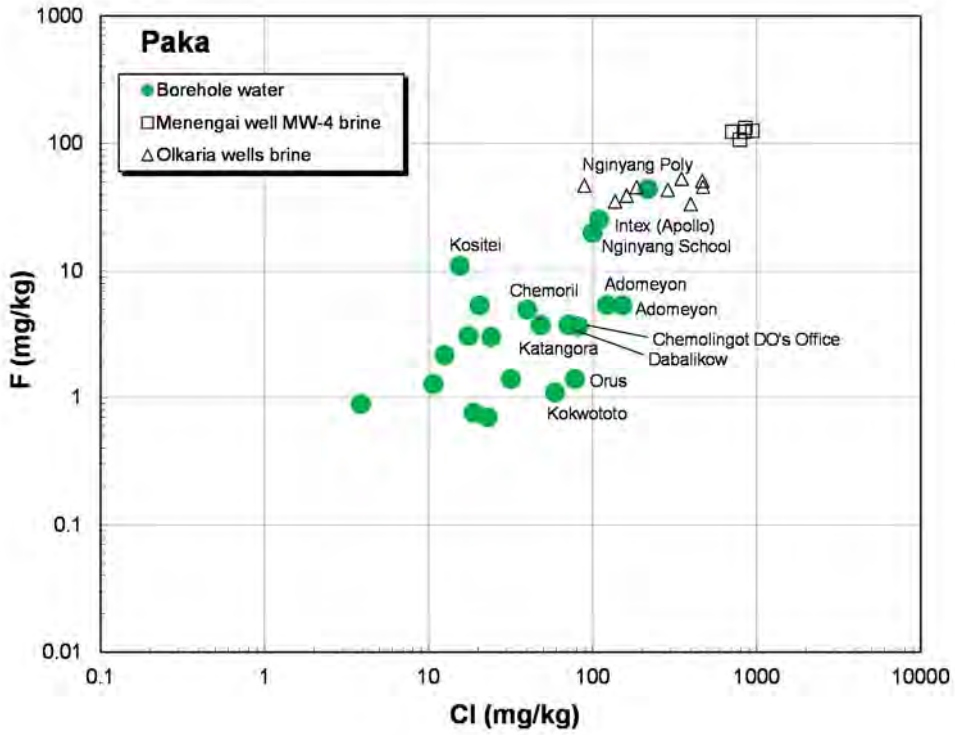

Plot of F vs. Cl concentration for spring and borehole water

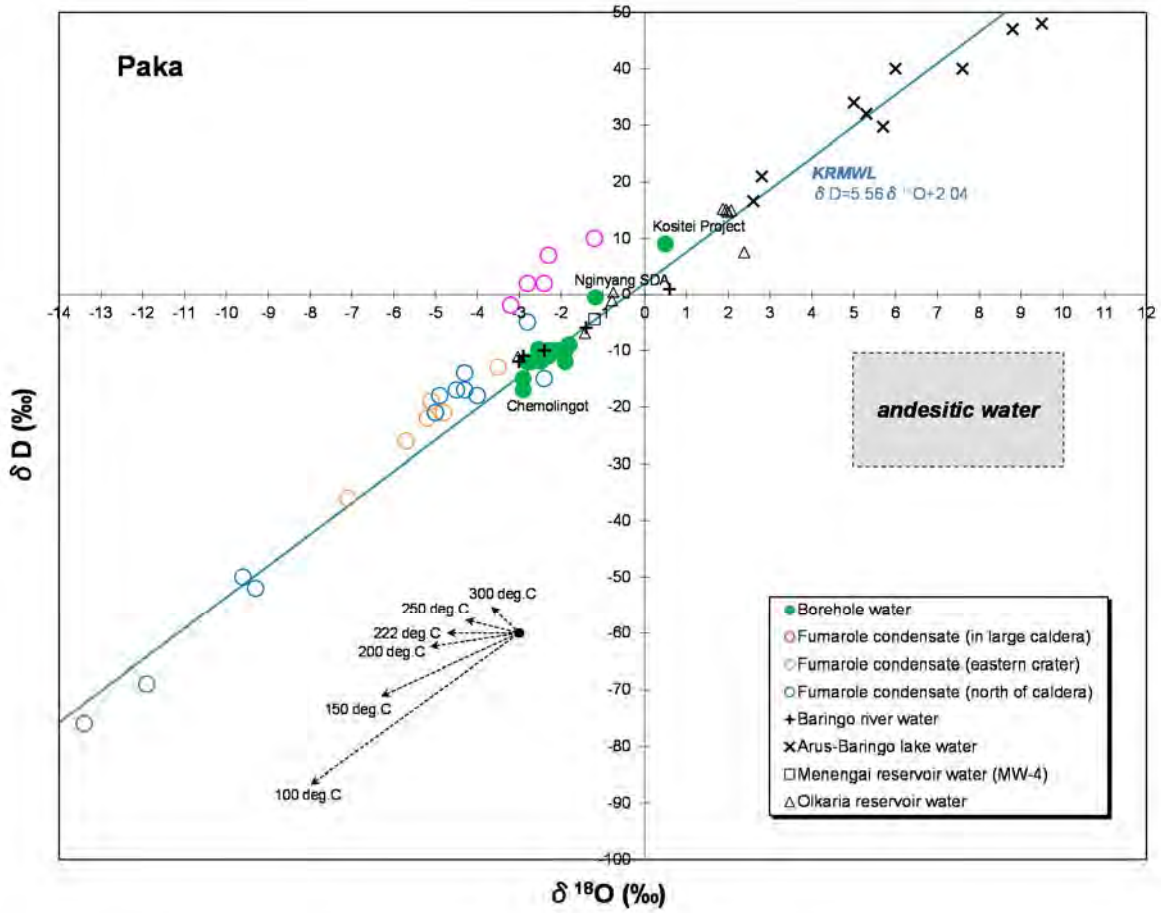

Hydrogen and oxygen isotopic composition

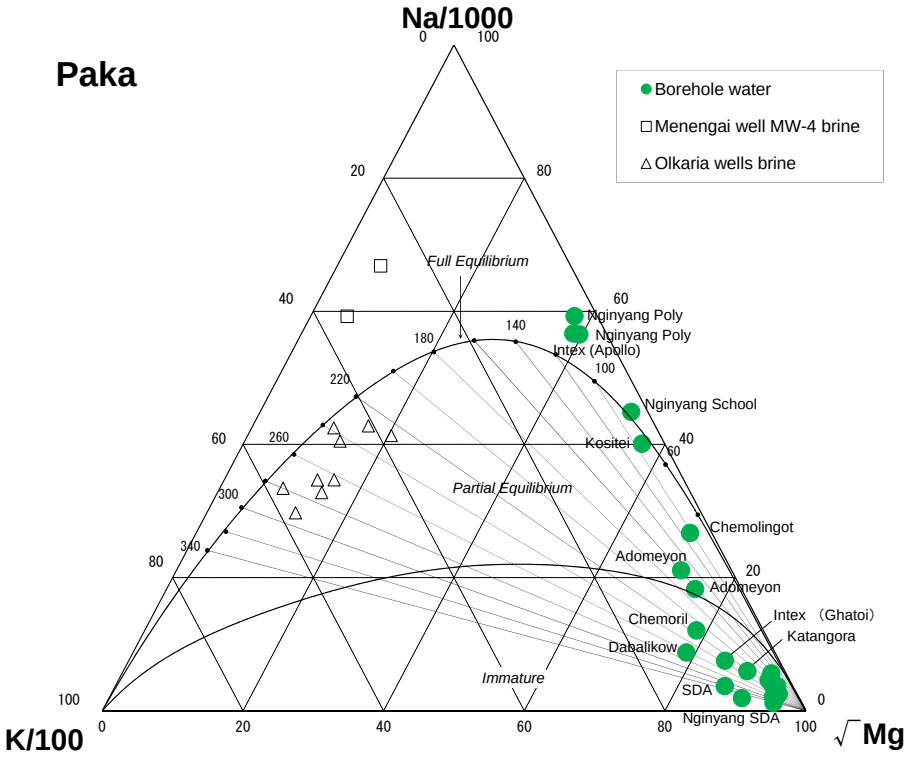

Ternary plot of Na-K-Mg composition for borehole water

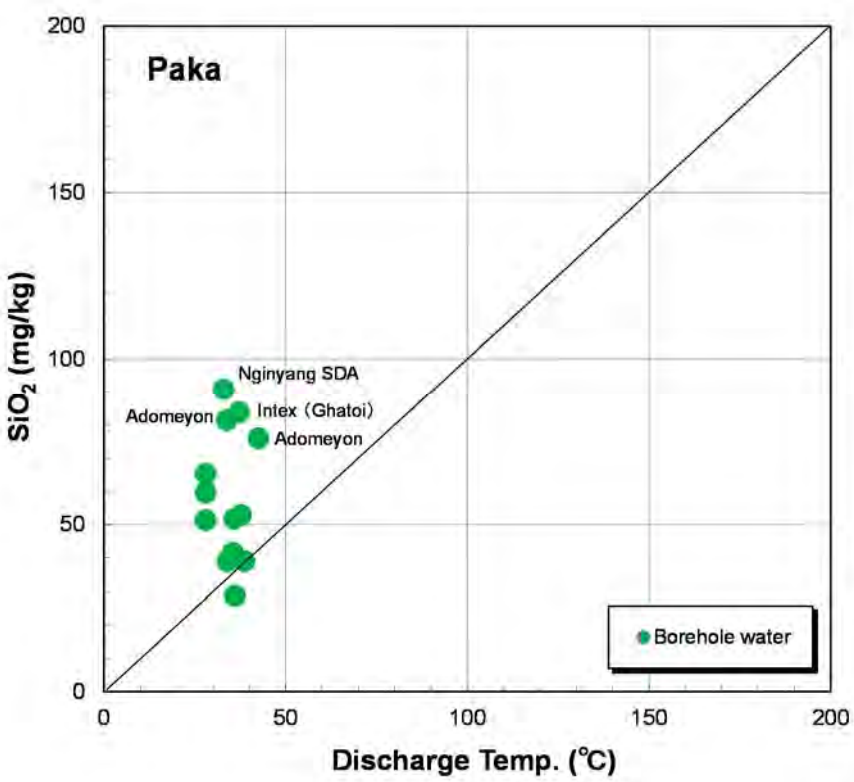

Comparison of measured discharge temperature and calculated silica temperature for borehole water

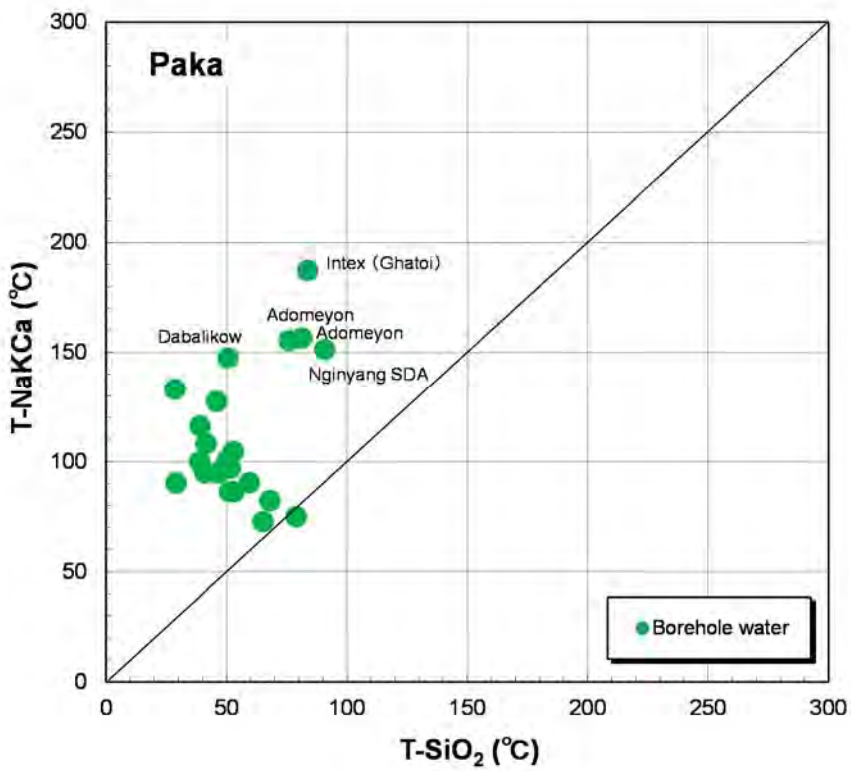

Comparison of silica temperature and NaKCa temperature for borehole water

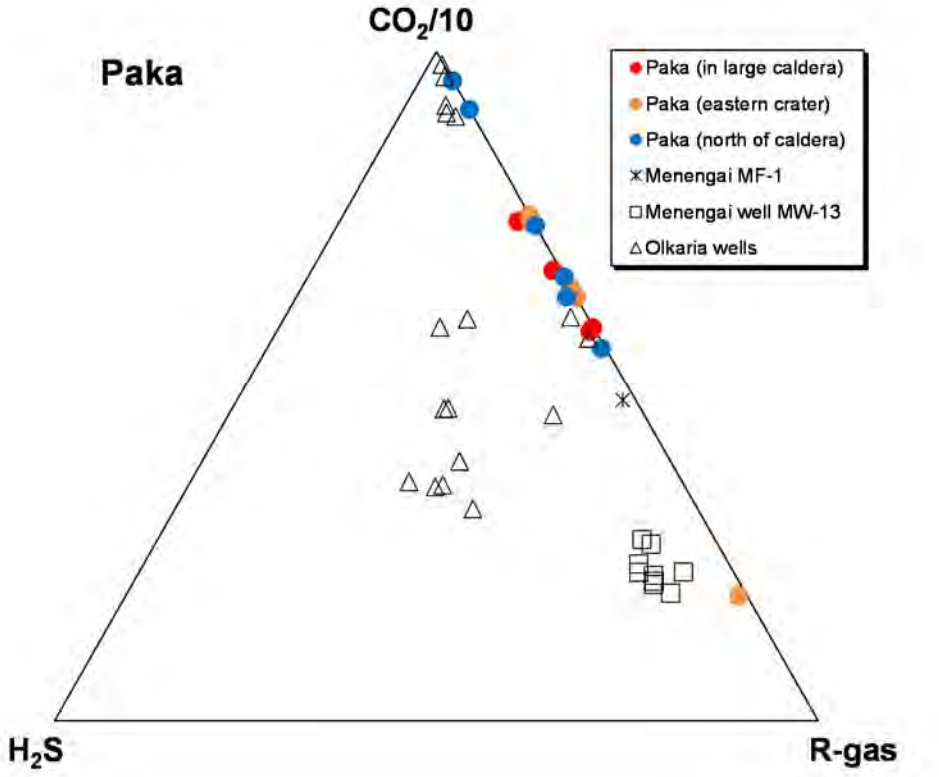

Ternary plot of major gas chemistry for geothermal gases

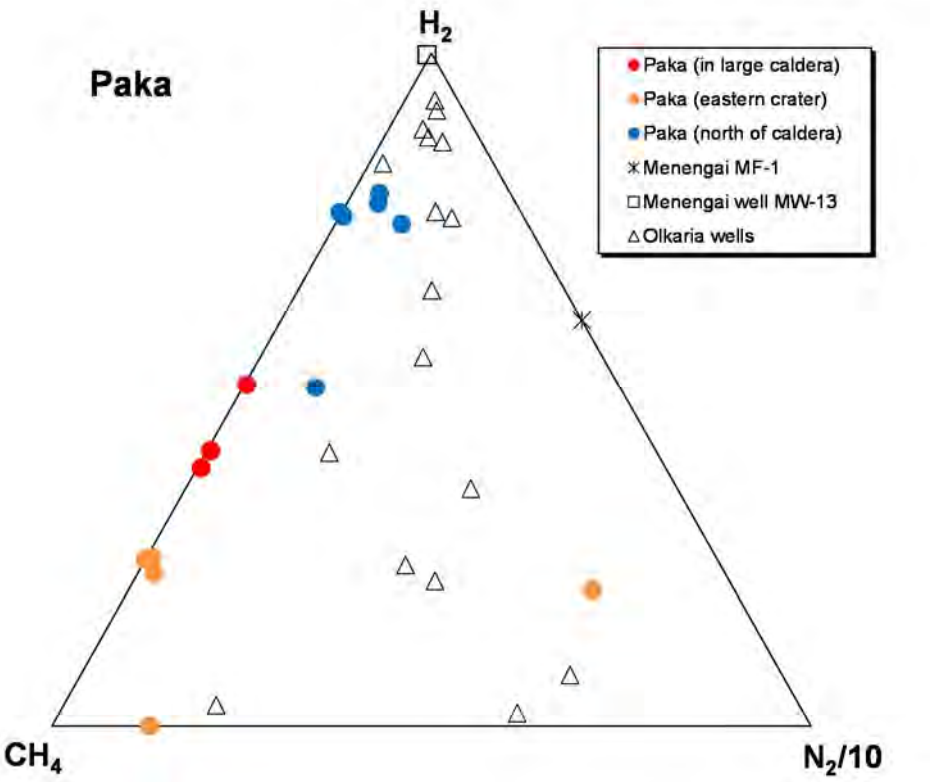

Ternary plot of minor gas chemistry for geothermal gases

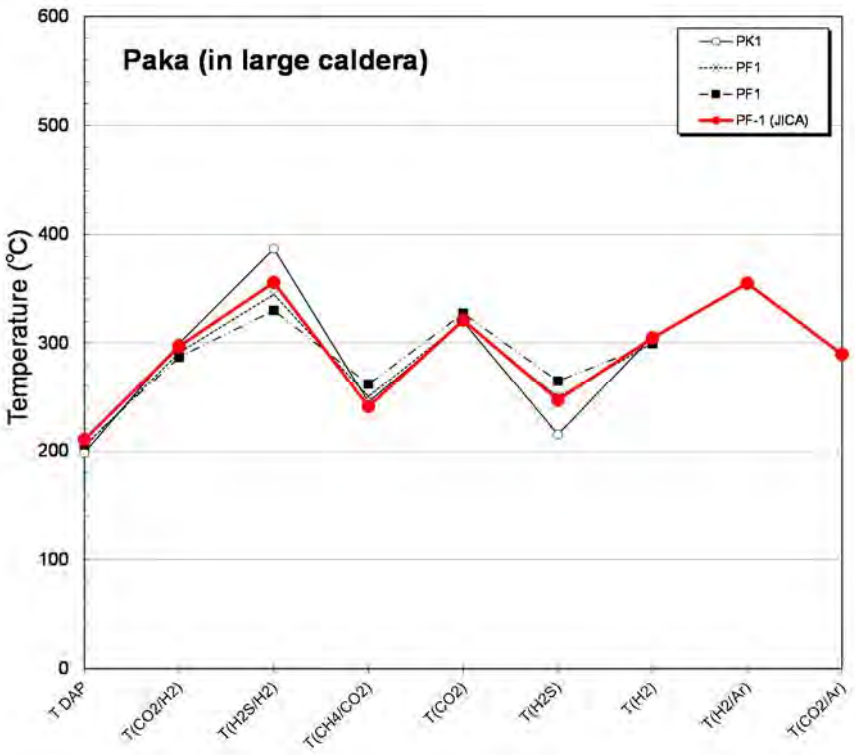

Comparison of gas chemical temperatures for fumarolic gases (in large caldera)

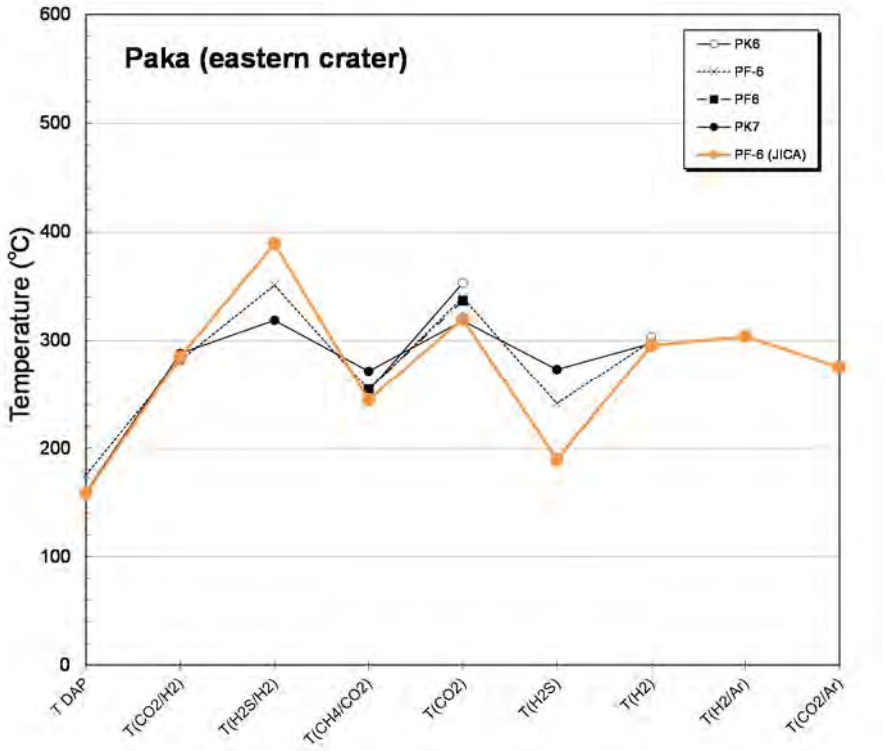

Comparison of gas chemical temperatures for fumarolic gases (eastern crater)

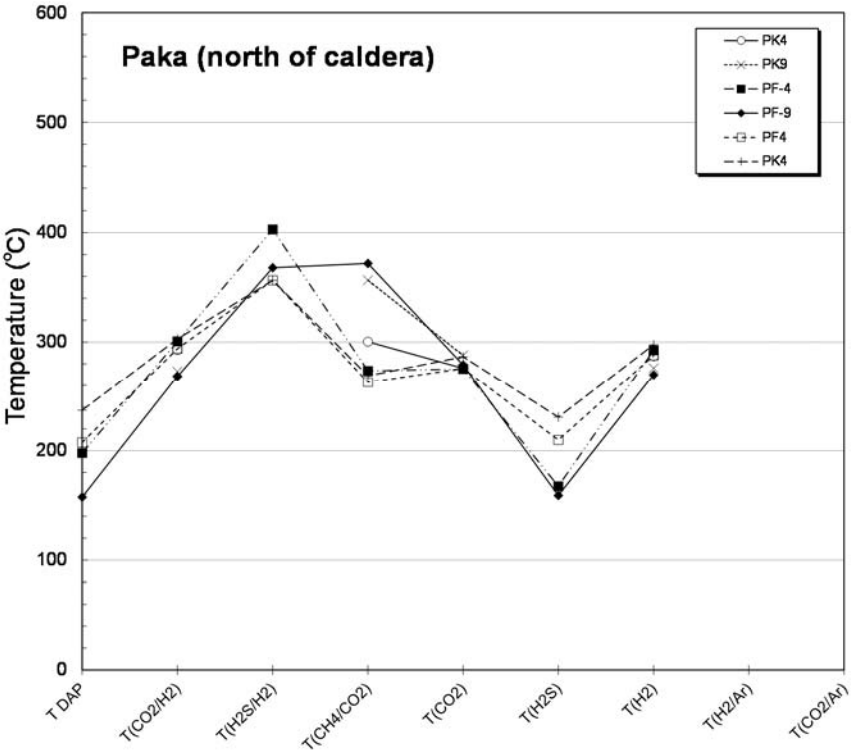

Comparison of gas chemical temperatures for fumarolic gases (north of caldera)

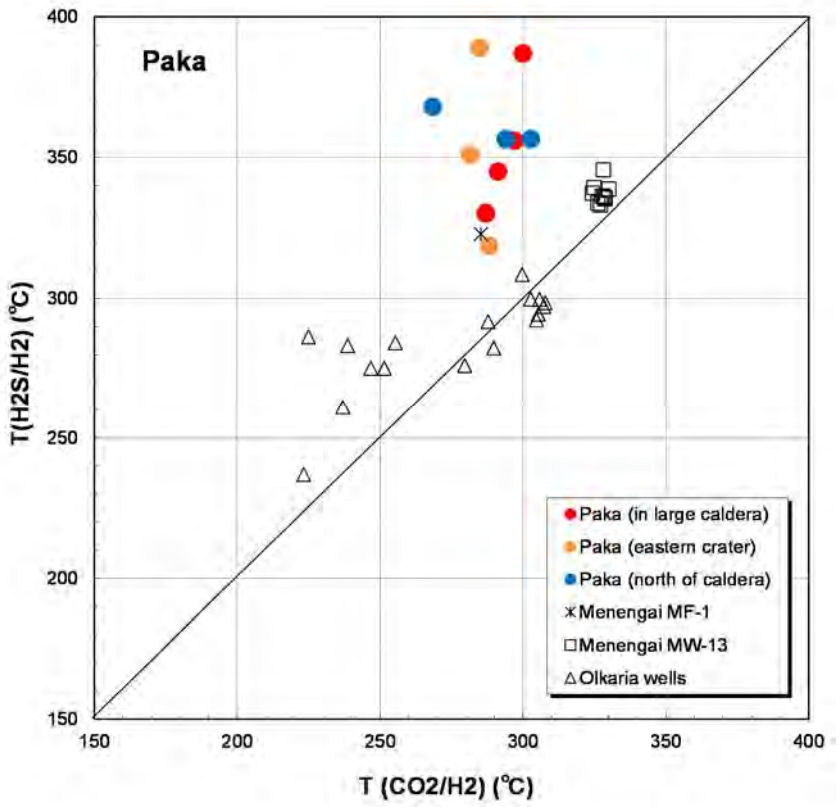

Comparison of H_2S/H_2 temperature and CO_2/H_2 temperature for geothermal gases

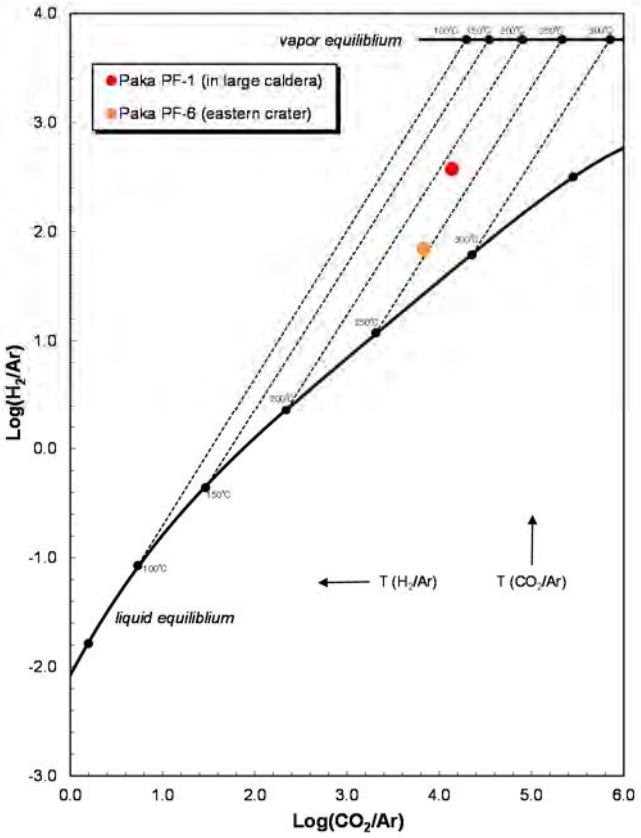

Plot of H_2/Ar vs. CO_2/Ar for fumarolic gas

APPENDIX

6. Methodology of MT Data Analysis and Results

Methodology of MT Data Analysis and Results

The data analysis procedure including the static shift correction, topography correction and the three-dimensional resistivity inversion scheme, and the basic interpretation method, “General Resistivity Structure of Geothermal Fields in Volcanic Areas” utilized in this study are described below:

1. MT station locations

The locations of the MT stations (UTM coordinates) used for the data analysis in Korosi-Chepchuk field and those used for the data analysis in Paka field are listed in Table MT-01 and MT-02 respectively.

Table MT-01 Locations of MT stations (Korosi and Chepchuk field)

Station	Easting (UTM)	Northing (UTM)	Elevation (m)	Station	Easting (UTM)	Northing (UTM)	Elevation (m)
BARMT02	170432.2	78062.4	994	KOR48	181165.3	83733.6	1337
BarMT03	170583.2	81899.2	1002	kor49	182972.7	83972.2	1062
BARMT19	167361.7	77563.2	1012	KOR50	184095.8	83645.6	1037
BarMT31	168748.2	82214.0	1007	KOR51	185575.0	83666.2	1037
BARMT39	182273.1	78780.5	1081	KOR52	172056.5	82030.4	1089
BARMT41Ar	175427.9	79277.4	1026	KOR53	173189.0	81842.1	1070
KORMT03a	178496.4	94928.6	891	KOR54	176008.6	82156.9	1173
KORMT09a	188786.5	87555.7	1156	KOR55	179071.9	81549.2	1231
KORMT13a	168967.9	95003.6	916	KOR56	180124.5	82068.1	1308
KORMT14a	185390.0	89190.4	1026	kor57	183064.2	81915.6	1071
KorMT15a	186428.5	91857.9	1006	kOR59	171904.1	80908.3	1045
KORMT18A	192944.0	90181.1	1168	KOR60	173572.1	80768.9	1011
KORMT19a	183077.2	96096.4	970	kor61	175595.9	80503.2	1039
KORMT21a	167043.6	92216.1	962	kor62	177415.4	80240.7	1200
KORMT25B	186291.7	90960.4	1021	KOR64	182345.7	80947.7	1067
KORMT28A	168950.5	83957.1	988	KOR74R	170045.0	91049.0	914
KORMT29a	180485.1	93353.1	904	kor78	176376.9	91155.0	972
KORMT31a	191616.1	84916.4	1132	KOR80	178982.5	91048.6	972
KORMT35a	172517.1	85999.2	1020	KOR82	181931.8	91243.2	962
KorMT37	168737.2	79702.1	1024	KOR88a	170316.5	80992.4	990
KORMT41A	193503.3	93598.9	1179	KOR89	174115.0	82748.4	1098
KORMT42A	189287.6	77540.4	1125	KorMT01	189639.6	94984.9	1115
KORMT43A	187473.1	80584.8	1060	korMT02	187165.6	97015.5	1182
KORMT44a	165112.2	87504.7	1004	KorMT03	189978.1	92341.1	1180
KORMT100	174308.4	93600.6	902	KorMT04	177217.6	89651.1	995
KORMT101	176440.5	93479.1	893	KorMT04(2)	168125.6	85992.9	966
KORMT102a	178541.3	92792.0	930	KorMT05	174910.6	95979.7	884
KORMT103	169603.6	92586.5	908	KorMT06	173886.4	92076.1	917
kormt104	171694.8	95459.5	889	KorMT07	172181.6	88449.6	936
kormt105	185971.1	83582.9	1049	KorMT08	176886.2	89276.3	1023
KORMT106a	189591.6	83728.1	1119	KorMT09	171565.7	92569.7	901
KORMT106b	180076.6	79780.9	1183	KorMT10	169959.5	88445.0	950
KORMT107	187659.5	86588.2	1060	KorMT11	176884.3	86632.4	1121
KorMT108	167254.7	84188.8	997	KorMT12(2)	174621.7	81499.9	1141
KORMT114	189732.0	89995.8	1236	KorMT13	168189.5	88790.6	938
KORMT115	174251.8	88134.5	967	KorMT14	170504.8	80334.3	1003
KorMT116	178421.7	85690.6	1343	KorMT15	177606.5	88267.4	1085
KORMT118	181104.1	84711.2	1181	KorMT15(2)	174006.6	87126.3	1022
KorMT119	177987.2	83803.7	1311	KorMT16	179227.9	88017.3	1192
KORMT120	179651.4	82692.5	1332	KorMT16(2)	167665.8	91988.5	941
KorMT121	181331.4	82095.0	1241	KorMT17	170042.3	82855.7	996
KORMT122	177558.3	81141.9	1304	kormt18	187590.1	84596.3	1055
KORMT123	180382.6	84106.1	1425	kormt19	187252.4	88531.2	1101
KORMTZL	191469.9	88476.1	1154	kormt20	184124.7	85213.4	1037
kor03	175100.9	89763.3	935	KORMT23	173207.9	86865.5	994
kor05	180476.2	89627.3	980	kormt26a	178264.9	87141.8	1175
KOR06	181708.1	89986.1	1000	KORMT28	173168.5	83505.3	1052
kor7	182985.8	89573.2	1015	kormt31	185540.3	87330.5	1020
kor11	171749.2	89648.9	921	KORMT34	173151.2	85310.0	1054
kor14	176372.1	88837.0	1000	kormt37	177418.6	85033.4	1304
KOR17	180605.2	88240.7	1070	kormt46	178596.8	83713.8	1296
kor18	182403.0	88067.3	1068	KORMT58	185976.3	82184.2	1048
kor19	183281.8	88023.7	1023	KORMT66	185232.8	80835.2	1037
KOR20	184925.1	88163.9	1014	kormt76	173207.9	91092.8	912
KOR21	170249.1	86560.2	968	kormtE	187182.0	89690.2	1197
kor22	171555.2	86688.4	971	kormtH	188323.0	88472.1	1141
KOR24	178953.8	89828.2	1013	KorMTm	191396.6	89859.4	1168
kor25	176265.4	86654.4	1127	korMTn	191159.1	90984.6	1163
KOR27	180198.7	86722.4	1211	korMTs	190526.5	93425.8	1162
kor29	183268.6	86818.6	1062	korC	189566.7	92602.6	1190
KOR30a	184620.8	81896.1	1059	KORD	188854.2	91407.4	1324
KOR31R	185945.3	86709.2	1056	KORF	188574.3	89510.9	1234
KOR32	170149.3	85413.5	978	korg	189991.5	89476.1	1205
kor33	171482.9	85151.3	997	korj	190216.6	88311.0	1184
kor34	172767.1	84864.5	1053	KORp	191556.5	92785.7	1163
KOR35	174766.7	85398.0	1125	KORU	190571.4	91270.9	1166
KOR36	176354.0	85031.1	1218	KORMT28n	184679.3	92498.6	984
KOR38	179089.7	85063.0	1313	pak28t	182458.8	94805.8	932
KOR39	180129.8	85415.9	1253	pak29	184194.6	94558.6	1029
kor40	182534.0	85039.2	1103	PAK31	187084.6	94279.8	1104
kor41	176303.7	83773.7	1148	PakMT27	180945.6	94868.4	888
KOR42	185566.6	84978.8	1042	PAKMT30	185568.5	94465.3	1071
KOR43	170129.5	83768.7	995	pakMT34	192982.6	94429.2	1166
kor44	171692.8	84274.9	1007	PAKAMT32	188545.6	94862.8	1068
KOR45	174799.9	84229.8	1138	pakamt33	191732.5	94368.6	1157
KOR47	179534.4	83602.5	1336				

Table MT-02 Locations of MT stations (Paka field)

Station	Easting (UTM)	Northing (UTM)	Elevation (m)	Station	Easting (UTM)	Northing (UTM)	Elevation (m)
PAK27	180758.2	95462.6	888	PakMT05	187907.7	101279.4	1659
pak28t	182271.4	95424.6	932	PakMT06	186268.2	101957.0	1518
pak29	184007.2	95165.0	1029	PakMT07	186362.4	103616.9	1429
PAK30	185381.0	95071.8	1071	PakMT09	188342.0	102693.1	1462
PAK31	186897.2	94874.0	1104	PakMT12	196107.5	101457.5	1235
PAK32	188358.1	95463.1	1068	PakMT14	182861.3	97963.3	984
PAK33	191544.9	94972.0	1157	PakMT15	181662.0	107371.1	891
PAK34	192795.0	95041.8	1166	PakMT18	189305.8	108409.9	956
PAK35	194382.3	94890.0	1184	PakMT20	180267.6	105097.4	906
PAK36	181086.9	96381.5	923	PakMT21	180830.2	100528.7	947
pak37	183002.4	96343.2	969	PakMT22	184178.5	100735.1	1164
PAK38	184756.8	96222.0	1098	PakMT23	185042.1	96934.9	1117
PAK39	186038.4	96934.2	1154	Pak102	191439.7	107043.3	977
PAK40	188405.3	96474.4	1090	PAKCRT1	186741.8	102196.4	1504
PAK41	189763.6	96350.4	1139	pkmt54R	183756.8	99579.6	1095
PAK42	191641.8	96299.9	1165	PAK13	192796.7	96233.7	1172
PAK43	194485.5	96439.2	1186	PAK34R	192894.4	94456.9	1163
PAK43A	181122.2	98023.1	928	PAK42	192226.7	95318.1	1172
PAK45	184746.0	98204.7	1147	PAK43R	193968.9	95618.0	1179
PAK46	185909.3	98004.0	1208	PAK50RR	193180.9	96986.5	1189
PAK47	188397.2	98051.3	1191	PAK55RR	186013.0	99072.9	1306
PAK48	189993.7	97924.1	1250	PAK60	181211.2	100097.3	960
PAK49	191639.9	97886.0	1165	Pak99a	187770.7	106959.5	1037
PAK51	194495.9	97945.4	1193	PAK100R	188318.0	106562.5	1050
PAK52	181067.5	99277.4	949	PAK107	187622.6	99729.5	1460
pak53	182420.0	99546.8	998	PAK108	186802.1	99093.9	1352
PAK55R	185774.3	99562.7	1300	PAK109	180198.6	99126.7	931
PAK56	189304.8	99394.0	1422	PAK110R	186926.6	96013.6	1157
PAK57	190477.4	99202.5	1327	PAK121	188101.1	98342.8	1259
PAK58	191910.1	99312.1	1322	PAK134	189867.2	97302.5	1217
PAK59	194178.3	99454.8	1209	PAK135	188219.7	99689.1	1469
PAK60	181167.7	100854.3	990	PAK145	187920.4	108447.2	950
PAK61	182421.2	101123.9	1065	PAK145B	189059.4	108732.1	941
PAK62	183671.2	100864.7	1160	PAK145C	188769.2	109593.0	933
PAK63	185688.8	100955.3	1430	PAK149A	179541.3	105207.9	887
PAK64	186115.7	100792.0	1420	PAK159	178091.8	103702.8	899
PAK65	189543.5	99888.7	1440	PAK162	177775.8	99408.3	893
PAK66	191017.1	100871.2	1483	PAK181	186966.1	110566.0	863
PAK67	192514.8	101039.1	1340	PAK189	186306.9	110391.3	859
PAK68	194210.5	101059.4	1297	PAK190C	186634.2	109597.9	891
PAK69	182521.4	102556.3	1006	PAK263	186301.2	107292.7	975
PAK70	183985.4	103040.9	1089	PAK400	180890.1	108403.9	872
PAK71	185646.7	102507.7	1466	PAK404	179781.9	104365.4	907
PAK72	191571.8	101937.5	1327	PAKA41R	189862.8	95522.7	1124
PAK73	192914.9	102293.0	1310	PAKC9	182849.2	108792.7	869
PAK74	194313.7	102504.0	1298	PAKCRT3	188647.7	100930.7	1560
PAK75	180808.1	103867.3	937	PAKE3	185423.2	108326.3	929
PAK76	182482.3	103973.5	1001	PAKMT03R	187230.9	97375.2	1201
PAK77	184131.9	104322.6	1110	PK47A	187707.1	96956.7	1154
PAK78	185765.6	104143.0	1362	PK101B	189002.1	106863.2	1050
PAK79R	186941.4	104169.7	1243	PK124	188839.2	100512.5	1655
PAK80	188785.6	104152.9	1333	PK125	189723.0	99005.6	1373
PAK81	189853.4	104527.1	1153	PK129	188299.6	98880.6	1316
PAK82	191913.4	103501.8	1217	PK138	188869.5	99636.4	1441
PAK83	193244.2	103921.9	1131	PK139	186436.5	98470.1	1273
PAK84	194379.8	104016.3	1228	PK140	186911.9	108733.9	939
PAK85	180939.3	105388.9	910	PK154	178226.4	105528.7	888
PAK86	182393.8	105513.7	949	PK154A	177657.0	105541.5	876
PAK87	184164.0	105788.9	975	PK154C	177381.0	104877.7	881
PAK88	185454.2	105529.7	1090	PK155	181921.4	105777.7	912
PAK89R	186886.9	105642.2	1156	pk162a	177147.5	99279.7	890
PAK90	188239.2	105782.5	1090	PK402	180273.9	104309.7	914
PAK91	189650.4	106021.2	1049	PKA	181784.1	108077.3	870
PAK92	191494.2	105561.6	1029	PKA2	181475.5	109116.6	857
PAK93	193060.5	106316.6	985	PKA4	182106.3	108615.0	867
PAK94R	194848.2	105442.2	1108	pkc4	182388.6	109414.0	879
PAK95	180804.6	107119.8	872	PKd	182105.5	107582.1	887
PAK95b	181940.0	106817.5	898	PKE4	186561.6	107931.9	971
PAK97	184366.2	107003.0	961	PKE6	186398.3	108685.1	933
PAK98	185728.0	107364.6	964	KorMT01R	189830.5	93632.2	1153
PAK99	187132.5	106985.4	1023	pk492	188450.5	101890.0	1528
PAK100	188518.7	106990.4	1046	pk493	189285.8	101701.8	1572
PAK101	189787.4	107093.8	1016	pk501	179638.7	99360.8	916
PAK103	193825.2	106930.7	1097	pk508	177391.0	97997.6	891
PAK104	194772.1	107022.2	1060	pk512	186366.0	99300.2	1324
PAK105B	182897.2	108037.2	886	pk540	187604.0	103519.9	1301
PAK106r	184194.2	108527.9	892	pk541	189289.5	102458.0	1475
PakMT01	181101.3	102883.3	961	pk543	186806.6	100800.0	1545
PakMT03	187131.9	98451.9	1265				

2. Topographic Correction

Topographic effects due to irregular terrain are known to influence electromagnetic field measurements and may prevent accurate interpretation of MT data. In order to reduce these topographic effects on the MT data, the following simple procedures were applied to the MT data acquired in and around the Korosi and Chepchuk geothermal fields.

1) First, a three-dimensional resistivity model including topographic variations was constructed and apparent resistivity (Appxy-topo and Appyx-topo) and impedance phase (Phsxy-topo and Phsyx-topo) responses at each station were calculated by using a three-dimensional MT forward modelling code. The resistivity of each block in the model was set to an average value of all the apparent resistivity values in a frequency range between 100 Hz and 0.01778 Hz.
2) Second, a three-dimensional resistivity model without topographic variations (flat earth) was constructed and apparent resistivity (Appxy-flat and Appyx-flat) and impedance phase (Phsxy-flat and Phsyx-flat) responses at each station were calculated by using a three-dimensional MT forward modelling code. The resistivity of each block in the model was set to an average value of all the apparent resistivity values in a frequency range between 100 Hz and 0.01778 Hz.
3) Finally, topography correction factors for apparent resistivity and impedance phase values at each station were calculated. These factors were then applied to the original observed apparent resistivity and impedance phase values in order to obtain corrected apparent resistivity and impedance phase values at each station in a frequency range between 100 Hz and 0.01778 Hz.

   Appxy-corr = Appxy-obs * (Appxy-flat / Appxy-topo)

   Appyx-corr = Appyx-obs * (Appyx-flat / Appxyxtopo)

   Phsxy-corr = Phsxy-obs + (Phsxy-flat - Phsxy-topo)

   Phsyx-corr = Phsyx-obs + (Phsyx-flat - Phsyx-topo)

   Where,

   Appxy-corr, Appyx-corr : Corrected apparent resistivity for xy and yx polarizations

   Phsxy-corr, Phsyx-corr : Corrected impedance phase for xy and yx polarizations

   Appxy-obs, Appyx-obs : Observed apparent resistivity for xy and yx polarizations

   Phsxy-obs, Phsyx-obs : Observed impedance phase for xy and yx polarizations

   Appxy-topo, Appyx-topo : Calculated apparent resistivity using a resistivity model including topographic variations for xy and yx polarizations

   Phsxy-topo, Phsyx-topo : Calculated impedance phase using a resistivity model including topographic variations for xy and yx polarizations

   Appxy-flat, Appyx-flat : Calculated apparent resistivity using a flat resistivity model for xy and yx polarizations

   Phsxy-flat, Phsyx-flat : Calculated impedance phase using a flat resistivity model for xy and yx polarizations

3. Static Shift Correction for MT data

Very shallow, small-scale inhomogeneities with dimensions much less than the skin depth at the highest recorded frequency can produce a shift in the log-log plot of the apparent resistivity versus frequency, moving it parallel to the undistorted curve. This parallel shift is commonly referred to as a static shift. Removing this effect from the data is important in interpreting the subsurface resistivity structure.

Since TEM is measuring a secondary magnetic field, it is relatively unaffected by local surface anomalies and also less affected by topographical conditions on the surface compared with MT. TEM data has high resolution for shallow resistivity structures (effective to a depth of approximately 300m below the surface) where MT data cannot predict the shallow zone in as much detail as TEM. Thus TEM data was utilized for correcting static shift problems in the MT data acquired in and around the Korosi and Chepchuk geothermal fields.

The following method was primarily employed to remove the static shift effect in the data processing.

a) First, one dimensional layered subsurface resistivity structure at shallow depths was analysed by GDC at each station by utilizing a one dimensional resistivity inversion technique using TEM data

b) MT apparent resistivity responses for frequencies between 1,000Hz and 10Hz were calculated using the one dimensional layered subsurface resistivity structure obtained in a) above

c) MT apparent resistivity curves and the apparent resistivity responses obtained from TEM data were displayed simultaneously, and the MT apparent resistivity curves were shifted up or down so that the MT apparent resistivity curves closely matched the apparent resistivity response obtained by TEM data for the high frequency range

d) Static shift correction factors were estimated from the difference between the shifted apparent resistivity values in step c) and the original observed apparent resistivity values

Apparent resistivity data corrected using the static shift correction factors was used for the three-dimensional resistivity inversion analysis. The static shift correction factors applied for MT data in the Korosi and Chepchuk field and the static shift correction factors applied for MT data in Paka fields are listed in Table MT-03 and Table MT-04 respectively.

The 3D MT inversion in the data analysis utilized the impedance values (Zxy and Zyx) after static shift correction and topography correction.

Table MT-03 Static shift correction values (Korosi and Chepchuk field)

Station	Static shift xy	Static shift yx	Station	Static shift xy	Static shift yx
BARMT02	1.188	1.138	KOR48	1.323	0.882
BarMT03	0.866	0.962	kor49	2.790	1.581
BARMT19	1.466	1.314	KOR50	2.634	1.646
BarMT31	1.166	1.115	KOR51	1.556	1.556
BARMT39	1.073	1.073	KOR52	0.674	0.898
BARMT41Ar	1.333	6.420	KOR53	4.433	6.915
KORMT03a	1.538	1.230	KOR54	1.324	0.916
KORMT09a	1.658	3.505	KOR55	1.937	1.259
KORMT13a	1.393	0.895	KOR56	0.831	0.748
KORMT14a	1.028	0.841	kor57	1.933	2.035
KorMT15a	1.150	1.150	kOR59	0.786	0.786
KORMT18A	0.909	0.808	KOR60	1.217	1.106
KORMT19a	1.175	0.784	kor61	1.186	3.235
KORMT21a	1.341	1.341	kor62	1.337	0.748
KORMT25B	0.732	1.172	KOR64	3.064	2.451
KORMT28A	0.814	1.424	KOR74R	1.001	1.041
KORMT29a	1.277	0.688	kor78	1.601	1.301
KORMT31a	1.097	1.447	KOR80	1.351	1.255
KORMT35a	0.745	1.242	KOR82	2.292	2.292
KorMT37	1.065	0.581	KOR88a	2.088	2.187
KORMT41A	1.011	1.685	KOR89	1.407	1.407
KORMT42A	1.041	1.249	KorMT01	2.154	2.997
KORMT43A	1.032	1.125	korMT02	2.341	1.658
KORMT44a	1.381	1.480	KorMT03	2.125	0.647
KORMT100	0.637	0.882	KorMT04	0.916	0.576
KORMT101	0.839	0.944	KorMT04(2)	3.018	1.107
KORMT102a	1.582	1.484	KorMT05	1.422	0.812
KORMT103	0.792	1.189	KorMT06	2.542	1.224
kormt104	1.295	0.896	KorMT07	1.181	0.885
kormt105	2.209	0.947	KorMT08	0.954	1.741
KORMT106a	1.792	1.095	KorMT09	1.383	1.284
KORMT106b	1.279	0.757	KorMT10	0.958	1.058
KORMT107	1.282	0.986	KorMT11	3.600	2.200
KorMT108	1.482	1.285	KorMT12(2)	6.499	2.315
KORMT114	0.808	0.856	KorMT13	1.012	1.114
KORMT115	1.052	1.263	KorMT14	0.860	0.765
KorMT116	1.072	0.643	KorMT15	1.363	1.635
KORMT118	1.639	0.883	KorMT15(2)	0.992	1.389
KorMT119	2.876	0.575	KorMT16	1.579	0.836
KORMT120	0.605	0.880	KorMT16(2)	1.304	1.195
KorMT121	2.346	4.692	KorMT17	1.019	1.019
KORMT122	3.537	4.653	kormt18	1.247	1.055
KORMT123	1.907	0.751	kormt19	1.067	1.334
KORMTZL	1.383	0.988	kormt20	2.355	0.631
kor03	1.210	0.943	KORMT23	1.626	1.219
kor05	0.739	1.866	kormt26a	1.241	1.448
KOR06	2.519	2.939	KORMT28	0.815	1.274
kor7	2.338	1.978	kormt31	0.793	1.990
kor11	1.213	1.011	KORMT34	0.951	0.951
kor14	1.487	0.683	kormt37	1.569	1.569
KOR17	1.680	1.867	kormt46	0.763	1.192
kor18	1.188	0.925	KORMT58	1.039	1.039
kor19	1.028	1.427	KORMT66	0.931	1.171
KOR20	0.863	0.953	kormt76	0.911	0.911
KOR21	1.369	1.369	kormtE	0.654	1.335
kor22	0.950	0.528	kormtH	1.367	1.998
KOR24	0.753	1.290	KorMTm	3.505	2.838
kor25	1.146	1.037	korMTn	1.671	1.018
KOR27	1.026	2.222	korMTs	0.962	0.642
kor29	1.931	1.931	korC	1.776	4.933
KOR30a	2.142	0.750	KORD	0.569	1.056
KOR31R	0.964	1.166	KORF	0.603	0.905
KOR32	1.314	1.142	korg	0.774	0.663
kor33	0.877	1.371	korj	0.596	0.476
kor34	1.139	1.139	KORp	0.860	0.968
KOR35	2.138	2.040	KORU	1.947	1.947
KOR36	3.597	1.609	KORMT28n	0.738	2.009
KOR38	0.482	1.446	pak28t	1.182	1.182
KOR39	0.457	1.980	pak29	1.398	1.677
kor40	1.335	0.970	PAK31	0.423	1.089
kor41	1.243	2.309	PakMT27	2.558	2.712
KOR42	1.006	0.910	PAKMT30	0.873	0.698
KOR43	1.401	1.926	pakMT34	3.134	1.880
kor44	0.730	1.004	PAKAMT32	1.000	1.105
KOR45	4.223	1.854	pakamt33	0.332	0.608
KOR47	2.298	2.941			

Table MT-04 Static shift correction values (Paka field)

Station	Static shift xy	Static shift yx	Station	Static shift xy	Static shift yx
PAK27	2.379	2.577	PakMT05	2.741	5.482
pak28t	2.079	2.079	PakMT06	1.185	1.137
pak29	1.587	1.904	PakMT07	1.455	1.662
PAK30	0.207	0.166	PakMT09	1.537	1.537
PAK31	0.604	1.509	PakMT12	0.827	0.786
PAK32	1.423	1.708	PakMT14	1.083	1.131
PAK33	0.549	0.998	PakMT15	0.945	1.134
PAK34	2.776	1.542	PakMT18	2.087	1.542
PAK35	1.411	1.663	PakMT20	0.862	1.006
PAK36	1.624	1.147	PakMT21	1.026	1.077
pak37	0.363	0.311	PakMT22	1.270	1.752
PAK38	4.453	2.163	PakMT23	0.921	1.439
PAK39	1.841	1.595	Pak102	1.482	2.646
PAK40	3.259	4.345	PAKCRT1	0.820	1.383
PAK41	2.001	2.477	pkmt54R	3.118	1.559
PAK42	0.702	0.439	PAK13	0.497	0.994
PAK43	1.032	0.928	PAK34R	1.681	1.978
PAK43A	1.446	1.726	PAK42	1.839	0.845
PAK45	0.979	1.031	PAK43R	0.809	1.163
PAK46	2.213	0.719	PAK50RR	0.710	1.466
PAK47	2.348	6.574	PAK55RR	1.843	1.570
PAK48	1.327	1.837	PAK60	1.086	0.802
PAK49	1.324	0.662	Pak99a	1.408	1.056
PAK51	0.734	0.596	PAK100R	2.311	2.512
PAK52	1.045	0.889	PAK107	1.093	0.519
pak53	1.949	3.118	PAK108	1.180	2.486
PAK55R	5.129	2.137	PAK109	0.537	0.831
PAK56	1.358	4.179	PAK110R	0.560	0.560
PAK57	2.965	2.965	PAK121	1.459	1.852
PAK58	1.520	2.229	PAK134	1.037	1.320
PAK59	2.924	2.339	PAK135	1.115	1.540
PAK60	1.418	1.229	PAK145	1.309	1.164
PAK61	1.386	2.033	PAK145B	1.096	0.548
PAK62	1.971	1.689	PAK145C	2.680	1.787
PAK63	0.936	4.212	PAK149A	0.967	0.870
PAK64	3.695	0.924	PAK159	0.964	1.065
PAK65	1.589	1.873	PAK162	1.834	2.344
PAK66	1.733	0.476	PAK181	2.906	3.487
PAK67	2.073	0.829	PAK189	1.171	1.081
PAK68	1.280	1.625	PAK190C	2.102	2.417
PAK69	1.700	0.850	PAK263	1.135	1.014
PAK70	0.744	1.163	PAK400	0.859	1.050
PAK71	2.369	1.545	PAK404	0.832	1.300
PAK72	1.131	0.668	PAKA41R	2.072	2.072
PAK73	2.102	1.911	PAKC9	1.164	1.164
PAK74	1.575	0.788	PAKCRT3	3.158	5.024
PAK75	0.896	1.394	PAKE3	1.601	1.201
PAK76	1.066	1.357	PAKMT03R	1.909	2.311
PAK77	1.594	5.517	PK47A	2.083	0.932
PAK78	1.174	1.062	PK101B	1.282	2.473
PAK79R	2.079	2.970	PK124	3.646	0.938
PAK80	1.178	0.785	PK125	1.383	2.028
PAK81	1.603	1.106	PK129	1.117	3.033
PAK82	0.821	1.314	PK138	1.510	1.342
PAK83	1.491	2.621	PK139	1.295	1.657
PAK84	1.301	2.914	PK140	1.494	1.892
PAK85	1.234	1.646	PK154	0.846	0.935
PAK86	1.016	1.016	PK154A	1.196	1.196
PAK87	0.725	1.315	PK154C	0.952	0.862
PAK88	1.555	1.710	PK155	2.017	1.467
PAK89R	2.435	1.507	pk162a	3.044	2.403
PAK90	2.387	3.938	PK402	0.890	0.890
PAK91	4.324	3.075	PKA	1.796	1.524
PAK92	1.539	1.624	PKA2	1.957	1.957
PAK93	2.736	2.105	PKA4	1.656	1.405
PAK94R	0.660	0.508	pkc4	1.362	1.412
PAK95	0.867	1.020	PKd	0.796	0.885
PAK95b	0.759	1.366	PKE4	0.805	0.890
PAK97	0.924	1.017	PKE6	1.008	0.912
PAK98	2.338	2.542	KorMT01R	1.716	2.080
PAK99	1.530	2.326	pk492	2.950	3.540
PAK100	4.294	0.791	pk493	0.650	0.130
PAK101	1.411	7.589	pk501	1.492	1.492
PAK103	0.953	1.049	pk508	0.086	0.774
PAK104	0.705	1.258	pk512	0.939	1.490
PAK105B	0.680	1.569	pk540	0.936	1.498
PAK106r	3.088	0.655	pk541	2.395	1.916
PakMT01	0.863	0.911	pk543	4.903	2.302
PakMT03	1.890	1.155			

4. Three Dimensional Resistivity Inversion Scheme

1) Concept of 3D Resistivity Modeling

In three-dimensional modeling, a three-dimensional resistivity structure whose resistivity distribution varies in the x and y (horizontal) directions and the z (vertical) direction, as shown in Fig. MT-01, is assumed. Resistivity values of each block in the 3D resistivity model are determined by iterating the calculation to minimize the value of Σ ((observed impedance values) – (calculated impedance values))^2 . This analysis is expected to lead to a more accurate subsurface resistivity model than that derived from 1D and 2D resistivity analysis.

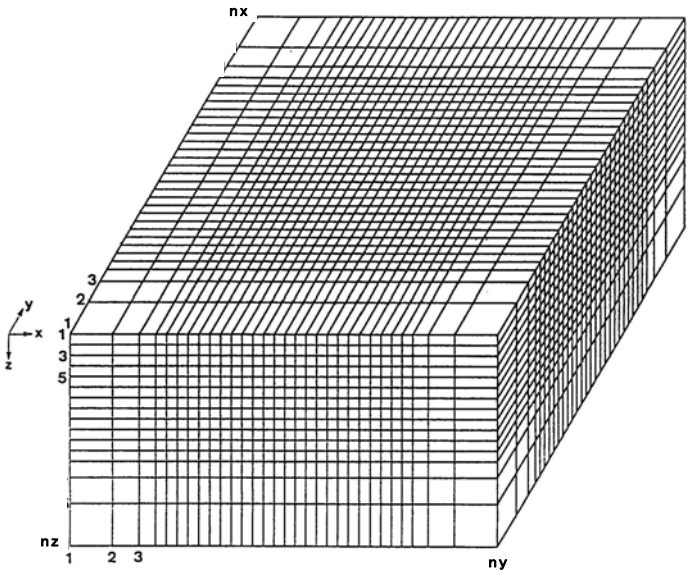

Fig. MT-01 Conceptual illustration of mesh for 3D Resistivity Modeling using the finite-difference method

2) Basic Theory of 3D Resistivity Modeling

In the forward modeling of the electromagnetic field, the earth is divided into a number of blocks of constant conductivity and so the forward modeling method needs to have the ability to handle a variety of conductivity values for the block in the model. The 3D electromagnetic field can be explained by Maxwell's equations shown below.

$$\nabla \times E = i\omega\mu H \qquad (1)$$

$$\nabla \times H = \sigma E \qquad (2)$$

where

ω : angular frequency

μ : magnetic permeability

σ : electric conductivity

The displacement current is ignored because it is very small. From equations (1) and (2), the following equations are derived.

$$\nabla \times (\nabla \times H) = \nabla \times \sigma E = \sigma \times \nabla \times E = k^2 H \qquad (3)$$

$$\nabla \times (\nabla \times E) = \nabla \times i\omega\mu H = i\omega\mu \times \nabla \times H = k^2 E \qquad (4)$$

where

$$k^2 = i\omega\mu\sigma$$

After introducing the orthogonal coordinate system, (3) and (4) lead to equations (5) and (6) respectively.

$$\left.\begin{aligned} &\partial^2 Hx/\partial y^2 + \partial^2 Hx/\partial z^2 - \partial^2 Hy/\partial x\partial y - \partial^2 Hz/\partial x\partial z - k^2 Hx = 0 \\ &\partial^2 Hy/\partial x^2 + \partial^2 Hy/\partial z^2 - \partial^2 Hx/\partial y\partial x - \partial^2 Hz/\partial y\partial z - k^2 Hy = 0 \\ &\partial^2 Hz/\partial x^2 + \partial^2 Hz/\partial y^2 - \partial^2 Hx/\partial z\partial x - \partial^2 Hz/\partial z\partial y - k^2 Hz = 0 \end{aligned}\right\} \quad (5)$$

$$\left.\begin{aligned} &\partial^2 Ex/\partial y^2 + \partial^2 Ex/\partial z^2 - \partial^2 Ey/\partial x\partial y - \partial^2 Ez/\partial x\partial z - k^2 Ex = 0 \\ &\partial^2 Ey/\partial x^2 + \partial^2 Ey/\partial z^2 - \partial^2 Ex/\partial y\partial x - \partial^2 Ez/\partial y\partial z - k^2 Ey = 0 \\ &\partial^2 Ez/\partial x^2 + \partial^2 Ez/\partial y^2 - \partial^2 Ex/\partial z\partial x - \partial^2 Ez/\partial z\partial y - k^2 Ez = 0 \end{aligned}\right\} \quad (6)$$

In a finite-difference scheme on a staggered-grid (Fig. MT-02), the solution region (including air) is discretized into rectangular cells (Fig. MT-01). To calculate the electric fields (Ex, Ey and Ez), the three equations in (6) should be solved simultaneously.

In solving the equations in (6) simultaneously, the tangential electric field on the boundaries of the model for each appropriate source polarization values must be assigned. These boundary values come from a one-dimensional (horizontally layered) calculation. The values obtained at the positions corresponding to the boundaries of the 3D model are then used as boundary values for the 3D electromagnetic forward modeling of MT responses. In addition, seven air layers were added on the top of the Earth model with a roughly logarithmically increasing thickness for each air layer. The layers should be extended far enough above Earth to allow the longest wavelength perturbations to be damped out (usually a value of three times the largest wavelength of the horizontal conductivity variations in the Earth model is used). These air layers are given a finite, but high, resistivity value of 10^8 ohm-m. At the top boundary of the highest air layer, a one-dimensional plane-wave impedance for outgoing fields is used. The 3D model does not include topographic conditions, however the input impedance data has been corrected by the topographic correction described previously.

The electric field (Ex, Ey and Ez) is first solved as a total field by the finite difference method using equation (6). Then, the magnetic field (Hx, Hy and Hz) is computed from the electric field obtained. After obtaining the electric fields and magnetic fields for two polarizations (Ex1, Ey1, Hx1, Hy1 and Ex2, Ey2, Hx2, Hy2), impedance values (Zxy and Zyx) can be calculated by using the equation (7).

$$\left.\begin{aligned} &Zxy = (Ex2 \times Hx1 - Ex1 \times Hx2) / (Hx1 \times Hy2 - Hx2 \times Hy1) \\ &Zyx = (Ey1 \times Hy2 - Ey2 \times Hy1) / (Hx1 \times Hy2 - Hx2 \times Hy1) \end{aligned}\right\} \quad (7)$$

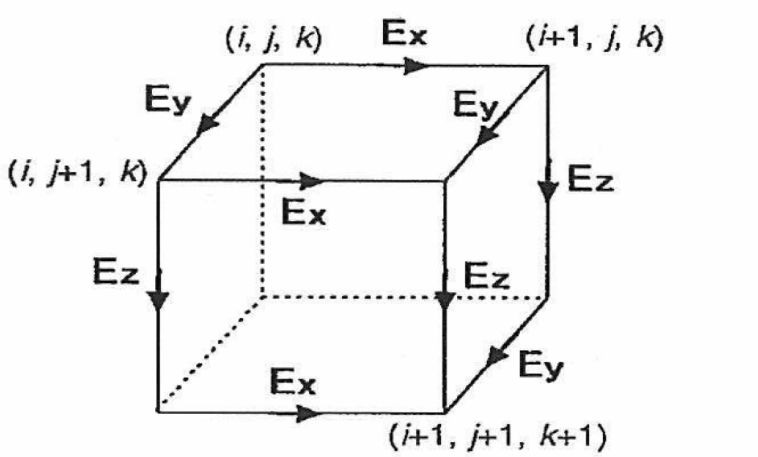

Fig. MT-02 Conceptual illustration for Staggered Grid configuration (Sasaki, Y., 1999)

3) Basic Theory in 3D Inversion Scheme

The 3D inversion algorithms use the principle of finite differences to discretize the model space into rectangular cells and follow Occam's inversion scheme to find a smooth resistivity model. Their advantage is the approach of performing the inversion in the data space, which can downsize the problem to a computational load that is manageable on a desktop computer. The resistivity of each block is treated as an unknown parameter in the inversion. The Jacobian matrix, consisting of partial derivatives (sensitivities) of MT responses with respect to block resistivities in the 3D model, should be evaluated from an estimated model at each iteration step.

To stabilize the model correction at each iteration step, smoothness regularization is adopted. The objective function W(m) to be minimized in the inversion is defined as

$$W(m) = (m-m_0)^T C_m^{-1}(m-m_0) + \lambda^{-1}((d-F(m))^T C_d^{-1}(d-F(m))) \qquad (8)$$

where m is the resistivity model parameter, m_0 is the prior model parameter, Cm is the model covariance matrix which defines the model norm, d is the observed data (impedance elements, Zxy, Zyx, Zxx and Zyy), Cd is the data covariance matrix, and F(m) is a non-linear function that works on the model m to produce MT responses. The second term of the right-hand side is for misfit minimization, and the first term is for equality minimization. The parameters λ (the so-called Lagrange multiplier) is a trade-off parameter controlling whether to heavily minimize the data misfit or the model norm. For large λ, the data misfit is less important and therefore the model norm is minimized to produce a smoother model. For small λ, the inversion tends to fit the data better, but often produces a rougher model. The model covariance matrix characterizes the smoothness of resistive variation relative to the base model.

Because of the nonlinearity of the magnetotelluric inversion problem, an iterative approach is required, based on the linearization of F(m) by using the Taylor expansion such that:

$$F(m_{i+1}) = F(m_i + \delta m) = F(m_i) + J_i \cdot (m_{i+1} - m_i) \qquad (9)$$

Where i denotes iteration number, and Ji is the Jacobian matrix (N(number of data) x M(number of model parameters)) calculated at each iteration i. Substituting (9) into (8), and applying the data space method, we obtain a series of iterative approximate solutions:

$$m_{i+1}-m_0 = C_m J_i^T C_d^{-1/2}[\lambda I + C_d d^{-1/2} J_i C_m J_i^T C_d^{-1/2}]^{-1} \times [d - F(m) + J_k(m_{i+1}-m_0)] \quad (10)$$

The final 3D model parameters (resistivity values in the 3D resistivity model blocks) can be obtained to solve equation (9) repeatedly until the misfit value between the observed data (impedance elements) and calculated data obtained from the 3D resistivity model becomes small. The approach using data space by Siripunvaraporn et al. (2005) is computationally advantageous, since in most practical applications, there are far fewer data points than model parameters.

5. General Resistivity Structure of Geothermal Fields in Volcanic Areas

The geoelectrical features of a low resistivity zone and a resistive zone at depth in and around a geothermal reservoir are as follows.

- A remarkable resistivity discontinuity can be continuously mapped from station to neighboring station. An uplifted structure is clearly identified along the resistivity discontinuity (An uplifted high resistivity zone sometimes indicates deep-seated intrusive rock. However, in a geothermal field, in cases where a remarkably low resistivity zone is distributed above the high resistivity uplifted zone, the uplifted high resistivity zone usually reflects a hydrothermally altered zone formed under high temperature conditions). The resistivity discontinuity usually reflects fractured zones along a fault.
- Resistivity values for the low resistivity zone along the resistivity discontinuity are smaller than those in the surrounding area and the low resistivity zone usually is an indication of the cap rock of the reservoir in geothermal fields. Such a zone is marked ρ_α in Fig. MT-03.
- The hotter parts of geothermal systems are characterized by higher resistivity than is seen in the overlying conductive zone, and the higher resistivity zone is often uplifted, causing a dome-like shape. The higher resistivity is due to the fact that the rock matrix is much less conductive than the saturating fluids, because low conductivity alteration products dominate the mineralization in this zone. High temperature alteration processes may increase the resistivity of some rocks by changing the resulting secondary minerals, for instance from smectite to illite or chlorite.

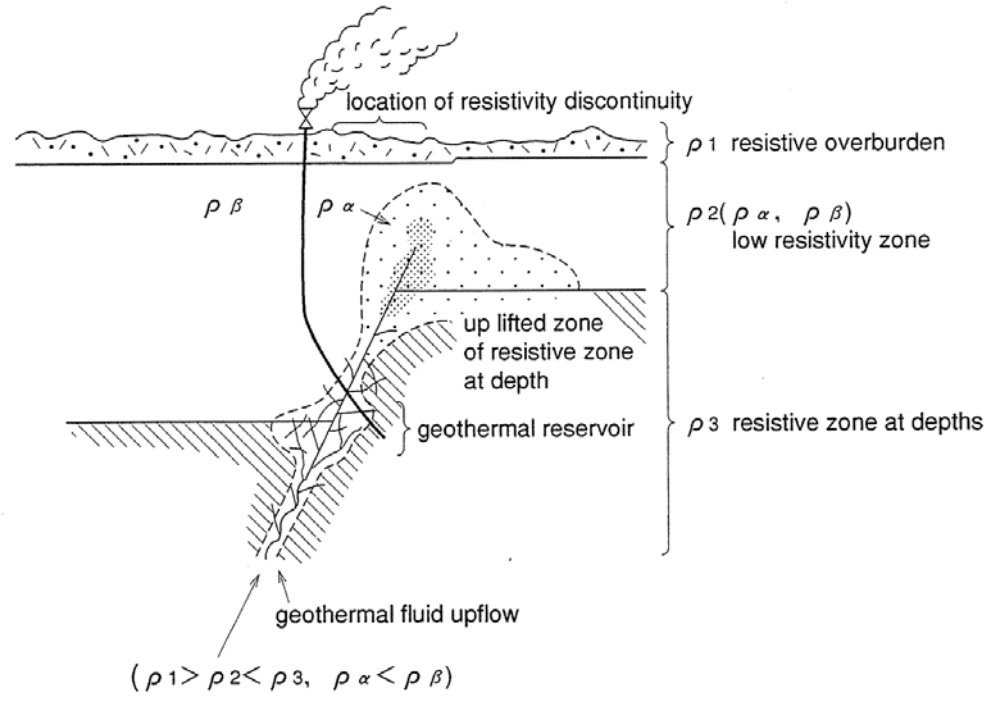

Fig. MT-03 Representative Model of Resistivity Structure in and around a Geothermal Reservoir

Considering that most geothermal reservoirs in volcanic areas are of the fracture-type and are controlled by faults, the low resistivity zone located around the faults obtained from resistivity surveys can be regarded as reflecting an impermeable zone, as a result of argillization, formed over the geothermal reservoir under temperatures ranging between approximately 70°C and 200°C. This impermeable zone functions as the cap rock of the reservoir in many geothermal fields. And a geothermal reservoir will be expected along a fault in a resistive zone at depth below a low resistivity zone. Therefore, when the drilling target is considered on the basis of the resistivity structure, the target must be decided not only on the basis of information concerning the low resistivity zones, but also after considering the geothermal structure, such as faults, and other geological and hydrological information.

6. Resistivity maps at different depths based on the three-dimensional resistivity inversion

Inverted resistivity maps at different depths both in Korosi-Chepchuk field and those in Paka field are depicted from Fig. MT-04 to Fig. MT-16 and from Fig. MT-17 to Fig. MT-29 respectively.

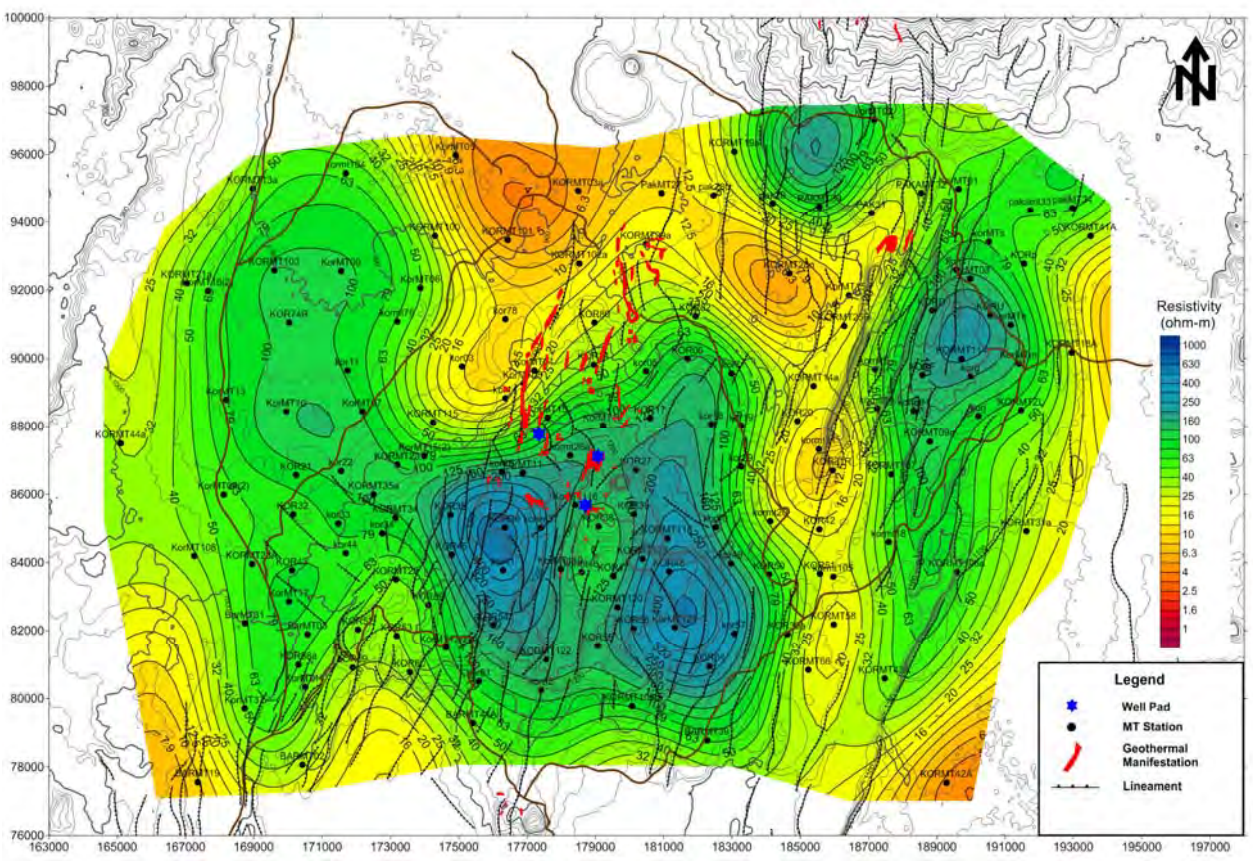

Fig. MT-04 Resistivity map at a depth of 100m (Korosi and Chepchuk field)

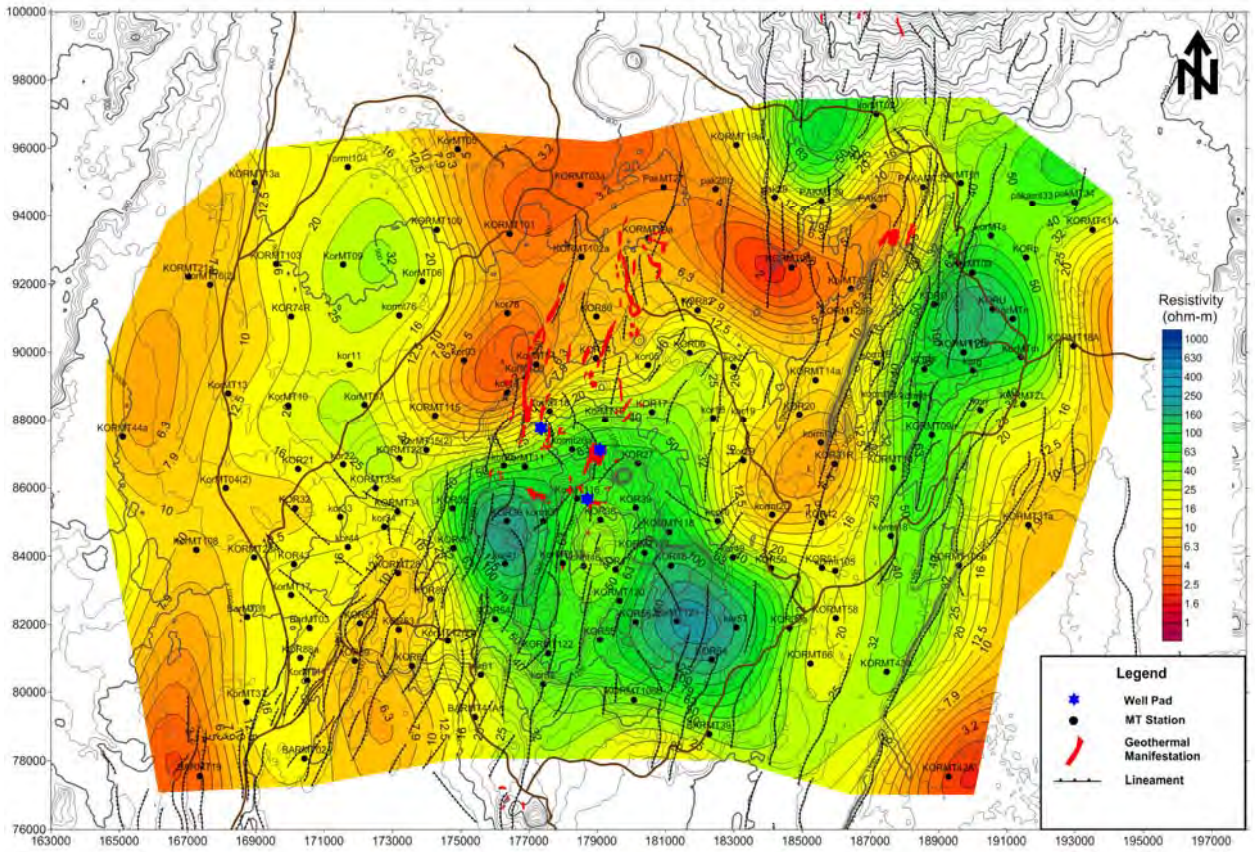

Fig. MT-05 Resistivity map at a depth of 200m (Korosi and Chepchuk field)

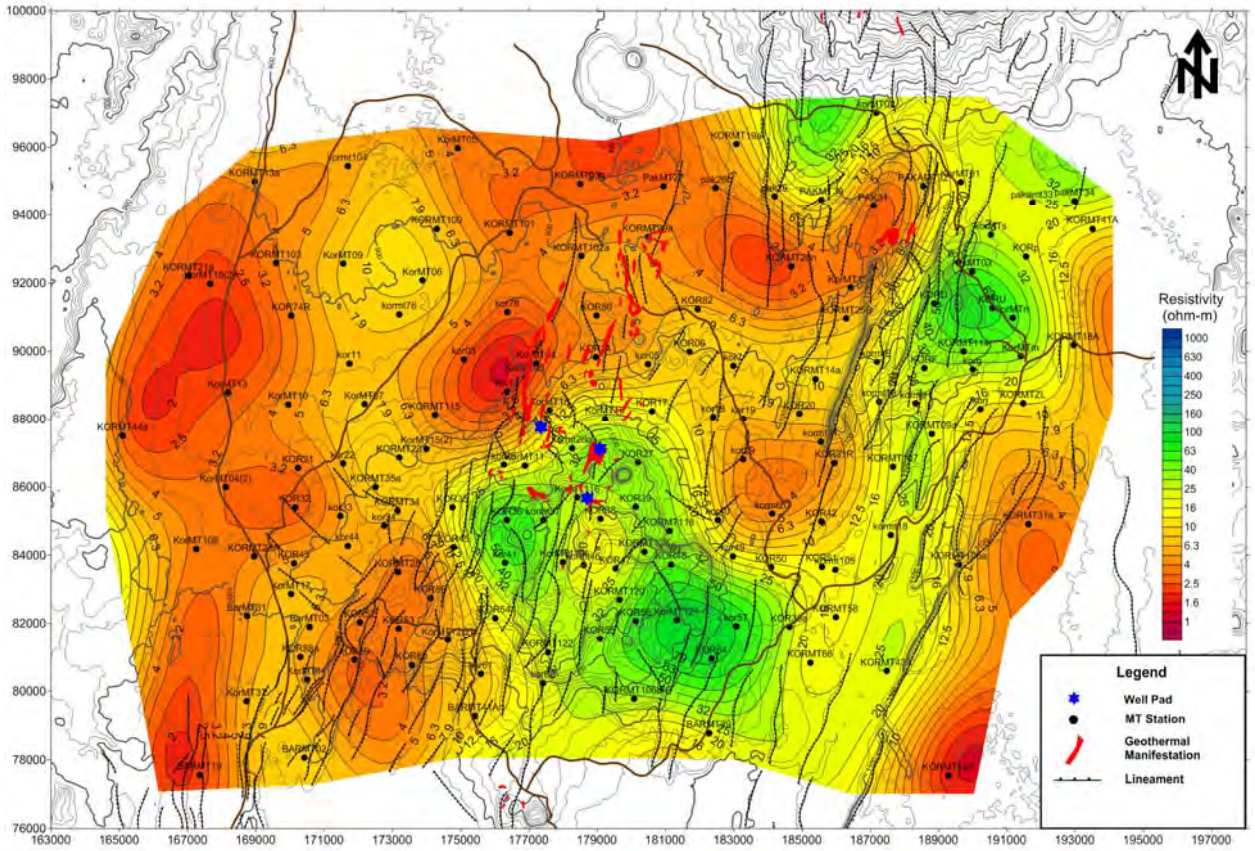

Fig. MT-06 Resistivity map at a depth of 300m (Korosi and Chepchuk field)

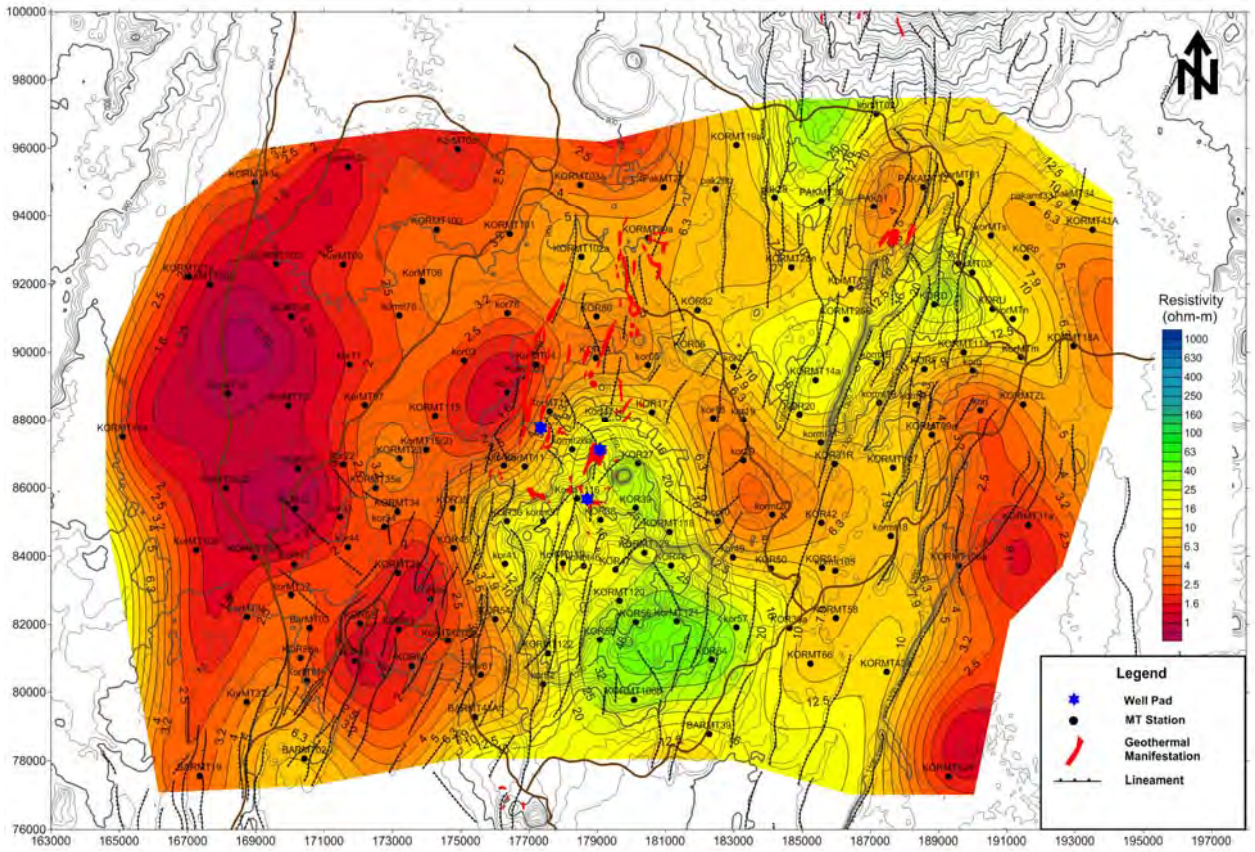

Fig. MT-07 Resistivity map at a depth of 500m (Korosi and Chepchuk field)

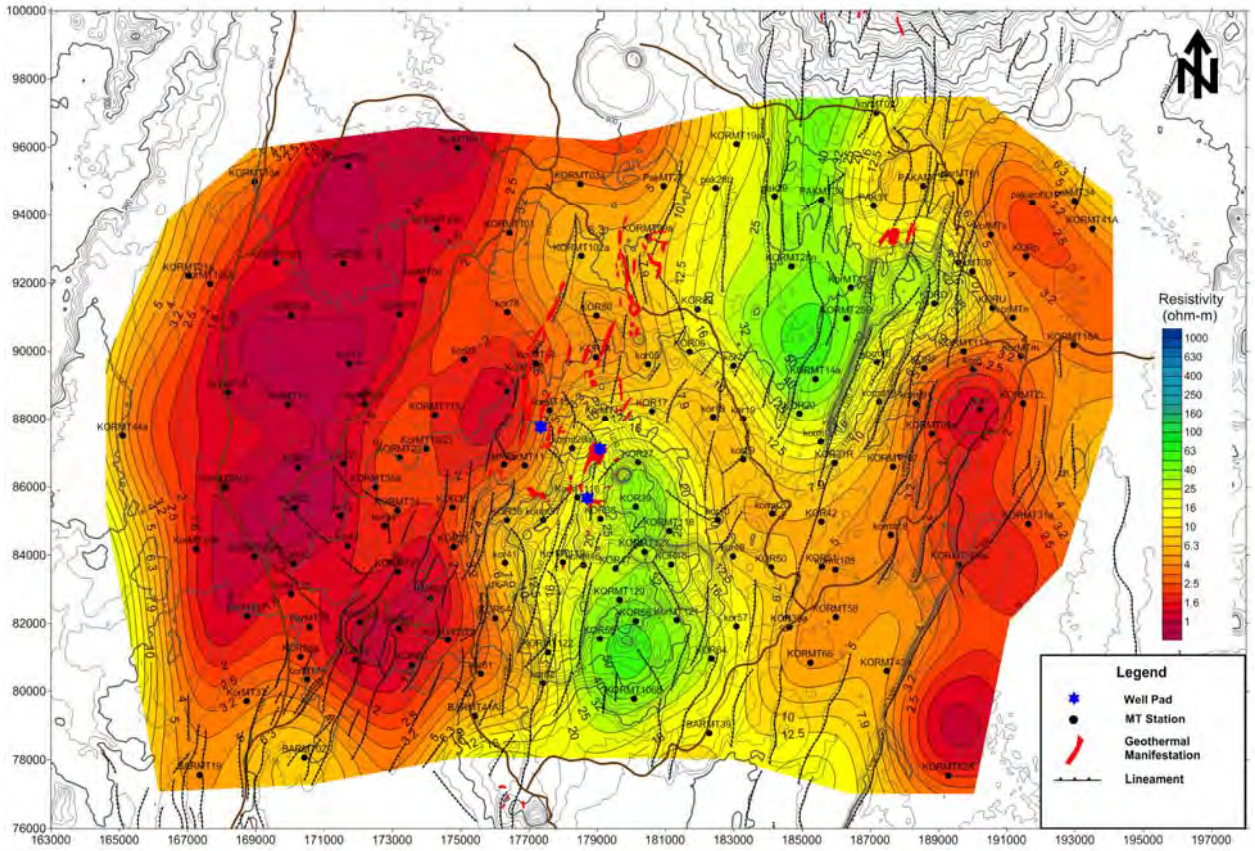

Fig. MT-08 Resistivity map at a depth of 750m (Korosi and Chepchuk field)

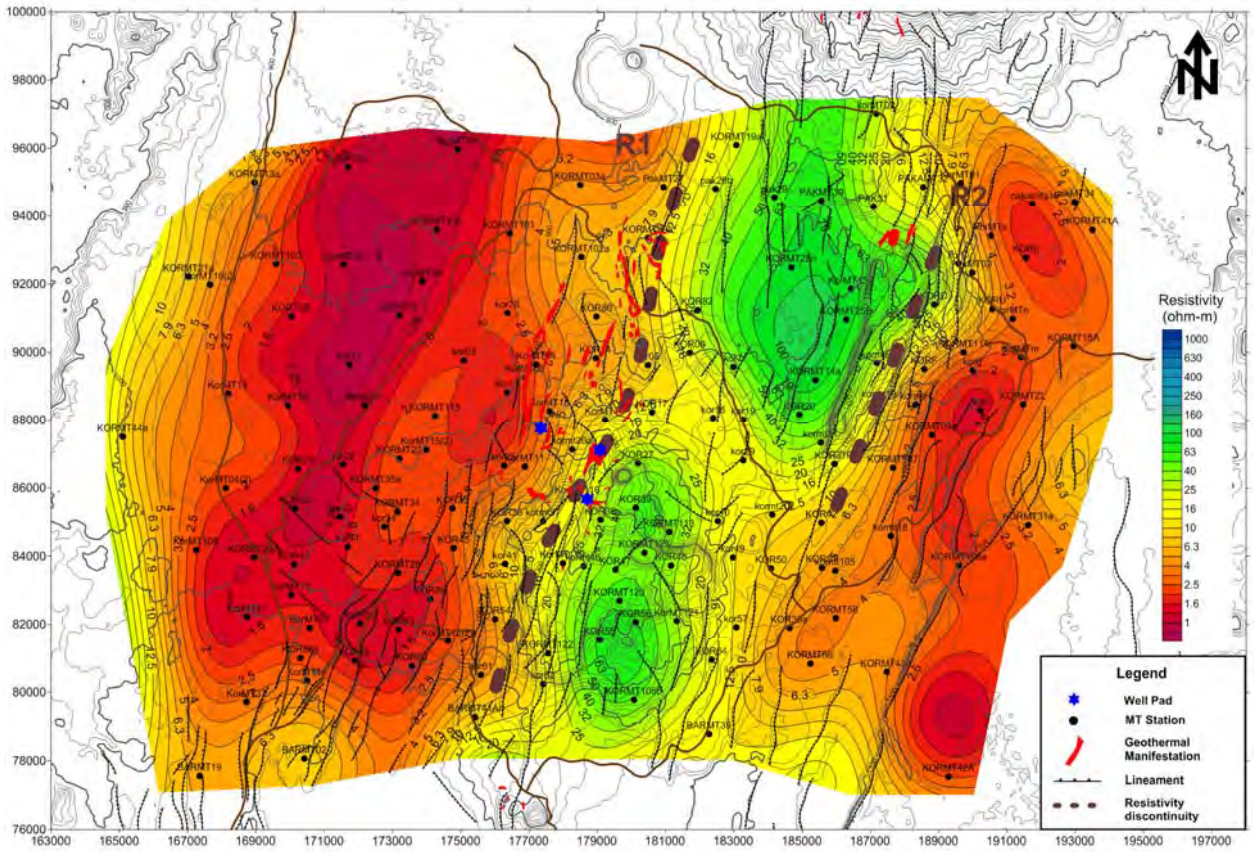

Fig. MT-09 Resistivity map at a depth of 1,000m (Korosi and Chepchuk field)

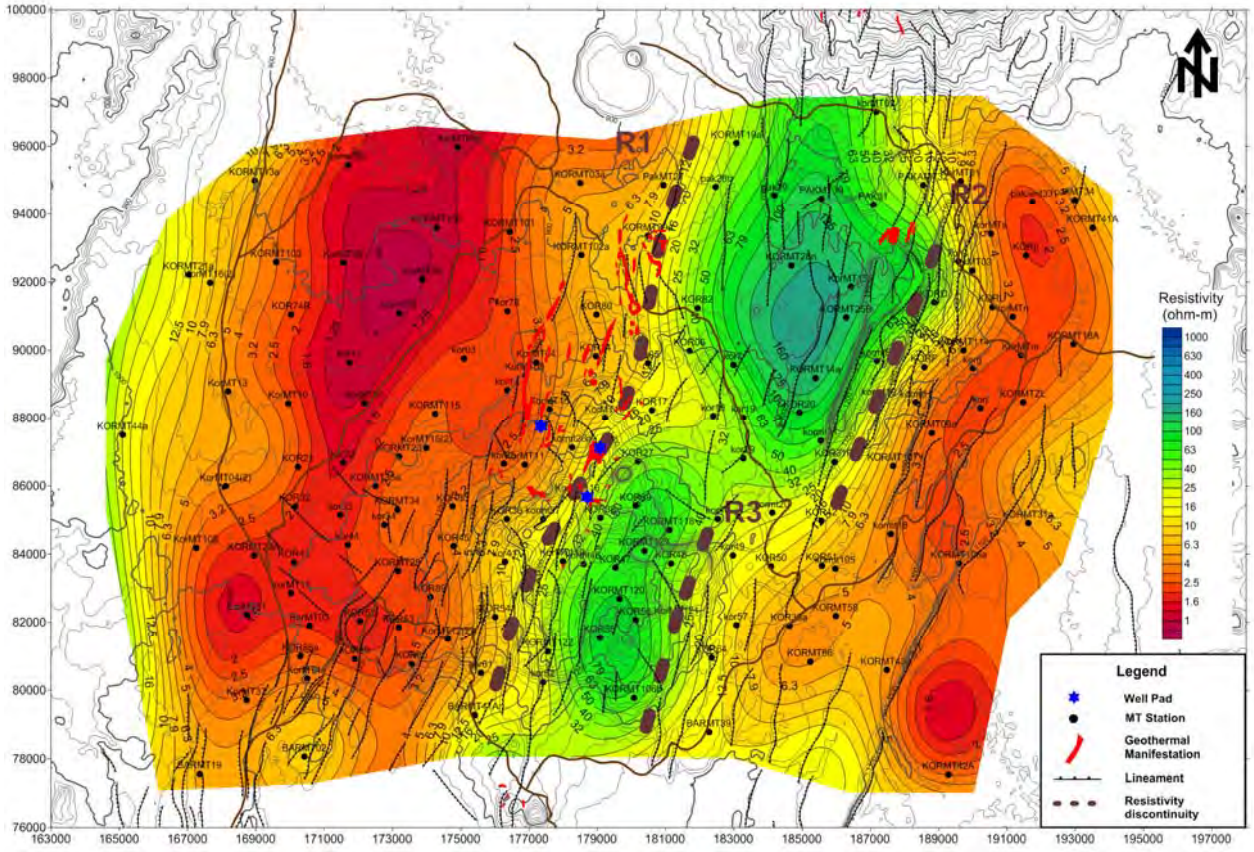

Fig. MT-10 Resistivity map at a depth of 1,250m (Korosi and Chepchuk field)

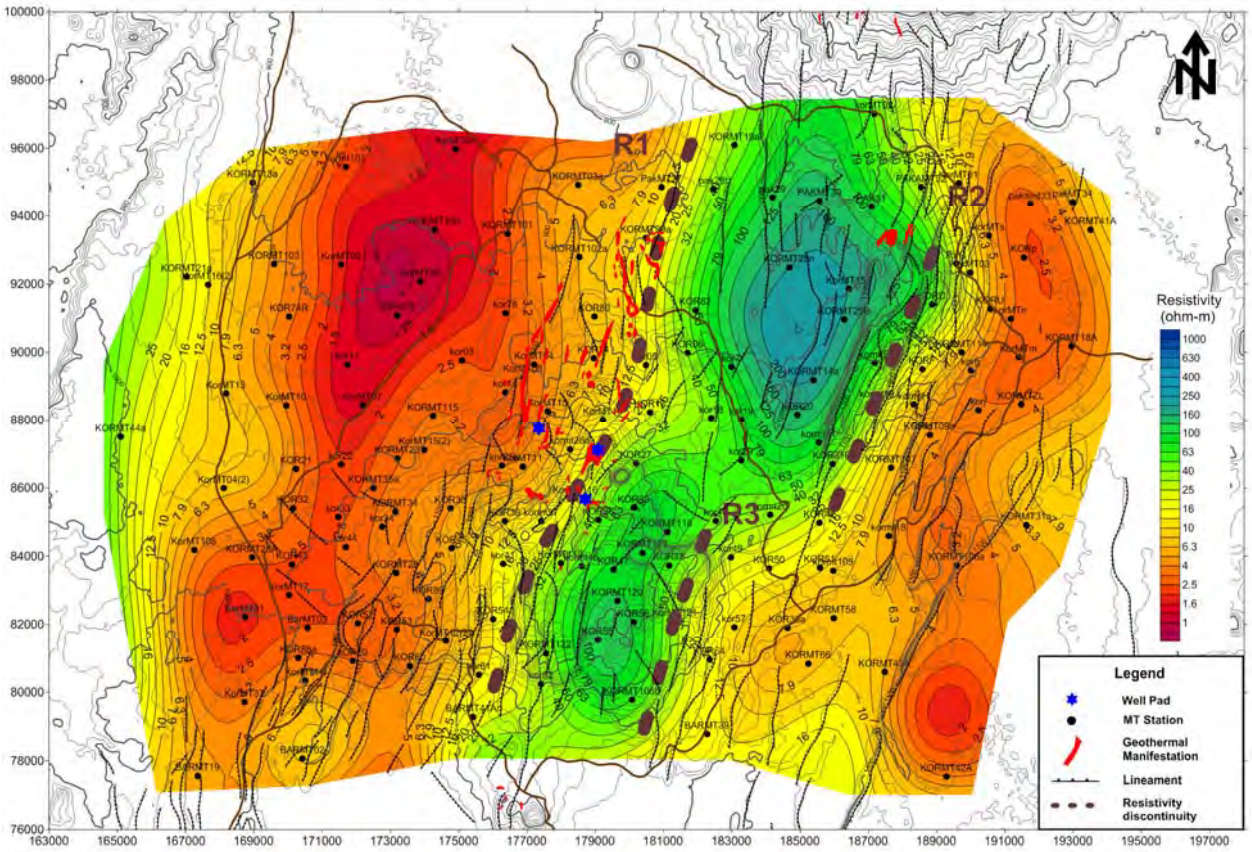

Fig. MT-11 Resistivity map at a depth of 1,500m (Korosi and Chepchuk field)

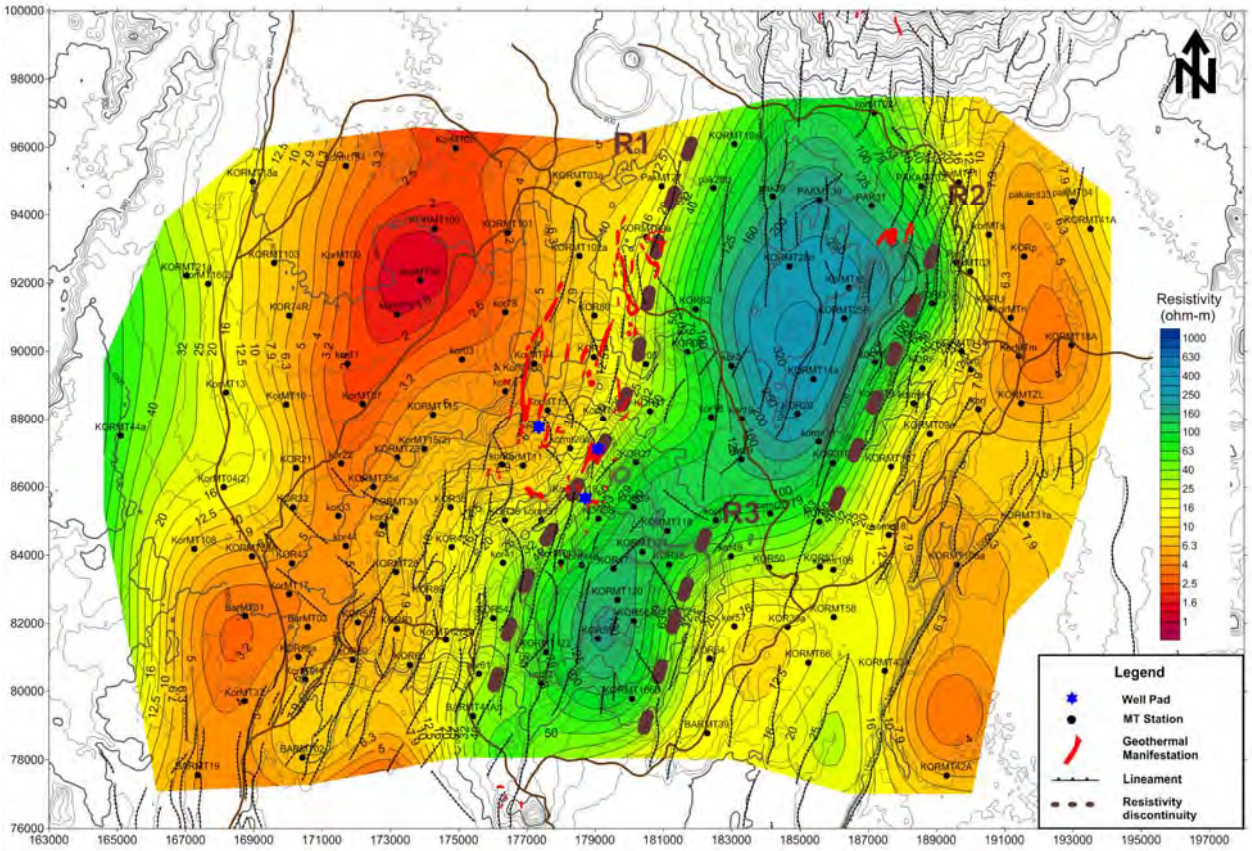

Fig. MT-12 Resistivity map at a depth of 2,000m (Korosi and Chepchuk field)

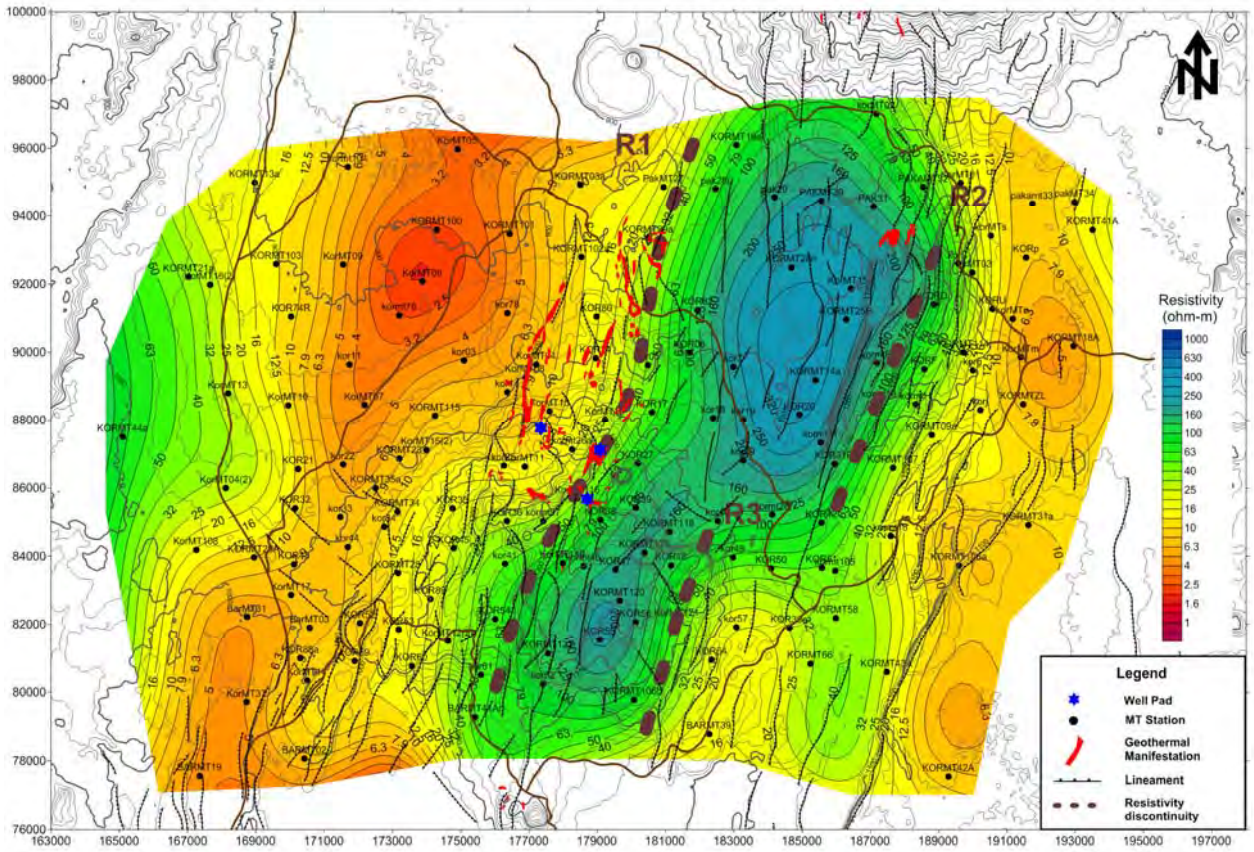

Fig. MT-13 Resistivity map at a depth of 2,500m (Korosi and Chepchuk field)

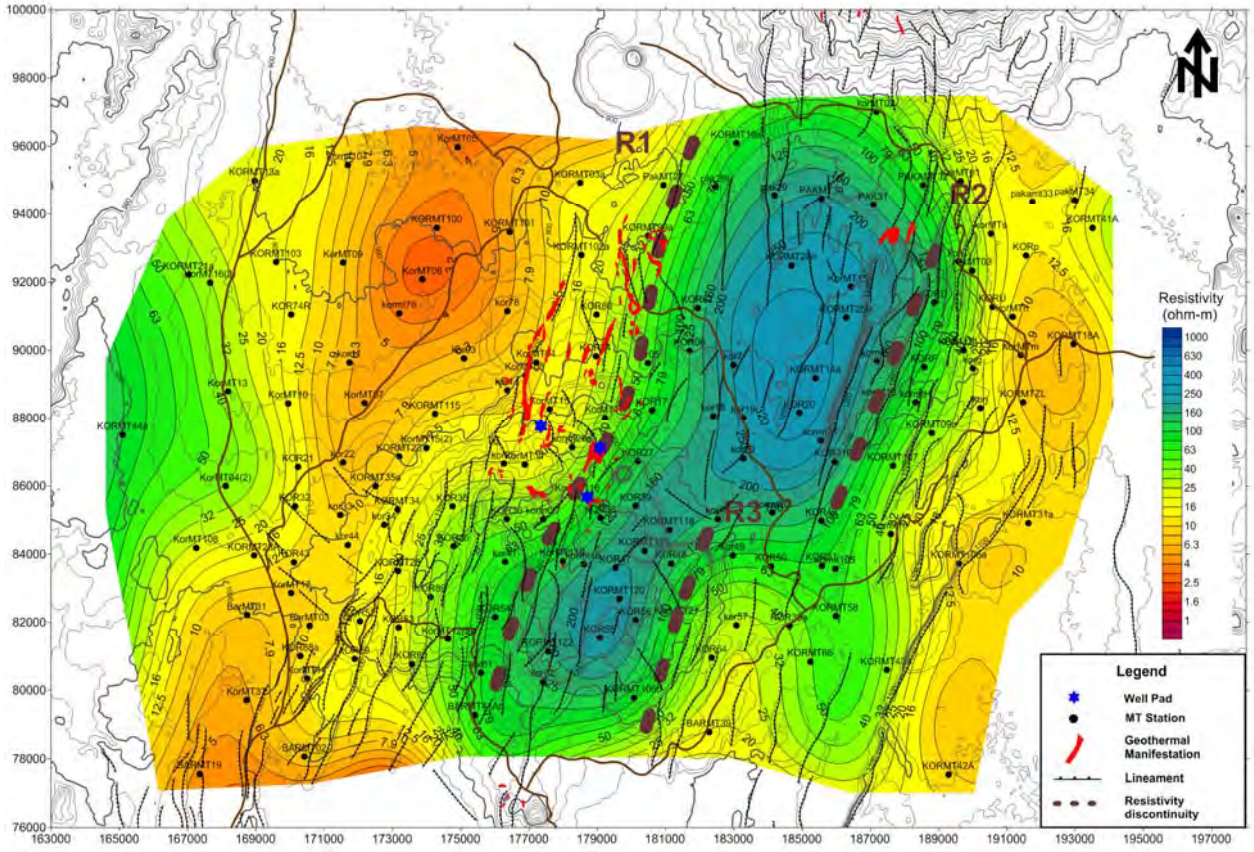

Fig. MT-14 Resistivity map at a depth of 3,000m (Korosi and Chepchuk field)

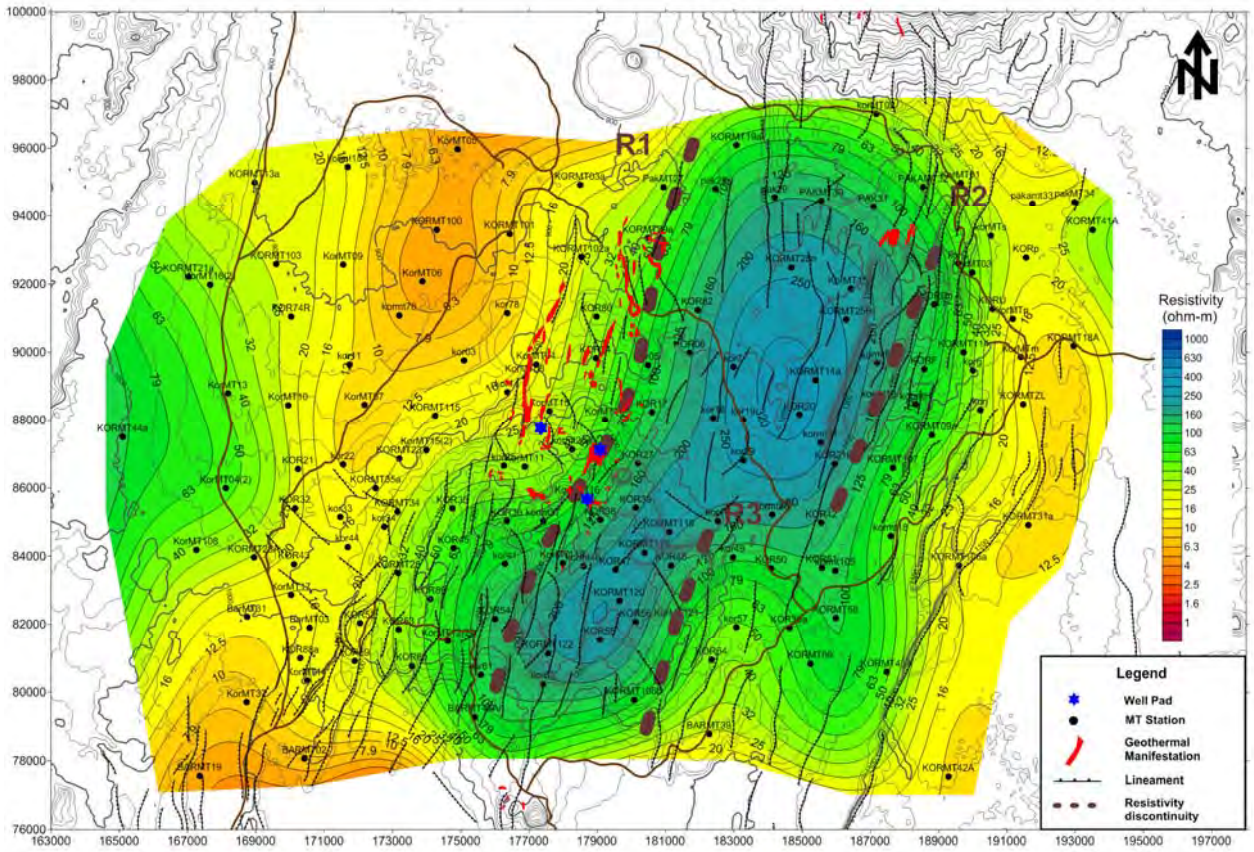

Fig. MT-15 Resistivity map at a depth of 4,000m (Korosi and Chepchuk field)

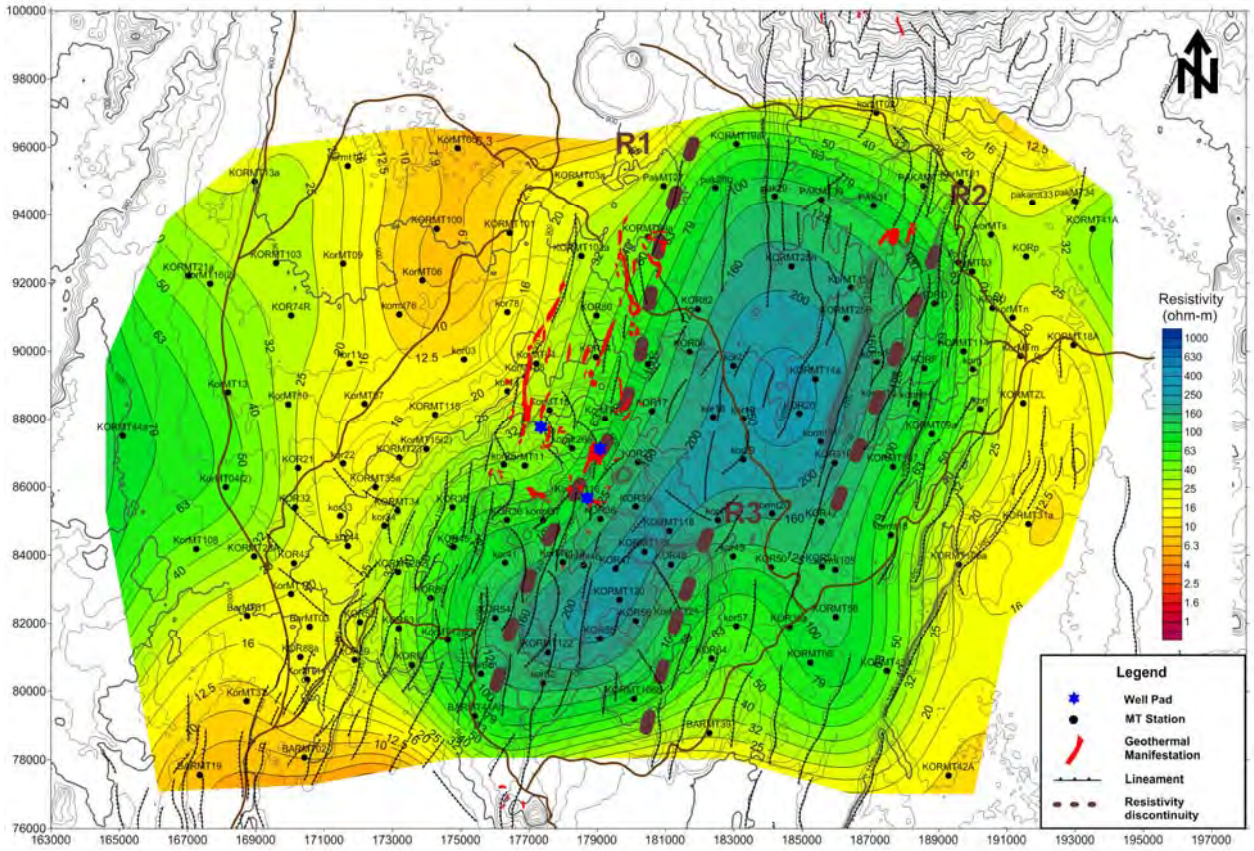

Fig. MT-16 Resistivity map at a depth of 5,000m (Korosi and Chepchuk field)

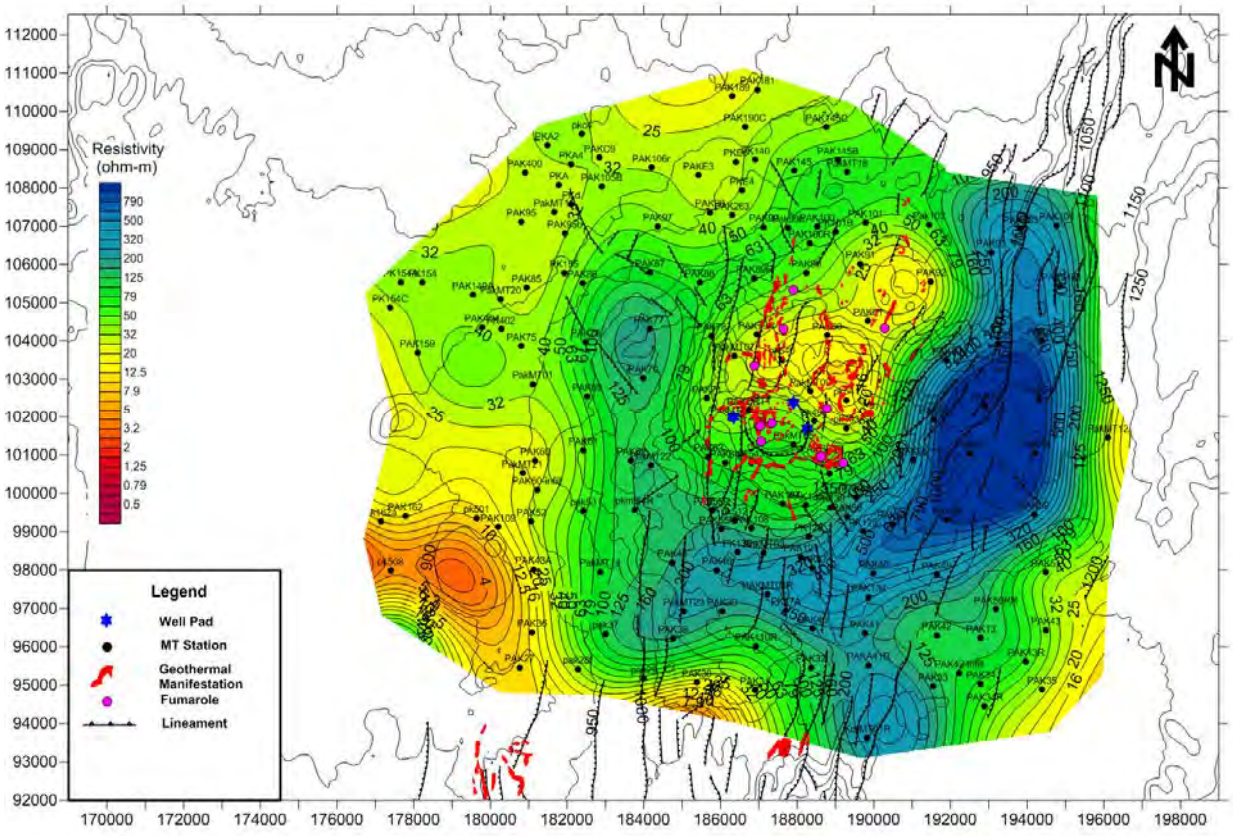

Fig. MT-17 Resistivity map at a depth of 100m (Paka field)

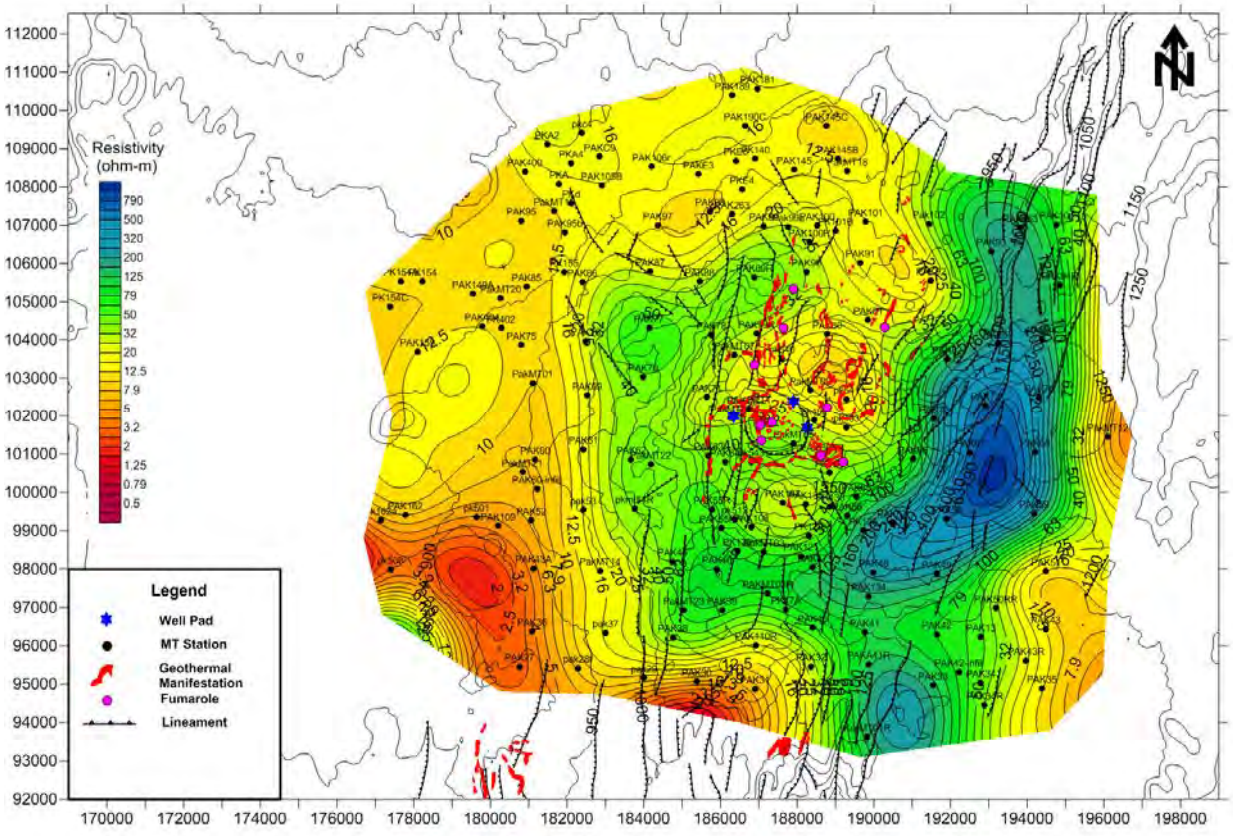

Fig. MT-18 Resistivity map at a depth of 200m (Paka field)

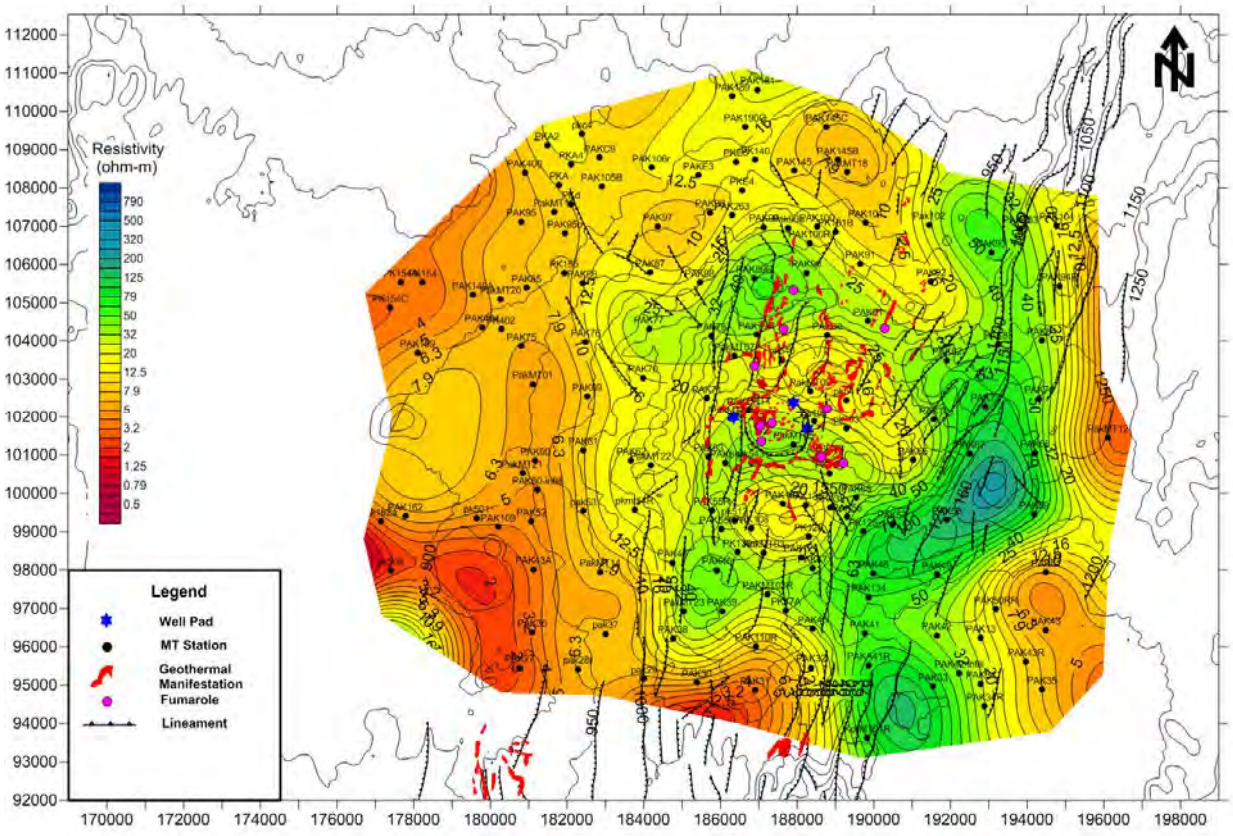

Fig. MT-19 Resistivity map at a depth of 300m (Paka field)

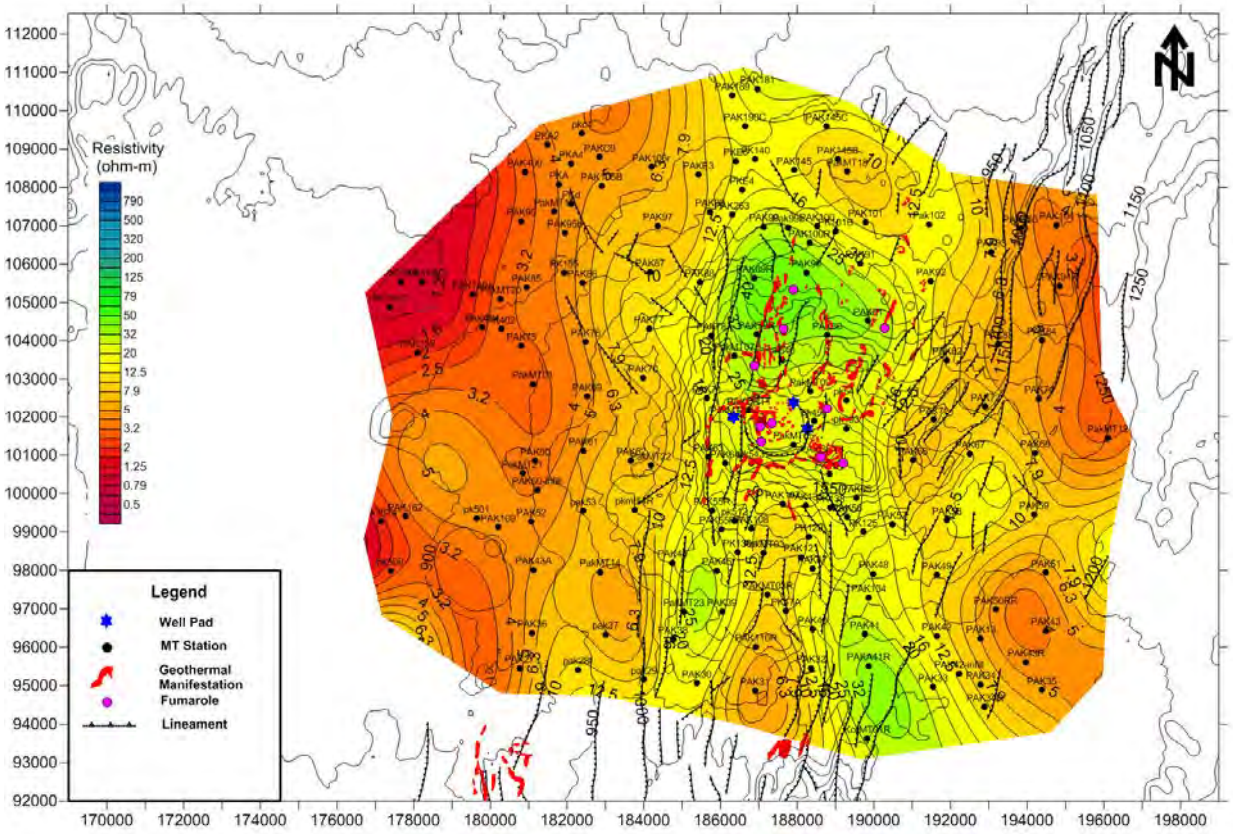

Fig. MT-20 Resistivity map at a depth of 500m (Paka field)

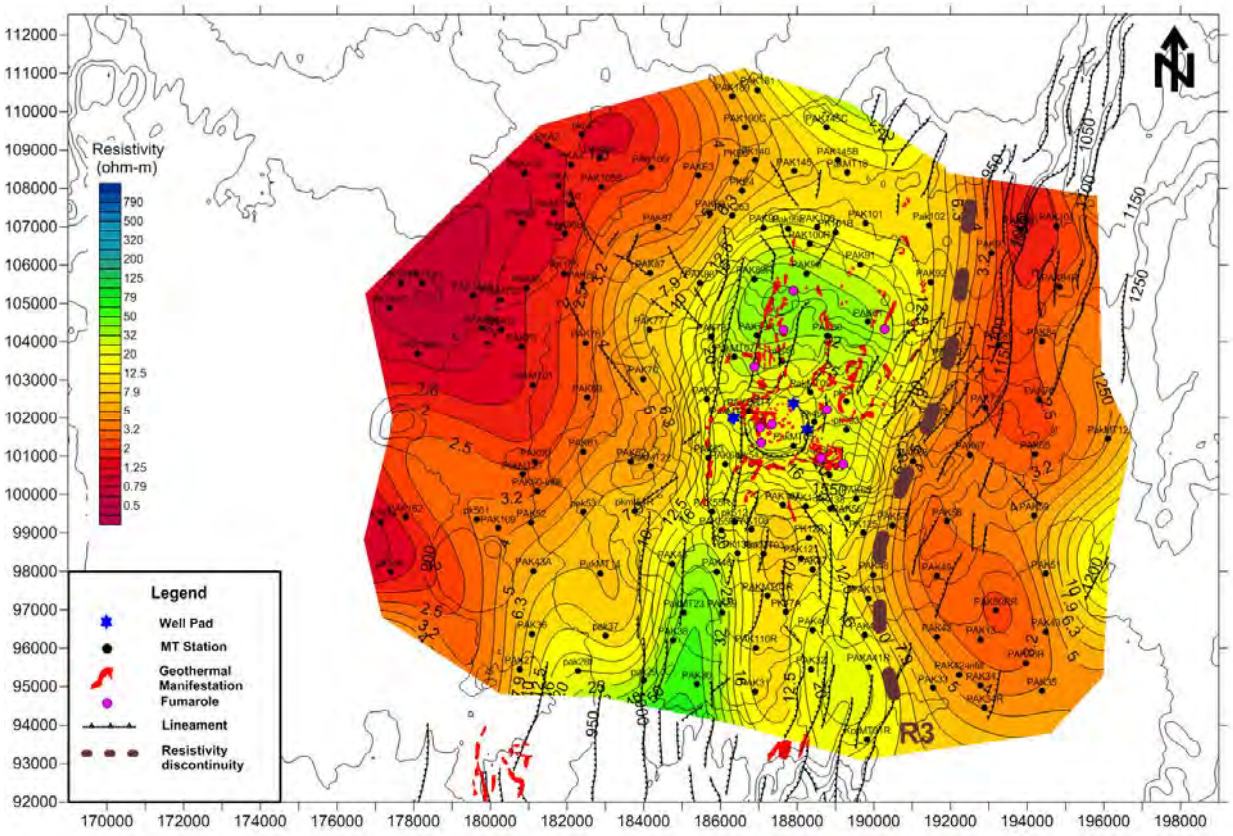

Fig. MT-21 Resistivity map at a depth of 750m (Paka field)

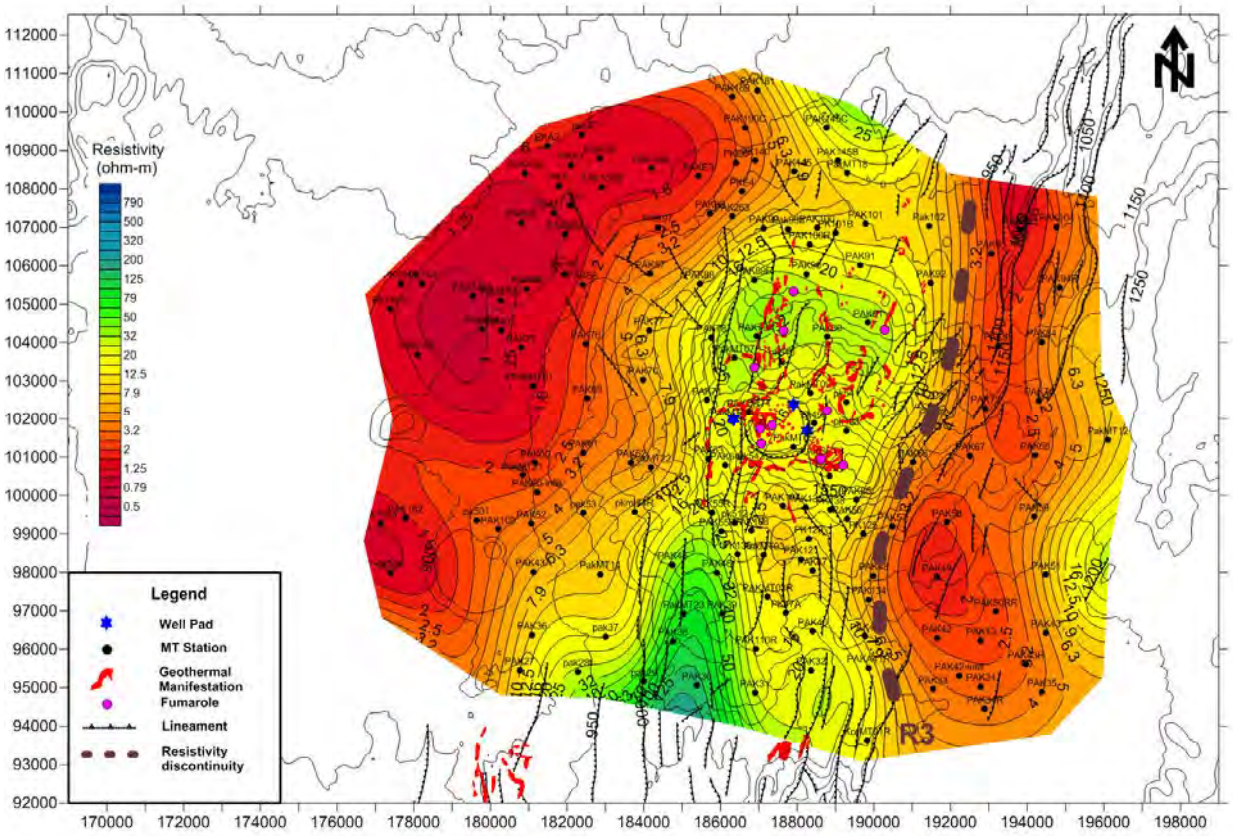

Fig. MT-22 Resistivity map at a depth of 1,000m (Paka field)

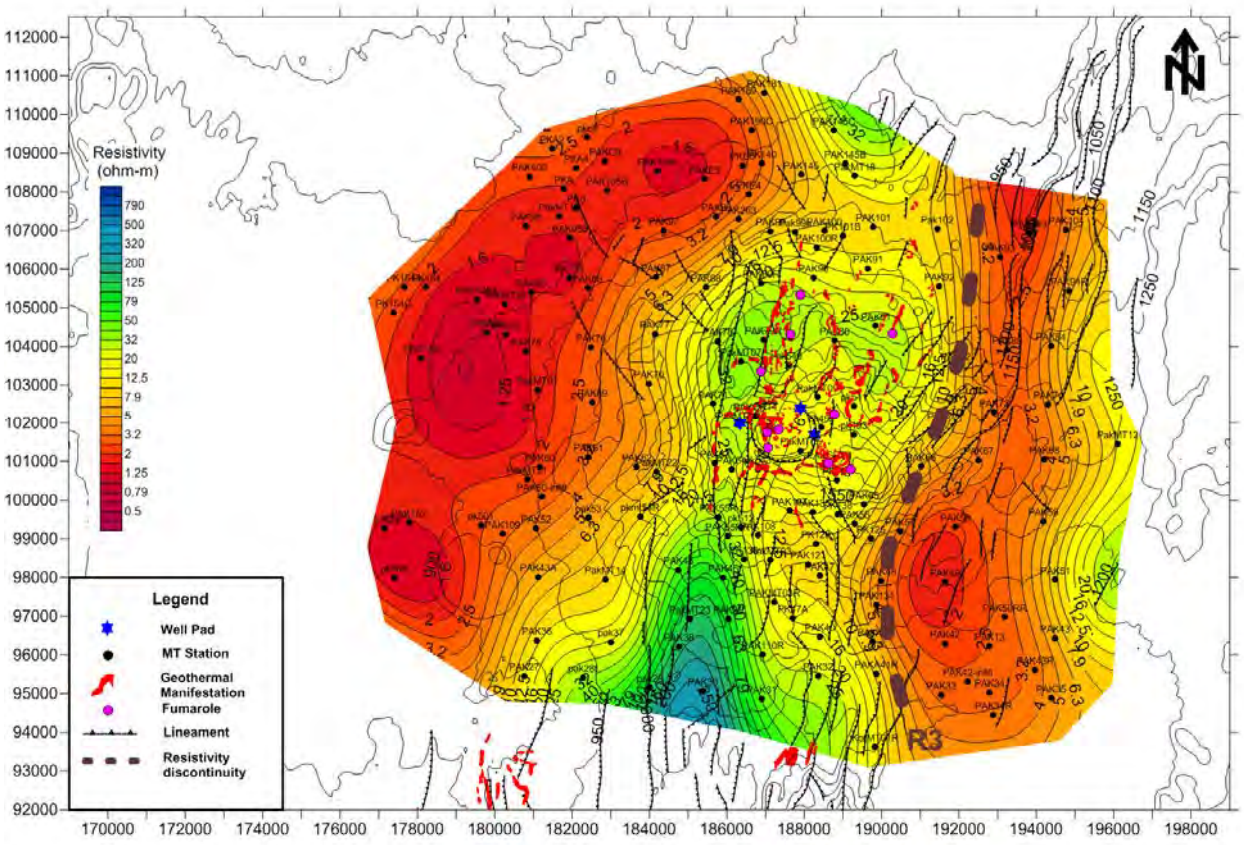

Fig. MT-23 Resistivity map at a depth of 1,250m (Paka field)

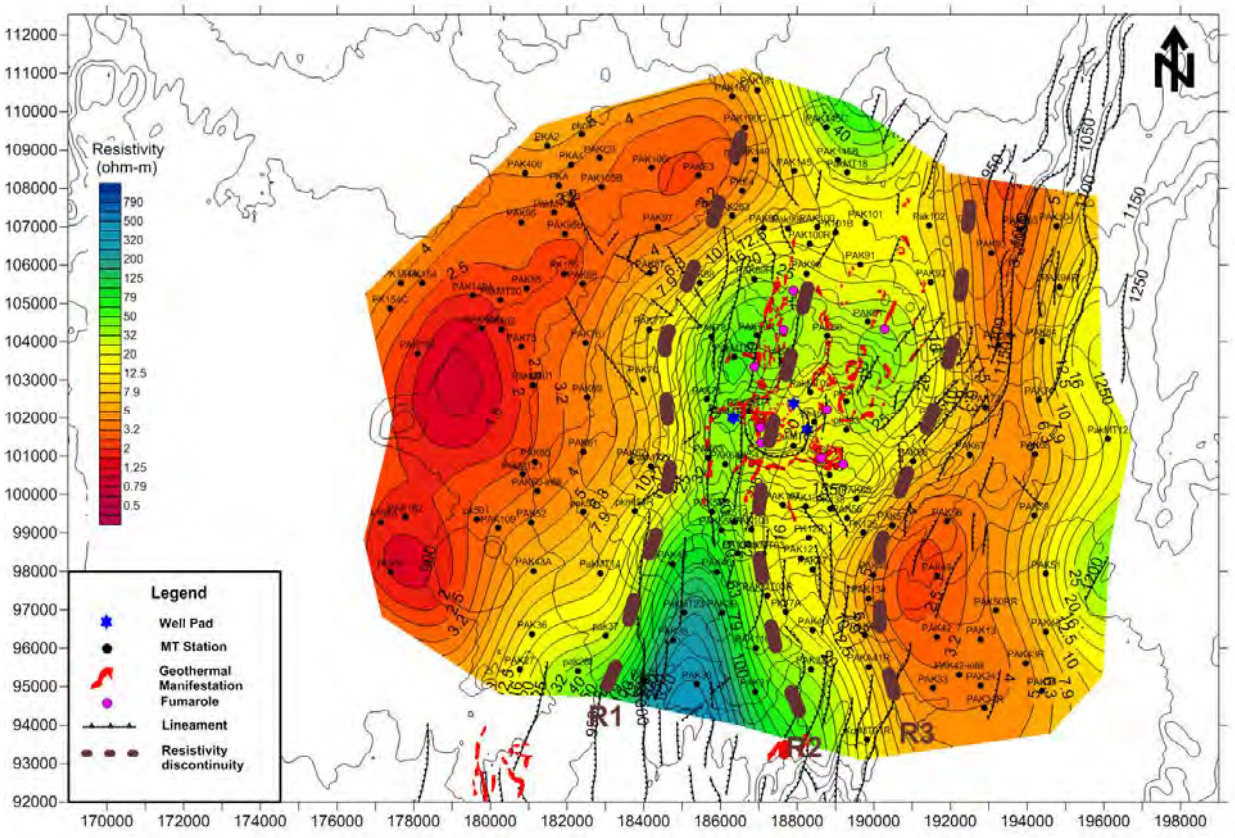

Fig. MT-24 Resistivity map at a depth of 1,500m (Paka field)

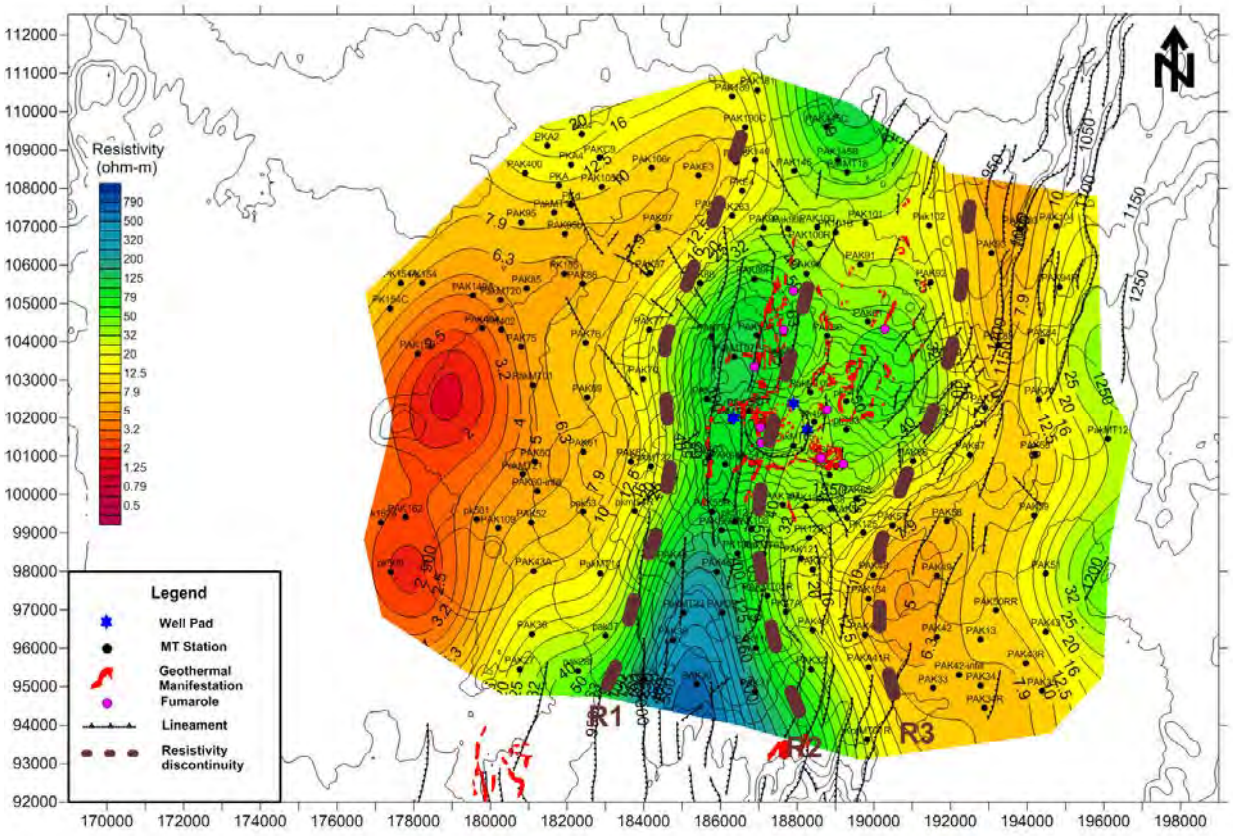

Fig. MT-25 Resistivity map at a depth of 2,000m (Paka field)

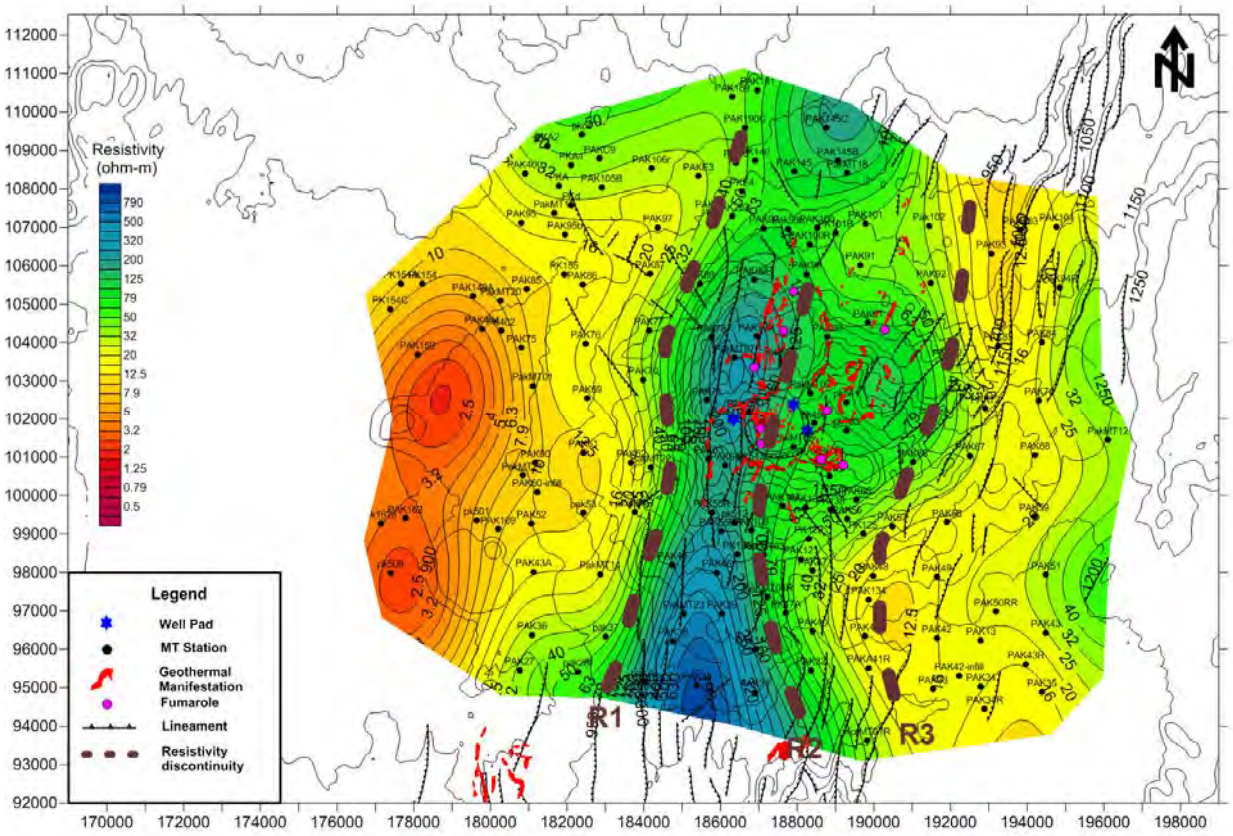

Fig. MT-26 Resistivity map at a depth of 2,500m (Paka field)

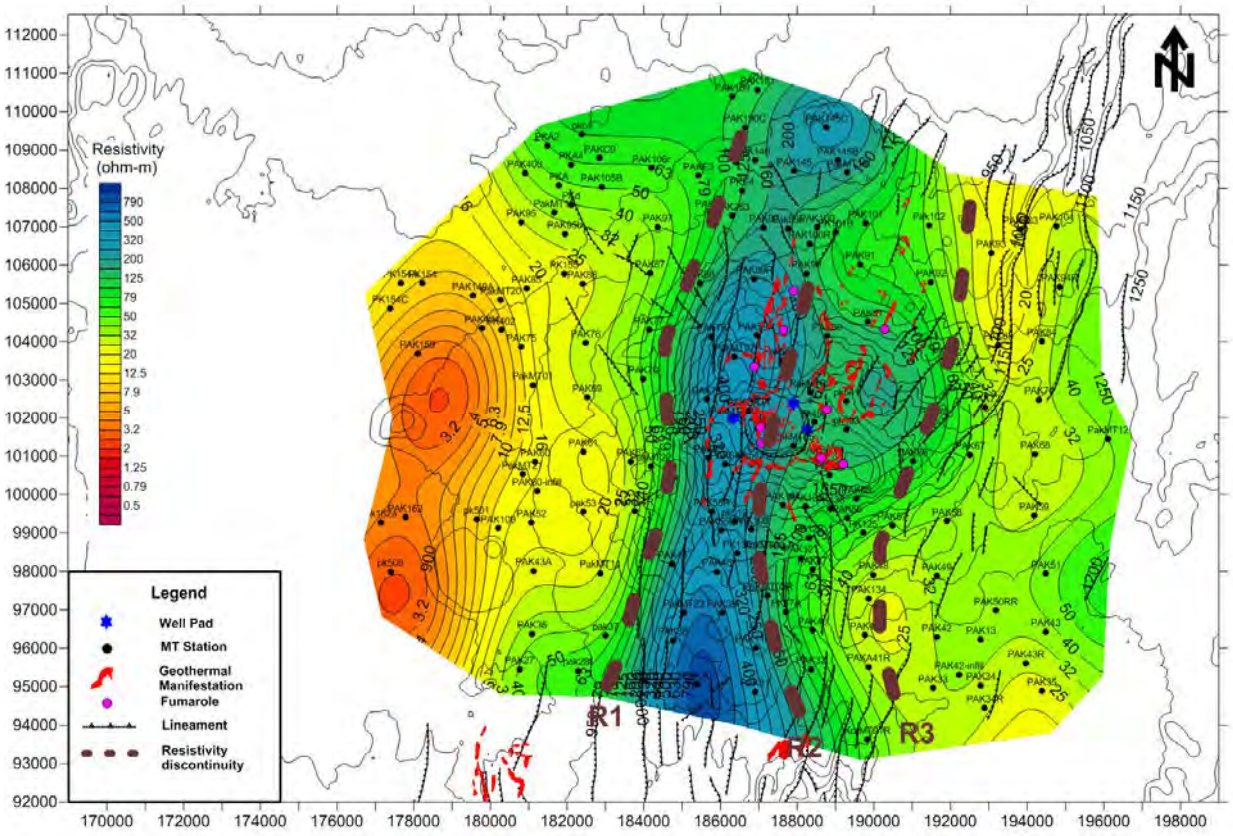

Fig. MT-27 Resistivity map at a depth of 3,000m (Paka field)

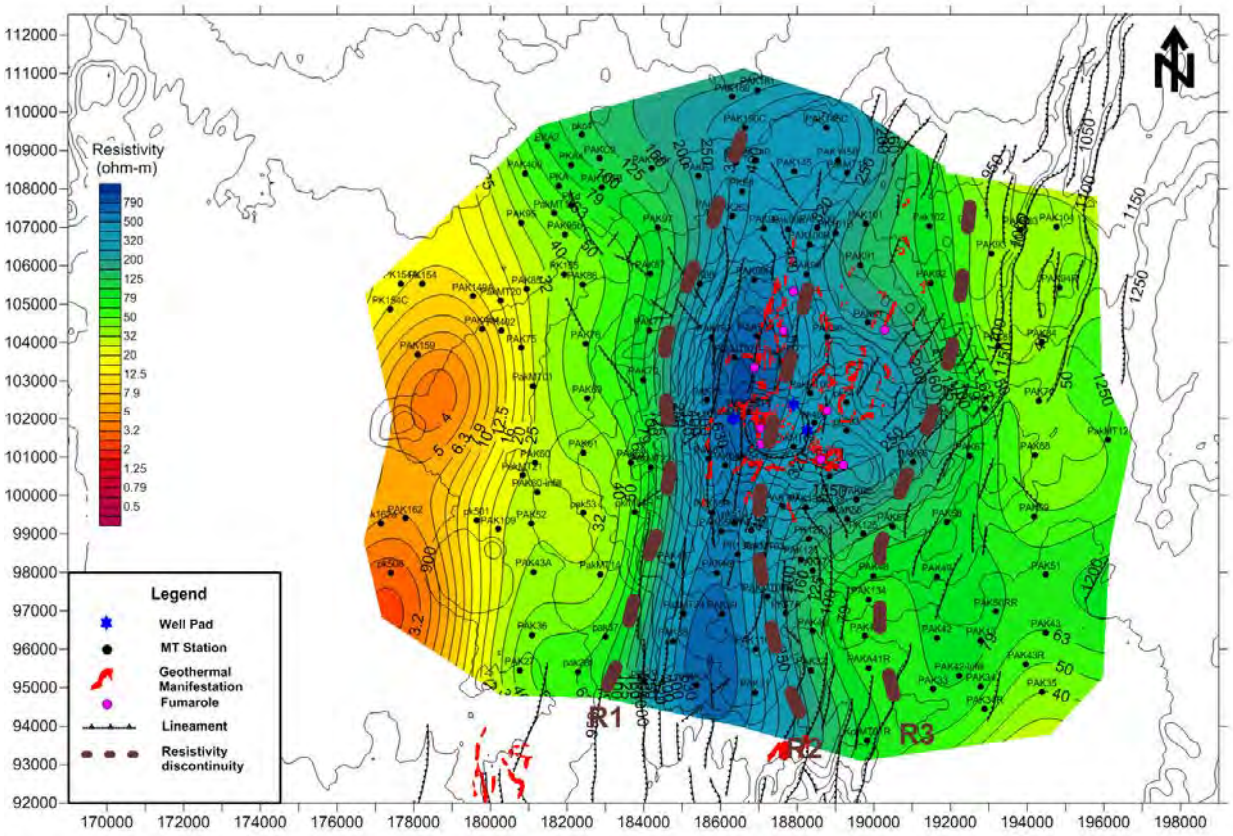

Fig. MT-28 Resistivity map at a depth of 4,000m (Paka field)

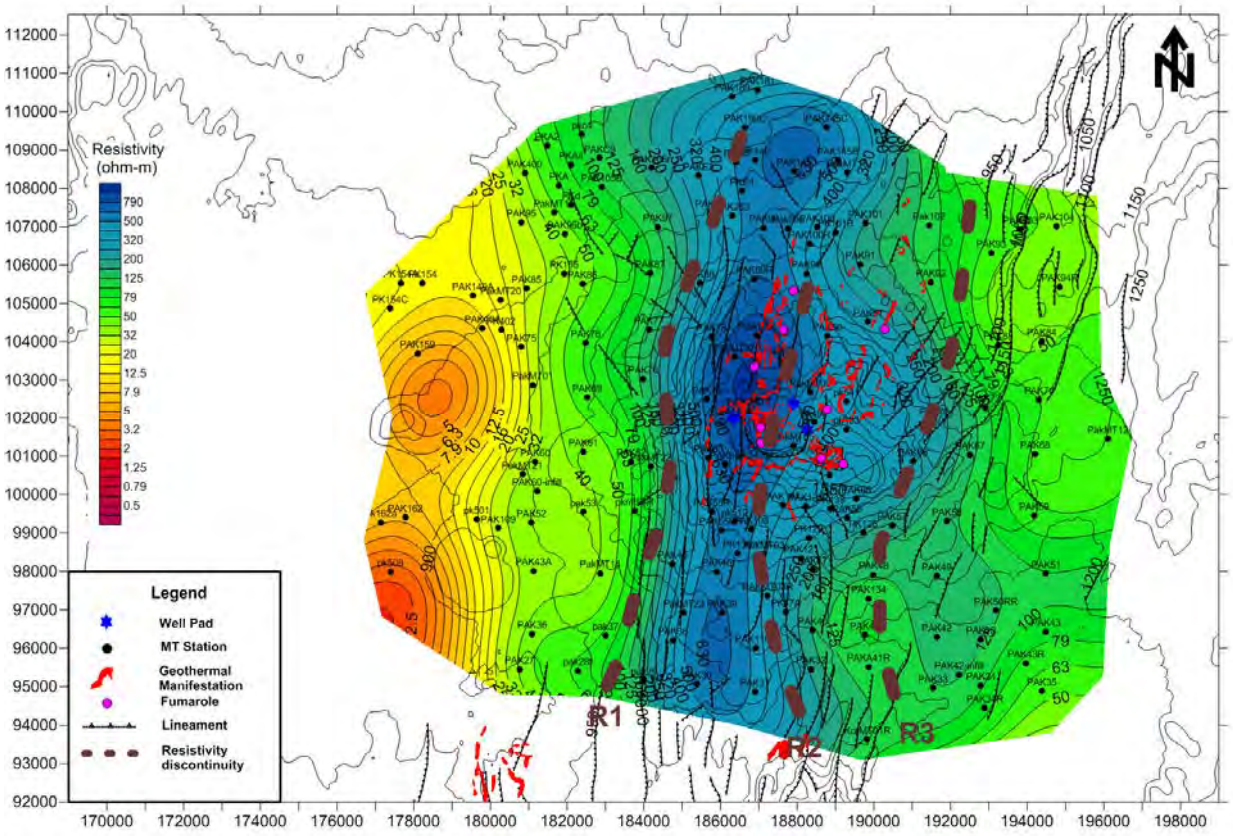

Fig. MT-29 Resistivity map at a depth of 5,000m (Paka field)